THE EFFECT OF COOLING RATE ON TOUGHNESS AND CRYSTALLINITY IN POLY(ETHER KETONE KETONE) (PEKK)/G30-500 COMPOSITES

by
Kedzie Davis

Thesis submitted to the Faculty of the
Virginia Polytechnic Institute and State University
in partial fulfillment of the requirements for the degree of

Master of Science
in
Materials Science and Engineering

Approved:

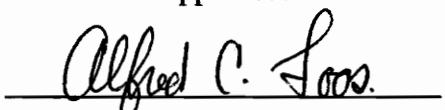

A. C. Loos, Chair

G.L. Wilkes

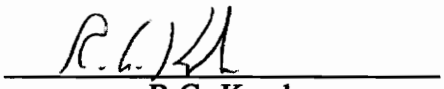

R.G. Kander

December 1996
Blacksburg, Virginia

Keywords: PEKK, Carbon Fiber Composites, Interlaminar Fracture Toughness, Mode I and Mode II Strain Energy Release Rates, Degree of Crystallinity

THE EFFECT OF COOLING RATE ON TOUGHNESS AND CRYSTALLINITY IN POLY(ETHER KETONE KETONE) (PEKK)/G30-500 COMPOSITES

by
Kedzie Davis

A.C. Loos, Chair
Materials Science and Engineering

(ABSTRACT)

Six poly(ether ketone ketone)/carbon composite panels were manufactured from powder coated towpreg. All six panels were initially processed using a hot press equipped with controlled cooling. Four of the panels were used to investigate the effect of cooling rate on crystallinity. A fifth panel was used to investigate the effect of annealing the composite after completion of the standard fabrication process. The sixth panel was used to investigate changes in toughness due to manufacturing towpreg with polymer that had been reclaimed from the towpreg fabrication system's air cleaner.

Cooling rates of 2°C/min, 4°C/min, 6°C/min, and 8°C/min resulted in composites with crystallinities of 33%, 27%, 24%, and 23%, respectively. The principal investigation of the effect of cooling rate on crystallinity and mode I and mode II strain energy release rates, G_{Ic} and G_{IIc}, respectively, showed that G_{Ic} and G_{IIc} values increase with increasing cooling rate. Comparison of the toughness values as a function of crystallinity showed that the dependence of toughness on crystallinity is approximately equivalent to the dependence of toughness on cooling rate.

Comparison of the data from the annealed panel to that from the analogous principal panel showed that annealing increased the crystallinity and decreased the mode I strain energy release rate. There was no effect, however, on the mode II strain energy release rate. Comparison of the data from the panel made with reclaimed polymer to that from its analogous principal panel showed that the reclaimed polymer panel had equivalent crystallinity and G_{Ic} values. On the other hand, the G_{IIc} values in this panel were lower than in the analogous principal panel.

Acknowledgments

The author would like to thank Dr. A.C. Loos, committee chair, for all of the time that he has spent with this project and for the support that he has provided. The insight and accessibility of committee members G.L. Wilkes and R.G. Kander are also sincerely appreciated.

The author would also like to gratefully acknowledge the financial support provided by the Office of Naval Research Graduate Fellowship Program and by the National Science Foundation Science and Technology Center for High Performance Adhesives and Composites.

There are several members of the Virginia Tech community who deserve special recognition for their invaluable assistance. Dr. G.L. Wilkes, Dr. S. Srinivas, and V. Ratta for help with the crystallinity analysis. Although the etching work for which they also provided assistance was not found to be useful, their assistance with that work is also still deeply appreciated. Dr. D. Dillard, R. Humfeld, and T. Chang for help with the double cantilever beam and end notch flexure testing. R. Humfeld for his development of a data reduction subroutine that significantly reduced the time required to analyze the end notch flexure data as well. J. Price-O'Brien for his near constant availability and never-ending willingness to work to keep all the electronics running in a less than ideal environment. And last, but certainly not least, A. Rau for his guidance throughout this project in all of the little ways that really made a difference.

The author would also like to thank all of the people who have made her time at Virginia Tech as pleasant as it has been and who have helped to smooth the way through trials in a variety of areas. In addition, the author would like to recognize the steadfast support and encouragement of her parents, Mary and Harvey Davis. Finally, the author would like to thank Christian Fernholz for being a such pillar of strength when she really needed it.

Table of Contents

List of Figures

List of Tables

Chapter 1 - Overview

Semicrystalline polymers are becoming more widely used in composite materials for a number of reasons, but primarily because they generally have higher strength, stiffness, and glass transition temperature than amorphous polymers. Semicrystalline polymers are thermoplastics so they also have many processing advantages in addition to the mechanical advantages provided by the crystalline nature of the material. Processing of these materials is of interest because processing conditions can be used to regulate the degree of crystallinity and the state of the amorphous phase. The material properties of the composite are dependent on these changes in polymer morphology. Knowledge of how processing conditions affect material properties can allow a manufacturer to tailor a material for a specific purpose. For instance, poly(ether ether ketone) (PEEK) with a relatively high degree of crystallinity generally has good solvent resistance[1] and high strength and stiffness[2]. In some applications, however, PEEK with a low level of crystallinity may be desirable because amorphous PEEK has greater toughness[1] and strain-to-failure[2].

1.1 - The Crystalline Phase

The degree of crystallinity and the crystalline structure in semicrystalline polymer composites can be affected by the composite processing conditions and the properties of the composite constituents. Spherulites can nucleate during processing in the bulk matrix between fibers or directly on a fiber surface. Furthermore, crystallinity can occur as a result of primary or secondary growth. These differences in crystalline morphology will affect composite properties.

The relative amount of primary and secondary crystallinity is important because this proportion will alter the mechanical properties of a polymer. The location of spherulitic nucleation in a composite may also affect composite properties, since some researchers[3,4] believe that spherulites which nucleate on the fiber create stronger bonds between the fiber and the polymer than spherulites which nucleate in the bulk polymer and then grow to touch the fibers. Although there is currently no conclusive evidence that the bond between the fiber and a spherulite varies based on the point of nucleation, the factors which affect the preferred nucleation site will be discussed.

1.1.1 - Formation of Crystallinity in Neat Polymers

The qualitative aspects of crystalline development in semicrystalline polymers is well understood. Unfortunately, there is limited understanding about the effect of the relative amounts of primary and secondary crystallinity in the polymer on mechanical properties. Issues regarding the growth of crystals will be discussed in this section, while the relationship of primary and secondary crystallization to mechanical properties will be discussed in Section 1.3.1.

The division of crystalline development into primary and secondary crystallization phases is well documented[5,6,7,8,9]. Primary crystallization is the initial stage of crystal development during which the spherulite grows at a nearly constant rate. This stage controls the size of the spherulites, so is dependent upon cooling rate and nucleation density. Secondary crystallization is a process in which spherulites do not grow larger, but lamellar development continues within the spherulite[5]. Secondary crystallization occurs in melt crystallization, i.e. when a polymer is crystallized from the melt state, and in cold crystallization, i.e. when a polymer is quenched and then annealed, so that crystallization occurs from the glassy state. This secondary growth is the primary mechanism for lamellar thickening and development of imperfect crystals between existing lamella[9,10]. The existence of imperfect crystals can be suggested by DSC scans. Cebe and co-workers[9,10] found that a low melting point endotherm seen in DSC scans can be a result of imperfect crystals that melt just above their formation temperature.

The transition from primary to secondary growth is primarily dependent on the nucleation density[11]. The higher the nucleation density, the more quickly spherulites will impinge upon each other. Under conditions of high nucleation density and fast spherulitic impingement, the resultant spherulites will be small and the material will have a high proportion of primary crystallinity[7].

The dependence of the transition from primary growth to secondary growth on nucleation density means this transition is also dependent upon cooling rate. Several groups[11,12,13] have shown that increasing the melt temperature, or correspondingly decreasing the cooling rate, will decrease the nucleation density. If a decreased cooling rate results in a lower nucleation density, primary crystallization will proceed for a longer period of time before spherulites impinge on one another. As a result, individual spherulites will become larger. A longer period of slower primary growth will also provide enough time for impurities and molecular imperfections to be driven to the spherulitic

growth front. Consequently, spherulites formed during slow primary growth will have few defects and a high melting point.

Larger individual spherulites, however, result in a larger proportion of secondary crystallinity. The proportion of crystallinity due to secondary processes can be quite large in some cases. Cebe found that in PEEK only about half of the total crystallinity formed through primary processes, i.e. prior to spherulite impingement[9]. The remaining half was then formed through secondary processes, such as development of crystals between existing lamellae or lamellar thickening.

The proportion of primary crystallinity to secondary crystallinity can influence the polymer's microstructure. Cebe, Chung, and Hong found that PEEK cooled from 370°C to room temperature in two to three hours had a crystallinity around 30%, while material cooled over a period of sixteen hours had a crystallinity around 32%. Although the two materials had relatively equivalent degrees of crystallinity, the spherulites in the material that was cooled more slowly contained larger, more perfect crystals[10]. Crystal imperfection is a concern because imperfect crystals have been shown to melt just above their formation temperature as discussed earlier. The resultant polymer is then less thermally stable than a polymer composed of more perfect crystals.

In addition to changing the crystalline morphology, the time-temperature profile during crystallization can influence the polymer unit cell and lamellar structures. Unit cell structures in poly(ether ketone ketone) (PEKK) have been shown to develop into two unique structures depending upon the temperature at which the polymer is crystallized[14]. If the polymer is cold crystallized, the less stable unit cell is formed as a result of relatively low molecular mobility and high chain stiffness. If the polymer is melt crystallized, a more thermodynamically stable form of crystal develops with a higher melting point[15]. Gardner, Hsiao, and Faron felt that this difference in preferred unit cell is primarily a result of the high chain stiffness in PEKK. They also found, however, that the nucleation rate can affect the preferred unit structure. Fast nucleation rates favored the less thermodynamically stable structure, while slow nucleation rates favored development of the more thermodynamically stable structure[14].

1.1.2 - Formation of Crystallinity in Composites

When dealing with neat polymer, the primary factors that determine the level of crystallinity are cooling rate and nucleation rate as a function of cooling rate. When a polymer is used as a matrix material in a composite, several other factors become important to the polymer's final crystalline structure. Fibers can provide heterogeneous nucleation sites, so the nucleating ability of the fiber and the fiber volume fraction (FVF) will affect the composite's crystalline structure.

In a composite, spherulites can nucleate in the bulk polymer or on a fiber surface. Nucleation of spherulites on a substrate results in "transcrystalline" formations. Hsiao and Chen[16] suggest transcrystallinity is a result of a large number of nuclei on the fiber surface. The high nucleation density causes the spherulites to grow into each other in a way that constrains further lamellar growth in the direction normal to the fiber surface. Cebe differentiates transcrystalline growth from spherulitic growth by describing transcrystallinity as radial growth around a fiber that essentially forms a concentric cylinder with the fiber at the cylinder center[9].

For spherulites to form as concentric cylinders around a fiber, the fiber must provide a large number of heterogeneous nucleation sites, as specified by Hsiao and Chen. Bessell and Shortall indirectly supported this supposition when they documented that if relatively few nucleation sites exist on a substrate, spherulites will form as fan-like structures[17] around a fiber. They claimed that the number of nucleation sites is important because a higher nucleation density causes the spherulites to impinge upon one another more quickly. This results in the more parallel, and less fan-like, morphology.

It is likely that spherulite nucleation on the fiber will occur at the same time as spherulite nucleation in the bulk; therefore, the relative nucleation rates will determine the characteristics of the microstructure. Incardonia, *et al* [18] found that transcrystalline growth formed more quickly than bulk crystallinity at high temperatures in the polymer J-1. Cebe[7] and Lee and Porter[13], on the other hand, found that bulk nucleation and transcrystalline nucleation occur simultaneously in PEEK. All three groups used carbon fibers in their work. This emphasizes that the preferred nucleation site can be a function of the compatibility of the matrix and the fiber, i.e. the nucleating ability of the fiber may differ depending upon the polymer matrix material.

The varying effectiveness of a type of fiber to nucleate spherulites in a particular polymer is evident from the work of Folkes and Hardwick[19] and Hsiao and Chen[16]. Folkes and Hardwick[19] summarized that, in general, spherulites nucleate on carbon and organic fibers, but not necessarily on glass fibers. Hsiao and Chen[16], on the other hand, found experimentally that PEEK, PEKK, and PPS polymers form transcrystalline growth on pitch-based carbon fibers and aramid fibers, but did not necessarily nucleate on PAN-based carbon fibers and glass fibers.

Differences in nucleating ability of the different types of fibers might imply that the surface chemistry of the substrate determines its nucleating ability. Huson and McGill[20], however, did not find this to be true for polypropylene. Teishev and Marom[21] found that plasma treatment increased the nucleating ability of polyethylene fibers. Nevertheless, this increased nucleation density could be a result of a change in surface energy or fiber morphology as well as a result of a change in surface chemistry.

The nucleation ability of the fiber does appear to be one of the more significant variables to morphological development in composites, Unfortunately the factors that influence the nucleation density are not clear. Campbell and Qayyum[22] found that imperfections in fiber surfaces improve the nucleating ability of the fibers. Lee and Porter[13] suggested that surface energy, temperature gradients, unit cell structures, and shear stresses might play a role in transcrystalline development. Whatever the reason, there is no doubt that the characteristics of the fiber can influence a polymer's morphology.

Not only are the characteristics of the fiber important, but the fiber volume fraction in the composite has also been shown to influence the proportion of spherulites that nucleate on the fibers versus those that nucleate in the bulk. He and Porter[23] found that the higher the fiber volume fraction, the higher the crystallinity in HDPE/PE composites. They claimed that the higher crystallinity is due to the higher heterogeneous nucleation density created by the increased number of fibers in the material. Additionally, higher fiber volume fractions appeared to result in preferential crystallization on the fiber surface. Campbell and Qayyum found that increasing fiber volume fraction in poly(ethylene terephthalate) (PET)/ polypropylene (PP) composite did cause preferential transcrystalline growth, but it also limited the width of the transcrystalline region[22]. Their work also showed that increasing the fiber volume fraction increased the number of spherulites formed in the bulk at high crystallization temperatures. This seems reasonable considering that they also found that the nucleation density decreases with increasing distance from the fibers.

In addition to the effects that nucleation rates and fiber volume fraction have on composite microstructure, addition of fibers to the system can alter the effect that the temperature has on microstructure. Moon[24] found that glass/PP composites cooled at slower rates showed more nucleation on fiber surfaces than in the bulk polymer. This seems reasonable since others[12,13] have found that faster cooling rates increase the nucleating ability of neat polymers. If the nucleating ability of the neat polymer is low, then it is likely that heterogeneous nucleation on the fiber surface will be more prevalent.

The nucleation rate on a fiber versus the nucleation rate in the bulk polymer will affect the composite microstructure because it determines the relative size of the spherulites that nucleated on the fiber with respect to the spherulites that nucleated in the bulk. Furthermore, preferential nucleation on fiber surfaces is likely to reduce the number and size of spherulites nucleated in the bulk, and vice versa, since the amount of polymer available for the formation of spherulites is limited. Campbell and Qayyum found that when nucleation occurs at the same rate in the bulk matrix as on the fiber, then the fiber nucleated spherulites will be the same size as the bulk nucleated spherulites[22]. On the other hand, if nucleation occurs more quickly on the fiber than in the bulk, as Incardonia, *et al* [18] found for J-1 polymer at temperatures below 245° C, the spherulites that nucleated on the fiber are likely to be larger than the spherulites that nucleated in the bulk. They, however, found that this preferential nucleation was temperature dependent. Although nucleation on the fibers was preferred below 245°C, nucleation in the bulk polymer was favored at temperatures above 270°C. This reemphasizes the additional complexity associated with the effect of cooling rate when fibers are included in the system.

1.2 - The Amorphous Phase

The first section of this review discussed only the crystalline phase of the polymer. Polymers, however, never reach 100% crystallinity, so one must also consider the state of the amorphous phase. Although the effect of cooling rate on a material's crystallinity is generally the only cooling rate dependent characteristic discussed, the thermal history will also regulate the state of the amorphous material.

The state of the amorphous phase is important because this phase is rarely in equilibrium after processing. As a result, the properties of the amorphous polymer will change over time as the amorphous phase attempts to reach an equilibrium state. This change of amorphous polymer properties over time is referred to as physical aging.

1.2.1 - The Phenomenon of Physical Aging in Amorphous Polymers

Physical aging is a phenomenon that occurs as an amorphous polymer relaxes over time to reach a lower energy state. This aging process only affects the amorphous phase of the polymer. The polymer does not degrade during aging or become more crystalline, so the effects of aging can be reversed by heating the polymer above it's glass transition temperature, T_g[25]. Above T_g the amorphous polymer is in a equilibrium state; therefore, when an aged polymer is heated to a temperature above its T_g, the amorphous material returns to the volume and energy state that existed before physical aging[26].

The main observable manifestation of physical aging is a reduction in free volume over time. This reduction has a significant impact on physical properties because as the free volume in the system decreases, so does the segmental mobility of the polymer[27]. Reduction in the mobility means that molecules will require more time to rearrange after a stress is applied, so the polymer becomes more stiff and brittle. This indicates that amorphous polymers which are cooled slowly, and therefore have a lower initial free volume, will show smaller changes in mechanical properties over time[28].

Characteristic effects of physical aging include increased density, stiffness, yield stress, and relaxation time and decreased free volume, enthalpy, impact strength, fracture energy, and elongation. Physical aging, however, appears to have no effect on the material's heat capacity, and therefore T_g[29]. Mijovic[27] detected this experimentally. He found that the characteristic decrease in enthalpy did not correspond to a change in the value of a graphite/epoxy composite's T_g.

The temperature range over which physical aging is a concern has been debated in the literature. Struik[30] states that physical aging will occur between the T_g and the secondary transition, T_β. Below T_β, relaxation may occur, but it does not change the free volume in the polymer[31]. Goodwin and Hay[32] claimed that physical aging occurred only in the temperature range from T_g to T_g- 50°C. Their claim, however, was developed from glass transition temperature data. As mentioned previously, T_g has been shown to be insensitive to reductions in free volume. Consequently, the possible effects of physical aging should be considered for application temperatures over the entire range from T_β to T_g.

1.2.2 - The Effect of Crystal Structure on Physical Aging

Just as the crystalline phase of a polymer can be affected by the amorphous phase of the polymer, the existence of crystallinity can affect the properties of the amorphous phase. The local structure of the amorphous phase of PEEK has been shown to be affected by the development of crystals[26]. This is due in part to tie molecules that exist between crystals. Tie molecules are contained in more than one crystal and the concentration of these molecules determines the mechanical continuity between crystals[8]. The interconnection of two crystals via tie molecules through an amorphous region will act to constrain the amorphous phase. At relatively low crystallinities the density of tie molecules between crystals can be rather high without causing excessive pressure in the amorphous melt. At higher crystallinities, the density of tie chains must be lower to reduce the pressure in amorphous material near the surface of the lamella. A low tie chain density reduces the number of molecules across the crystalline-amorphous interface. This decreases the material's ability to transfer load. Consequently, fracture often initiates near the crystalline/ amorphous interface[8] in highly crystalline polymers. Similarly, increasing the proportion of polymer in the crystalline phase also increases the number of tie molecules which are constrained by surrounding crystals. This reduces the effect of physical aging, because constrained tie molecules reduce the polymer's ability to relax into a lower energy state[26,29].

The change in polymer properties over time as a result of physical aging is also likely to be diminished by increasing crystallinity because higher proportions of crystallinity reduce the amount of amorphous polymer in the system. Additionally, the chemical structure of the polymer can alter the significance of physical aging. Carfagna, et al. expected that in polymers with relatively stiff molecules, e.g. PEEK, the effects of physical aging would be reduced because of molecular constraints[33].

1.3 - The Effect of Polymer Morphology on Mechanical Properties

Fracture properties of polymers have been shown to be dependent upon both the crystalline morphology and the amorphous morphology of the polymer. Very fine spherulitic structure has been shown to increase ductility, yield strength, and impact strength[8]. Similarly, large deviations from equilibrium in amorphous materials have also been shown to increase ductility. Highly crystalline materials, however, are strong and stiff, but brittle, while the properties of amorphous materials that are far from an equilibrium state may change significantly over a relatively short period of time. Consequently the relationship between both phases and the resultant mechanical properties will be discussed more fully.

1.3.1 - The Effect of Crystallinity on Mechanical Properties

The dependence of material properties on the degree of crystallinity in semicrystalline polymers is well documented. The exact crystalline structure can, however, alter the significance that crystallinity has on material properties. For instance, Lee and Porter[13] and Folkes and Hardwick[19] found that in carbon/PEEK composites and glass/PP composites, respectively, the interfacial shear strength increased with increased nucleation on fiber surfaces rather than simply increased crystallinity. Additionally, the size of the spherulites[8] and the proportion of primary to secondary crystallinity[6,7] can affect the modulus, yield stress, toughness, and melting temperature of a polymer or polymeric composite. The addition of fibers to a polymer can also reduce the extent to which the degree of crystallinity will independently determine the material properties.

The location of crystal nucleation in composites is of interest because of its potential to influence a number of mechanical properties. Lee and Porter[13] examined four carbon/ PEEK composites processed under different conditions. They found that toughness was more dependent on the type of crystallinity than the percent crystallinity. The samples were preheated for various lengths of time to manipulate the number of existing nucleation sites in the bulk polymer after the melt stage. The samples heated for a longer period of time had fewer remaining bulk nucleation sites and, therefore, had a much higher level of transcrystallinity in the composite. The composites with more transcrystallinity had a higher toughnesses than the samples which were preheated for shorter period of time.

Folkes and Hardwick also found that transcrystalline regions may provide a toughening mechanism even though these regions have been shown to have a low strain to failure. In a 1990 paper[19] they reported that if the interfacial bond between glass fibers and polypropylene is weak, a crack can be deflected between transcrystalline layers. This study showed that the presence of transcrystalline layers improved the strain energy release rate, G_c, of the composite even though the layers themselves had a low failure energy. Folkes and Hardwick felt that their work provided evidence that the nucleation of spherulites on fibers may act as a crack stopping mechanism. If transcrystalline regions crack easily, a large number of cracks will result when the material is loaded. This will increase the amount of energy absorbed during composite failure.

Lustiger[34] and Carvalho and Bretas[35] have also investigated the mechanism for fracture in composite crystalline regions. In general, there seems to be a consensus that cracks form between spherulites, regardless of whether the spherulites were nucleated in the bulk polymer or on the fiber. Although Chu and Schultz[36] worked with neat PEEK samples, they proposed a interspherulitic cracking mechanism that is similar to the mechanisms that have been proposed for composite transcrystalline regions. Existence of weak boundaries connecting crystalline regions is reasonable since crystallization theory states that impurities which cannot be crystallized are pushed to the growing edge of the crystal. When two crystals impinge, these impure, amorphous regions are weak compared to the surrounding crystal. Propagation of cracks through weaker, but tough, amorphous regions might explain the toughening mechanism which was seen empirically by Lee and Porter.

The size of the spherulites has also been shown to affect mechanical properties. Schultz[8] reported that any means of reducing the size of spherulites resulted in improved ductility and strength. Large spherulites have been shown to result in a more rugged fracture surface[36]. Weak boundaries between large spherulites were discussed in Section 1.1.1. This comparatively weak layer may act as a pathway for fracture[36].

The distinction between primary and secondary crystallization appears to be important to mechanical properties because the formation of more perfect primary crystals at lower cooling rates can result in higher crystallinity and, therefore, a higher modulus[6]. This higher stiffness is often retained at elevated temperatures, thus increasing the material's potential end use temperature. Cebe showed that neat PEEK samples with equivalent crystallinities but differing thermal histories had differing thermal properties[9]. She did not, however, speculate about the mechanism that causes the changes in thermal properties. The discussion of primary and secondary growth in Section 1.1.1 indicates that differences

between thermal histories could have resulted in differences in the proportion of primary growth to secondary growth. This might explain the differences in observed tensile properties, since tensile properties have been shown to be dependent on spherulitic size.

Although there are general trends for the dependence of a property on the degree of crystallinity and the morphology of the crystallinity, the degree of dependence of composite properties may not be equivalent to the degree of dependence of neat polymer properties. For instance, the tensile strength and stiffness of neat PEEK has been shown increase with increasing crystallinity[2]; however, the transverse strength and stiffness in PEEK composites was shown to be generally independent of the degree crystallinity[13]. Lee and Porter did, however, find that the nucleation density of PEEK in composites was always higher than the nucleation density in neat PEEK. This higher nucleation density may then result in smaller spherulites which should improve ductility and toughness[8].

If the degree of crystallinity in a composite differs from the degree of crystallinity in a neat polymer when the two materials have been subjected to the same thermal history, then the degree of crystallinity may also be dependent upon the fiber volume fraction (FVF) of the composite. There was little documentation of the combined effect of fiber volume fraction and crystallinity on material properties. The effect of fiber volume fraction, however, on the tendency of polymers to nucleate on fibers has been well documented. He and Porter[23] found that the higher the FVF, the higher the crystallinity in high density polyethylene (HDPE)/PE composites. Additionally, higher FVF resulted in preferential crystallization on the fiber surface. This presumably is because the increased number of fibers increased the nucleation density. Campbell and Qayyum[22] found that increasing fiber volume fraction in PET/PP composites also caused preferential transcrystalline growth.

Although He and Porter and Campbell and Qayyum found that increasing FVF can increase nucleation of fiber surfaces, other researchers question whether increased transcrystallinity has any effect on mechanical properties in high fiber volume fraction composites. Chen and Hsiao measured debonding forces for single fiber, 20% FVF, and 60% FVF AU-4/PEKK composites[4]. Comparison of the force required to debond a filament from a single filament composite with and without transcrystallinity showed there was a nearly 50% increase in the force required to debond a single filament when the crystallinity increased from 0% to 28%. However, for the 60% fiber volume fraction composite the debond force was essentially constant regardless of the crystallinity. This clearly indicates that increasing the fiber volume fraction can decrease the effect of transcrystallinity on some properties.

1.3.2 - The Effect of the Amorphous Phase on Mechanical Properties

Although the degree of crystallinity is usually considered to govern the mechanical properties of polymers and their composites, the state of amorphous material will also alter the material properties. The affect of the state of the amorphous material is rarely discussed directly. Nevertheless, a number of reports[10,37,38] have published data showing that the mechanical properties of polymeric materials can differ between specimens with equivalent degrees of crystallinity when different thermal histories are used to crystallize each specimen. The differences in properties as a result of thermal history could be a result of differences in the crystalline structure or of differences in the amorphous phase. If the differences in properties are due to differences in the amorphous phases, these differences may only be a transient phenomenon due to physical aging. The reduction in properties over time that occurs with physical aging will determine the long term properties of polymers and polymeric composites.

The importance of the state of the amorphous phase is implied by the results of Cebe, Chung, and Hong. They found that in melt crystallized films having approximately equal degrees of crystallinity, that the tensile properties were still dependent upon the cooling rate used during processing[10]. These particular results suggest that there are differences between the energy states of the amorphous materials in these polymers. Amorphous regions are able to maintain an equilibrium energy configuration to lower temperatures at slower cooling rates[31]. As a result, slower cooling rates reduce the material's initial departure from its equilibrium state and reduce the effects of physical aging[28].

Talbott, Springer, and Berglund reported improvements in tensile and compressive strength[37] for polymers that were quenched and annealed rather than simply melt crystallized. Nevertheless, their work provides no way to determine whether differences are due to changes in the crystalline state or changes in the amorphous state. Their work also showed that fracture toughness and the tensile and compressive moduli in neat PEEK are not dependent upon the thermal history of the polymer, only the degree of crystallinity. Tregub, Harel, and Marom, however, seem to contradict that result with their finding that the flexural fatigue behavior is improved by quenching and annealing a composite rather than simply isothermally crystallizing the specimens[38]. These differences in properties of materials with equivalent degrees of crystallinity but differing thermal histories indicate that one must consider the effect of the state of the amorphous phase on mechanical properties.

Unfortunately, differences in mechanical properties are only of interest if they exist throughout the lifetime of the composite. If the differences are a result of changes in the amorphous state, these differences may disappear over time as the polymer physically ages. Physical aging of amorphous regions effects many polymer properties. The most significant effect is to make the polymer less compliant[26]. Consequently, the yield stress will increase, but the polymer will fail at smaller strains[39]. In fact for PEEK, aging has been shown to result in an effect on fracture toughness that is equivalent to the effect of increasing the degree of crystallinity. Kimmish and Hay found that the fracture toughness of purely amorphous PEEK can drop to a tenth of its original value as a result of crystallization or as a result of physical aging[29].

Little documentation is available about the effect of physical aging on thermoplastic composites. Several studies have been completed that discuss the effect of physical aging on thermosetting, epoxy composites. Unfortunately, epoxy composites can simultaneously chemically age, i.e. crosslink, and physically age[27,28], so the aging process in these materials is not necessarily thermodynamically reversible. Changes due to increased crosslink density may not be readily differentiated from changes due to physical aging, so the results from these studies may not necessarily correlate directly to effects of physical aging in thermoplastic matrix composites.

1.4 - Summary and Research Objective

The properties of composites are indirectly dependent upon fabrication cooling rate because of the effect that cooling rate has on the composite microstructure. The morphology of the crystalline and amorphous phases of a semicrystalline polymer are interdependent, so changes in both phases as a result of changes in the cooling rate must be considered. Materials that are crystallized from the melt have been shown to have good fracture properties while materials that are quenched and annealed often have good tensile and compressive strength. This dependence of mechanical properties on polymer morphology seems, however, to be dependent upon the particular property of interest, the composite constituents, and the composite fiber volume fraction.

Although there has been a significant amount of research investigating the temperature dependence of PEEK composite properties, there has been relatively little that pertains specifically to the similar polymer PEKK. The PEKK polymer has higher chain stiffness than PEEK as a result of the substitution of a second ketone group for PEEK's second ether group. This difference in polymer chain stiffness will cause some differences in the properties of these two materials.

PEKK is a semicrystalline, thermoplastic polymer that has been one of the polymers of choice for recent work at the National Science Foundation Science and Technology Center for High Performance Polymeric Adhesives and Composites at Virginia Tech. Not only are the properties of the material of interest, but also how we can control properties through processing conditions. Some properties, such as flexural strength, short beam shear strength, and compressive strength have been reported[40] for continuous carbon fiber reinforced PEKK. Similar investigation of the effect of crystallinity has been completed for Iosipescu shear, transverse flex, and meso-indentation.[41]

Polymers in the poly (aryl ether ketone) family have been developed specifically for applications which require good fracture properties as well as high strength and stiffness. Although these polymers do provide improved toughness over more traditional epoxy composites, the material's toughness has not necessarily been quantified. A number of studies on the toughness of carbon/PEEK composites have been compiled by Moore and Seferis[1], but there are currently no reported data for either mode I or mode II interlaminar fracture toughnesses of carbon/PEKK composites.

Crystallinity in PEKK matrix composites has been shown to be dependent upon the cooling rate used in the consolidation cycle[41]. Cooling rates of up to 8°C/min were achieved with the hot press used in the investigation. Although presses which can cool parts much more quickly can be built[37], these are often complex to build and operate, and are therefore ordinarily undesirable in industrial settings. For this reason it was determined that it was unnecessary to study the effects of cooling rates greater than 8°C/min at this time. There are no physical limitations for the lower limit on the cooling rate, but there is a practical limit. Slow cooling rates increase the processing time for each part, which would reduce the product throughput in an industrial application. A lower bound on the cooling rate of 2°C/min results in both a factor of four difference in the upper and lower cooling rate bounds and provides a reasonable length for the processing cycle.

Although the minimum and maximum cooling rates vary only by a factor of four, measurable differences in both the crystallinity and toughness as a function of cooling rate should still be evident. These bounds will also indicate whether relatively small changes in the carbon/PEKK composite processing cycle can have a significant effect on final composite properties. If this is found to be true, composite properties could be manipulated in industrial settings without requiring expensive modification to existing processing equipment or extensive changes in processing operations.

This study is intended to establish bounds for carbon/PEKK mode I and mode II fracture toughnesses for the range of cooling rates most likely to be used in commercial manufacturing. Changes in the interlaminar fracture toughnesses and degree of crystallinity as a result of changes in cooling rate will be determined. The changes in toughness will be correlated to changes in crystallinity.

Chapter 2 - Manufacture and Evaluation of Composite Specimens

Composite panels were manufactured from G30-500 carbon fiber and powdered poly(ether ketone ketone) (PEKK) polymer. Panels were consolidated in a hot press at 370°C under 2.1 MPa pressure. The panels were then evaluated ultrasonically and cut into specimens for double cantilever beam testing and end notch flexure testing. Following mechanical testing of these specimens, the crystalline content was measured for each panel.

2.1 - Manufacture of Composite Panels

Composite panels were manufactured from stacks of towpreg lamina. The towpreg was fabricated using a continuous powder impregnation procedure and then wound into approximately 160 mm wide strips. 152.4 x 152.4 mm lamina were cut from these strips and stacked to form unidirectional laminates. The panels were processed using a hot press equipped with controlled cooling.

2.1.1 - Towpreg Manufacture

G30-500/PEKK towpreg was manufactured with the Virginia Tech Electrostatic Powder Prepregging Facility[41]. The final fiber volume fraction (FVF) target for these composites was 60%; therefore, operating variables were chosen so that towpreg with approximately 58% FVF was produced. This allowed for a small amount of resin flash during processing. Operational variables were tow tension, line speed, fluidization velocity, polymer bed depth, and powder charge. The two most controllable variables in the system were line speed and fluidization velocity. The response surfaces reported by Bucher[41] were as used as guidelines to determine operational parameters. Line speed was set at a nominal speed of 5.2 m/min. This resulted in an actual tow speed of 4.5 m/min. The tension was fixed to provide the minimum resistance that would maintain a taught tow. Increased tension decreased the line speed and increased fiber damage. The powder charge was maintained at 20 kV and the polymer bed depth was maintained at approximately 38 mm. The fluidization velocity was kept below 8.5 m^3/hr and altered periodically during the run to maintain the necessary volume of deposited polymer.

G30-500 carbon fiber is a PAN-based fiber available from Toho Carbon Fibers. The 12k tow used in this work was unsized and had no particular surface treatment. The

PEKK powder from DuPont had a median diameter of 27 μm. This was much smaller than the powder used in previous work[41], which had a median diameter of 48 μm. The smaller particle size caused a significant amount of polymer to cling to the sides of the deposition chamber during towpreg fabrication. Although there was a electromagnetic vibrator attached to the deposition chamber, it did not provide enough motion to prevent the polymer from accumulating on the chamber walls. As a result, the accumulated polymer had to be manually dislodged from the walls occasionally or it fell as clumps onto the fiber. If this occurred, the polymer clumps were brushed off of the fiber to maintain the target fiber volume fraction.

Approximately 150 m of tow was manufactured at a time. The fiber volume fraction of the last six meters of tow from each spool was measured and recorded. Fiber volume fraction (FVF) was measured by cutting a 1.5 m length of tow from the spool and weighing it on a laboratory scale. A 1.5 m long tow with 58% FVF was calculated to weigh 1.85 g. The average weight of the four measured lengths from each fabrication run had to fall between 1.83 g and 1.87 g or the tow was rejected.

Towpreg was manufactured using either polymer which had not been used previously in the system, i.e. "new" polymer, or polymer which was recovered from the air cleaner's powder collection bin. Six spools of approximately 150 m of towpreg were manufactured using new polymer. One spool of 150 m of towpreg and one spool of 75 m of towpreg were manufactured using recovered polymer.

2.1.2 - Towpreg Ply Preparation

Towpreg was wound on a drum winder in a manner similar to that described by Bucher[41]. In this case, however, 152.4 x 152.4 mm plies were required, rather than 76.2 x 76.2 mm plies, so strips were wound approximately 160 mm wide. One hundred twenty plies of first use polymer towpreg were required to make five 3 mm thick panels. The drum winder had a diameter of 300 mm, so twelve 160 mm wide strips had to be fabricated to provide the necessary plies. After each strip was completed, masking tape was placed on the towpreg at 160 mm intervals. The strips were removed from the drum, masking tape was placed on the other side of the strip, and plies were cut from the strip. These plies were then trimmed to exactly 152.4 mm wide while the length was left at 160 mm. Thirty plies of recovered polymer towpreg were created in a similar fashion from three 160 mm wide strips.

All six panels were unidirectional panels. To distribute the random variability in the towpreg, the ten plies from each of the twelve strips of new polymer towpreg were distributed equally and uniformly among the five panels. Two plies from each strip were placed symmetrically about the centerline of the panel. The same ply stacking sequence was used for all five new polymer panels. The plies selected for the single panel made with recovered polymer were also chosen so that plies from the three strips were interspersed through the thickness of the panel. Plies from each strip were again ordered symmetrically about the centerline of the panel to distribute the variability in the towpreg as well as possible.

2.1.3 - Panel Processing

Panels were processed using a hot press and a standard PEKK consolidation cycle with varying cooling rates. Before each panel was processed the six piece 152.4 x 152.4 mm steel mold was cleaned and treated with Frekote. The two side pieces of the mold that were the same length as the mold bottom plate were put in place. The towpreg plies were stacked in two groups, a top group and a bottom group. The bottom stack of plies was placed into the partially assembled mold, followed by a 40 mm x 152.4 mm piece of Teflon coated Kapton film that was 0.07 mm thick. The top twelve plies were then placed on top of the stack that was already in the mold. At this point the mold top plate was put in place and secured with two c-clamps. The c-clamps were used to compress the towpreg between the top and bottom plates so that the fibers would not shift when the excess towpreg was cut from the ends of the plies. The towpreg plies were cut flush with both ends of the mold using a utility knife. A thermocouple was inserted on the same end of the laminate as the Kapton film, and the last two side pieces of the mold were put in place.

The fully assembled mold was placed in a hot press and the composite was consolidated using a consolidation cycle shown in Figure 2.1. The mold assembly was heated from room temperature to 370°C at a rate of 5° C/min under contact pressure ranging from 50 kPa to 200 kPa. Once the mold reached 370°C, approximately 2 MPa pressure was applied to the mold. The temperature was held at 370°C for 20 minutes and then the panel was cooled to room temperature at the appropriate cooling rate. Panels were cooled at rates of 2°C/min, 4°C/min, 6°C/min, or 8°C/min, as indicated in Figure 2.1. Figure 2.2 is a plot of the actual thermal history seen by the panel cooled at 6°C/min as measured by the mold thermocouple. The actual history is superimposed over the nominal cycle.

Although there was some lag in the system, the overall correspondence of the actual and nominal cycles was excellent. The panel manufactured with recovered polymer towpreg was processed using the consolidation cycle shown in Figure 2.1 with a cooling rate of 4°C/min.

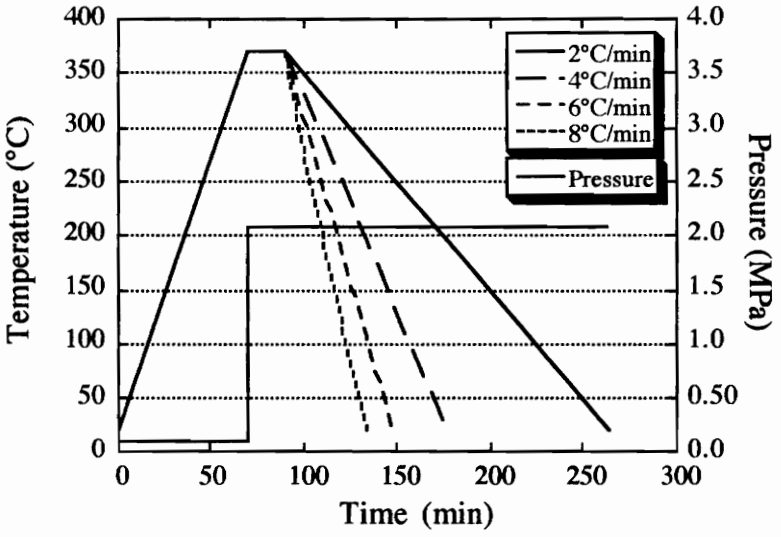

Figure 2.1: G30-500/PEKK Composite Consolidation Cycle

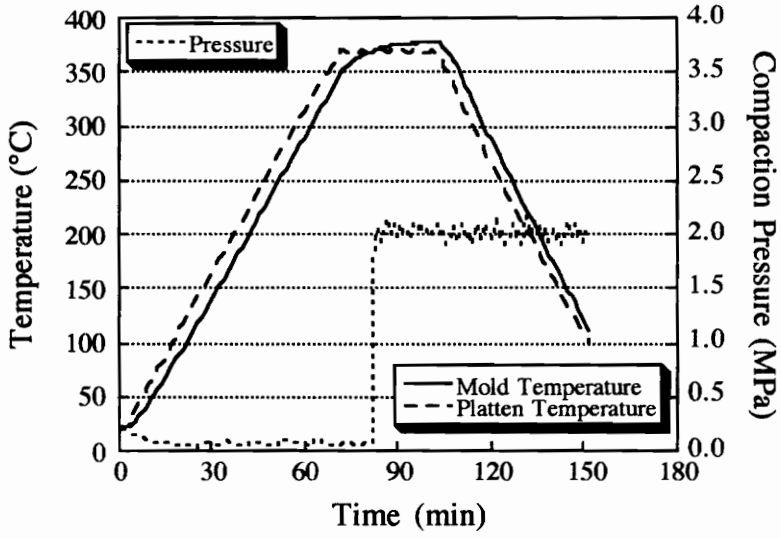

Figure 2.2: Nominal and Actual Thermal Histories for the Panel Cooled at 6°C/min

Two panels were processed using a cooling rate of 8°C/min. After consolidation, the second panel was annealed for two hours in a convection oven that was set at 250°C. The temperature of the panel would not immediately reach 250°C, therefore the temperature profile of the panel needed to be monitored. The glass transition temperature, T_g, of PEKK is 144°C, so a thermocouple could not be attached directly to the panel without damaging the surface. To avoid possible damage, the panel was placed on an aluminum plate and a thermocouple was attached to the plate about 30 mm from the panel. This thermocouple was then used to monitor the temperature of the aluminum plate before and after the annealing process. This is an indirect method of measuring the panel temperature, but does provide and approximate thermal profile.

The thermal conductivity of PEKK was not available in the literature; however, the value for poly(ether ether ketone) (PEEK), a similar polymer in the poly(aryl ether) family, was listed as 0.25 W/m•K. Carbon fibers and aluminum have thermal conductivities ~~of~~ 15 to 20 W/m•K and 237 W/m•K, respectively. These differences in constituent thermal conductivities indicate that the composite panel is unlikely to have experienced the same temperature profile during annealing as the aluminum plate. The differences also indicate, however, that the cooling rate experienced by the plate will give a conservative estimate of the maximum cooling rate that the panel would have experienced after it was removed from the oven. The temperature of the aluminum plate during annealing as measured by the thermocouple is shown in Figure 2.3.

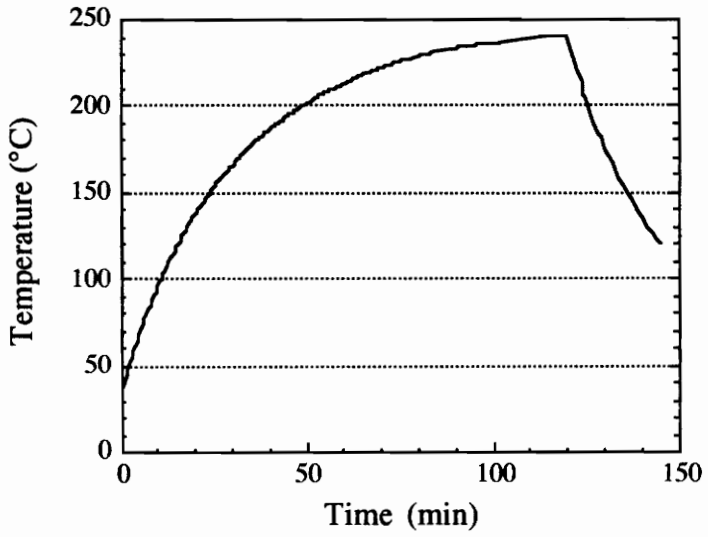

Figure 2.3: Aluminum Support Plate Surface Temperature Profile

The exact cooling rate experienced by the panel is important because it will control the energy state of the amorphous phase. The observed temperature dropped from 240.7°C to 221.5°C during the first three minutes following the anneal. This provides an initial post-annealing cooling rate lower estimate of 6.4°C/min. The temperature profile was monitored using a hand held thermocouple thermometer, however, so there was lag between the last temperature measurement and the time at which the panel was removed from the oven. If one estimates that it took one minute to put on gloves, open the oven door, and remove the panel and then assumes that the panel and plate temperature remained constant during that minute, the resulting upper bound estimate for the cooling rate is 9.6°C/min. The actual initial cooling rate should have fallen between these two bounds. After twenty-five minutes the apparent instantaneous cooling rate had dropped to 2.8°C/min.

2.2 - Nondestructive Panel Evaluation

Prior to being cut into mechanical test specimens, each panel was ultrasonically scanned to identify voids and other macroscopic anomalies. Two outer edges of the panel were inserted into metal brackets before the panel was submerged in the tank. The metal brackets held the panel in place during the scan. Less than 5 mm of each panel edge was obscured by the brackets. A 25 MHz transducer with a 25 mm focal length was used in the scan. The scan rate was set at 2.54 mm/min while the detector gain was set between 25 dB and 30 dB. The Virginia Tech scanner created a hard copy image of the panels, so digital analysis of the quality of the panels was not possible.

2.3 - Preparation of Test Specimens

Test specimens from each panel were used for both double cantilever beam (DCB) tests and end notch flexure (ENF) tests. Specimens were required to be at least 12.5 mm wide. ASTM Standard D5528 recommended that DCB specimens be 20 to 25 mm wide, but round robin testing showed that the width of the specimen was not critical[42]. Data from the round robin tests show that there was no significant difference between G_{Ic} values measured from specimens that were 12.5, 25, and 37.5 mm wide. The amount of material available in this study was limited, so specimens were made 12.7 mm wide to maximize the number of specimens available for testing.

2.3.1 - Cutting Mechanical Test Specimens

Panels were cut into 12.7 mm wide specimens. A strip approximately 5 mm wide was trimmed from one longitudinal edge of each panel to reduce edge effects. A 10 mm wide strip was then trimmed from the transverse edge of the panel which contained the Kapton film. This removed the resin rich cap that formed over this edge of the panel during processing. Each panel was then cut into ten, 12.7 mm wide specimens. After the specimens had been cut from the panel, the edges were ground to smooth the surface.

2.3.2 - Tabbing Specimens for Double Cantilever Beam Testing

DCB tests required that hinges or loading blocks be attached to the upper and lower edge of the cracked end of the specimen. The hinges or blocks provided a means to apply load to the specimen in a crack opening mode. The t-shaped loading blocks used in this work were aluminum with nominal dimensions as shown in Figure 2.4.

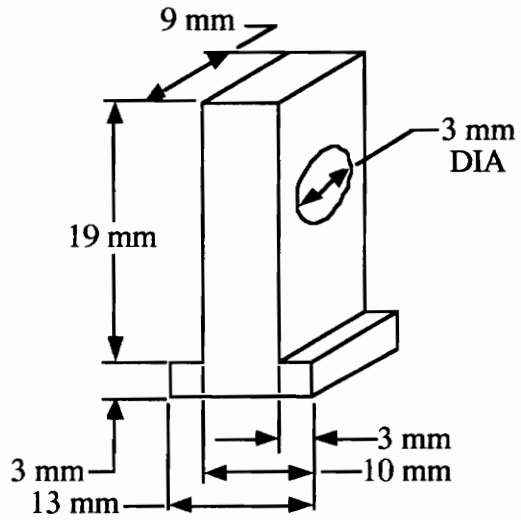

Figure 2.4: Diagram of the T-Tabs Used in Double Cantilever Beam Testing

The surface of the tab that was to be attached to the specimen was sanded lightly with 250 grit emery cloth and then washed with acetone. The same cleaning procedure was completed on both faces of the cracked end of each specimen. The adhesive used to attach the tabs to the specimens was a room temperature curing, strain gage adhesive, M-Bond 200 from M-Line Accessories. This adhesive is a modified alkyl cyanoacrylate compound.

For strain gage uses, a conditioner, neutralizer, catalyst, and adhesive are used in series to create a very strong bond between the specimen and the gage. In this application, the t-tabs were to be used on more than one specimen. This required that the bond between the tab and the specimen be strong enough to transfer the load during testing, but weak enough that the tabs could be removed after testing. For this reason only the catalyst and adhesive were used to bond the tab to the specimen. In some cases the t-tabs debonded before the crack opened along the Kapton tape. When this occurred, the failed adhesive was sanded from both the tab surface and the specimen surface with 250 grit emery cloth. The surfaces were then wiped with acetone and the tab was rebonded to the specimen.

2.4 - Double Cantilever Beam Testing

Double cantilever beam (DCB) tests were completed as specified in ASTM D5528. After all required specimen measurements were obtained, both edges of the specimens were coated with a white paint marker. A line, at each delamination length specified in ASTM D5528, was scratched into the paint marker coating with the sharp point of a caliper.

The specimen was placed into the grips of an Instron test machine via loading pins through the t-tabs. The opposite end of the specimen was supported as specified in ASTM D5528. Load was applied using a controlled displacement mode at a constant displacement rate of 0.5 mm/min. The load was measured using a 1 kN or 5 kN load cell. LabVIEW was used to acquire data and monitor the load-displacement curve during testing. The specimens were precracked to initiate the crack along the Kapton tape before testing. During precracking the specimen was loaded at a displacement rate of 0.5 mm/min until one surface separated from the Kapton. The load was increased until the delamination length reached about 5 mm less than the length of the Kapton insert. The specimen was then unloaded at a rate of 2 mm/min.

After precracking, the specimen was immediately reloaded at a rate of 0.5 mm/min. The growth of the delamination front position was observed with a 10x lighted magnifying glass. The load and displacement when the delamination front reached each of the specified delamination lengths was marked in the data file. After the delamination had propagated more than 25 mm beyond the end of the Kapton insert, the specimen was unloaded at a rate of 2 mm/min.

2.5 - End Notch Flexure Testing

End notch flexure (ENF) tests do not yet have an official ASTM specification. The test procedure followed was obtained from Rau[43]. ENF testing measured the changes in compliance as a function of increasing crack length and characterized the load as a function of displacement during loading up to crack propagation in a shear mode. The compliance of each specimen was measured prior to double cantilever beam (DCB) testing to determine the compliance of the uncracked specimen. After DCB testing, the compliance was measured at crack lengths of 20 mm, 25 mm, 30 mm, 35 mm, and 40 mm. All compliance measurements were completed in the flexural mode following specimen dimension requirements and loading specifications dictated in ASTM D790. DCB testing was used to precrack the specimen so that the mode II strain energy release rates will be valid for a natural crack.

All compliance measurements were completed using a three point flexure loading fixture with a span of 100 mm. Load was applied through a controlled displacement mode at a constant displacement rate of 0.5 mm/min. A 1 kN load cell was used to measure the load. Load and displacement data were monitored and recorded using the LabVIEW data acquisition program. Data was recorded every 0.75 seconds in the compliance tests and every 1.25 seconds in the crack propagation tests. For the uncracked (zero crack length) compliance measurement, the specimen was placed in the fixture so that the Kapton insert lay outside the 100 mm test span. The specimen was loaded to 200N and then unloaded instantaneously.

Following zero-crack length compliance testing and DCB testing, the resultant termination point of the propagated crack was identified. A 10x lighted magnifying glass was used to help locate the end of the crack. Lines were drawn on the previously unmarked side of the specimen at distances of 20 mm, 25 mm, 30 mm, 35 mm, and 40 mm from the end of the crack. The specimen was placed on the three point flexure loading support so that the crack length mark of interest laid over the centerline of one support. The specimen was then loaded to 200 N at a displacement rate of 0.5 mm/min as described earlier. After each measurement was completed, the specimen was shifted to the next specified crack length and the test was repeated. This process was repeated until the compliance was measured at all five crack lengths.

After all five compliances had been measured, the crack propagation test was completed. It is important to note that the crack extension was from an arrested initial crack, not from the root of the starter crack. The specimen was placed in the fixture with a

crack length-to-half span ratio of 0.5 (i.e. a crack length of 25 mm). The specimen was then loaded at a rate of 0.5 mm/min until the load dropped with increasing displacement. The specimen was again unloaded instantaneously.

It should be mentioned that not all specimens were tested in both DCB and ENF experiments. There were several specimens in which the crack did not propagate along the centerline during DCB testing. These specimens were not included in ENF testing. There were also specimens, however, which exhibited anomalous loading curves during DCB testing. These specimens were included in the ENF specimen pool.

2.6 - Measurement of Composite Fiber Volume Fraction

Two methods were used to calculate the global fiber volume fraction in each panel. The first computation is based on the areal weight of a ply, while the second is based on the composite density. Equation 2.1 is used to calculate the areal weight, ξ, of a ply of dry fibers.

$$\xi = \frac{l \times \frac{W}{l} \times n_t}{A} \tag{2.1}$$

In this equation l represents the length of a tow, $\frac{W}{l}$ represents the weight per unit length of a tow, n_t represents the number of tow in a ply, and A represents the area of the ply. Equation 2.2 is the equation used to calculate the fiber volume fraction from the areal weight, V_f^{ξ}.

$$V_f^{\xi} = \frac{\xi \times n_p}{t_c \times \rho_f} \tag{2.2}$$

In this equation, n_p represents the number of plies in the panel, t_c represents the final thickness of the composite, and ρ_f represents the density of the fiber. The density of the composite, ρ_c, is calculated using Equation 2.3.

$$\rho_c = \frac{m_c}{A \times t_c} \tag{2.3}$$

In this equation m_c is the mass of the composite. The equation used to calculate the fiber volume fraction based on the density of the composite, V_f^{ρ}, is shown as Equation 2.4.

$$V_f^{\rho} = \frac{\rho_c - \rho_m}{\rho_f - \rho_m} \tag{2.4}$$

In this equation, ρ_m is the density of the polymer.

2.7 - Measurement of Composite Crystallinity

The degree of crystallinity was measured for five specimens from each panel using a differential scanning calorimeter (DSC). Two specimens were taken from the outside edges of the panels. Three additional specimens were taken from just beyond the propagated crack in DCB/ENF specimens that had originally been located in the middle of panel. The mass of polymer in the sample was calculated assuming that each specimen contained exactly 60% fiber volume fraction. Scans were completed at a rate of 10°C/min from 100°C to 400°C. The heat of fusion (ΔH_f) as a result of crystallinity in the sample was computed from the area under the DSC endothermic melting peak minus any area under an exothermic cold crystallization peak. The sample ΔH_f was computed by dividing the calculated heat flow by the calculated mass of polymer in the sample. Crystallinity of the samples was computed as the ratio of the sample ΔH_f to the ΔH_f of purely crystalline PEKK.

Chapter 3 - Mode I Strain Energy Release Rate

Double cantilever beam (DCB) tests provide mode I interlaminar strain energy release rate, G_{Ic}, values. G_{Ic} values are generally used to determine failure criteria for damage tolerance and durability analyses. Currently there are no published G_{Ic} values for carbon fiber/poly(ether ketone ketone) (PEKK) composites. Published values for a similar material, carbon/poly(ether ether ketone) (PEEK) range approximately from 1400 J/m^2 to 3200 J/m^2 [1]. PEEK and PEKK are both members of the poly (aryl ether) family of polymers. In addition to having very similar chemical structures, they have been shown to have similar values for mechanical properties. Comparing PEKK composite G_{Ic} to reported G_{Ic} values for PEEK composites can indicate whether the measured PEKK values fall within a reasonable range.

3.1 - Specimen Testing Anomalies

Specimens are expected to exhibit certain behaviors during DCB tests. Furthermore, the loading curves generated during testing are expected to show certain characteristics. Unfortunately, these expectations were violated at times by different specimens during actual testing.

A crack is initiated at the centerline of the DCB specimens. This crack is expected to propagate along the centerline of the specimen. In two cases, specimen 5 from the panel that was cooled at 6°C/min (designated 6-5) and specimen 6 from the panel that was cooled at 8°C/min and then annealed (designated 8A-6), the crack did not propagate along the centerline of the specimen. This is considered to be a major deviation from acceptable behavior, since the crack must propagate along the centerline to undergo pure mode I fracture. Crack propagation between arms of differing thicknesses results in mixed mode fracture which is not of interest to us at this time. The data from both of these specimens is, therefore, excluded from both the DCB data analysis and subsequent ENF testing.

In addition to expecting the crack to propagate along the centerline of the specimen, the two halves of the specimen are expected to split cleanly, i.e. no fibers from one arm should remain attached to the other arm. When fibers remain attached to both arms of the specimen, this is called fiber bridging. Fiber bridging occurred in all sixty of the specimens, but the extent of bridging varied from specimen to specimen. Some specimens

exhibited relatively minor fiber bridging, while others exhibited significant fiber bridging. We believe that the fiber bridging in these specimens was a result of using towpreg, rather than more sheet-like prepreg, to manufacture the panels. The towpreg sheets fabricated on a drum winder maintained their integrity to some extent, but when they were stacked into a panel, tows from adjacent plies could mingle together. This intermingling of fibers from adjacent plies resulted in panels with no distinct ply boundaries. The intermingling of plies is demonstrated microscopically in Figure 3.1. This figure shows the equivalent of more than six plies even though the boundaries between individual plies are not discernible.

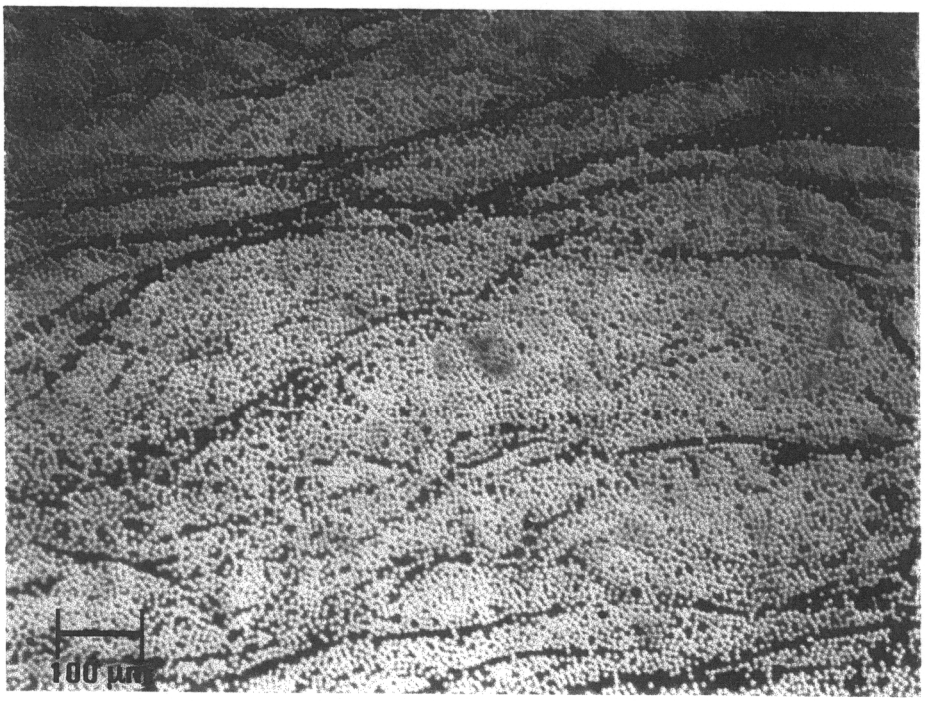

Figure 3.1: Optical Micrograph of Six Plies of a Sixteen Ply G30-500/PEKK Laminate

ASTM Standard D5528 states that fiber bridging in unidirectional materials is an artifact of the testing method. In this case, however, fiber bridging is likely to be a characteristic of the material. While fiber bridging may not have a significant effect on the G_{Ic} initiation values, the propagation values reported in this study are likely to be much higher than corresponding values for composites made from prepregs. Fortunately, the initiation values are the values used to determine failure criterion. G_{Ic} propagation values are plotted and reported, but not generally used to predict allowable failure limits for a material.

A characteristic DCB load versus displacement curve increases linearly before the crack propagates. The load should then decrease with increasing displacement as the crack begins, and then continues, to grow. In some of the specimens used in this study the Kapton insert did not debond cleanly from the composite. One primary requirement in DCB testing was that a nonadhesive insert be used to initiate the crack. In most cases the Kapton debonded readily from one of the arms of the specimen, but there were a few cases where the Kapton essentially acted as a film bridge between the two arms during the early part of the testing. In these cases the load-displacement curves did not show a single, clearly defined, linear slope, but changed slope when the Kapton finally debonded from one of the arms. This left no definitive slope to use to determine G_{Ic} initiation values. The data from these cases (specimens 7 and 9 from the panel cooled at 2°C/min (designated 2-7 and 2-9), specimens 5 and 10 from the panel cooled at 4°C/min (designated 4-5 and 4-10), specimen 5 from the panel cooled at 8°C/min (designated 8-5), and specimens 8A-6 and 8A-7) were eliminated from the DCB analysis. These specimens were included in the ENF specimen pool, however, since the Kapton had debonded completely from one arm of the specimen by the end of the DCB test. The loading curves for each specimen included in the data analysis are provided in Appendix A. This appendix also includes the fiber volume fraction of each panel, the dimensions of each specimen, the modified beam theory method intercept for each specimen, and the delamination resistance curves.

3.2 - G_{Ic} Initiation Values

Values for mode I strain energy release rate were calculated using the modified beam theory method. This method was recommended for data reduction in ASTM standard D5528 since it has been shown to provide more conservative values than the compliance calibration and modified compliance calibration methods. Initiation values were computed at two critical points: the point at which the load-displacement curve deviated from linearity (denoted as onset of non-linearity, or NL) and at the intersection of the loading curve with a line drawn at 95% of the original compliance (denoted as 5% compliance offset, or 5%). In some specimens the point of local maximum load occurred before the intersection of the load-displacement curve and the line of 95% compliance. In these instances, the load and displacement values that correspond to the local maximum load were substituted for the values that correspond to the intersection at 5% compliance offset. These initiation values

are, therefore, denoted 5% offset/max load or 5%/Max. The three critical points in a DCB load-displacement curve are illustrated in Figure 3.2.

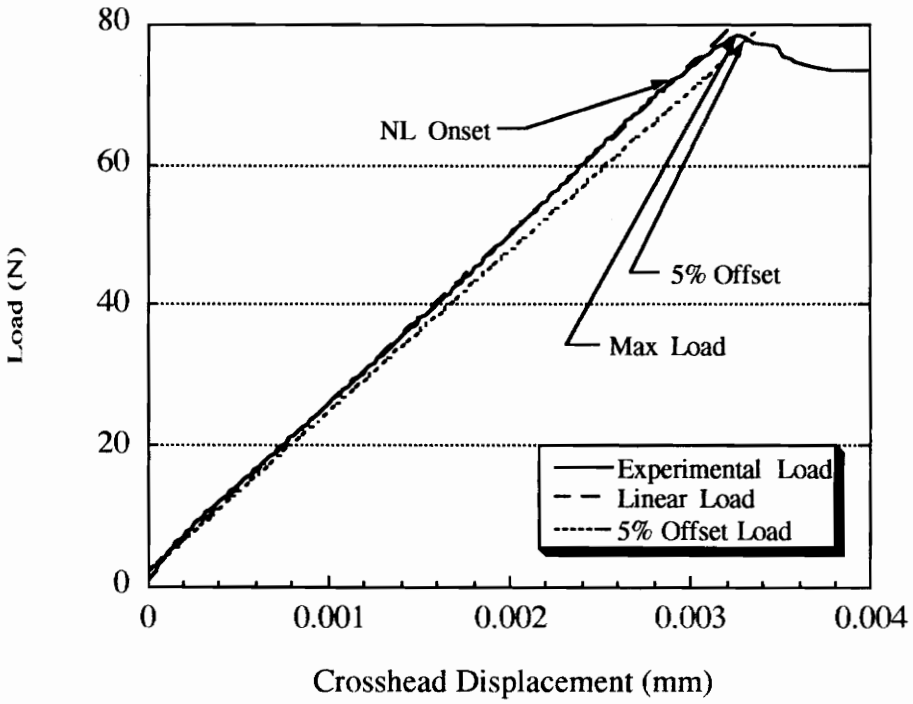

Figure 3.2: Representative Load-Displacement Curve from a DCB Test

In the load-displacement curve shown in Figure 3.2, the point of local maximum load occurs before the intersection of the 5% compliance offset with the load-displacement curve. As a result the load and displacement used to calculate the 5%/Max G_{Ic} value would correspond to the point of local maximum load. Table 3.1 indicates whether values corresponding to the point of 5% offset compliance intersection or to the point of maximum load were used to compute the 5%/Max initiation value for each specimen in the DCB analysis.

ASTM D5528 also suggested that an initiation value be computed based on the point at which the crack was first visually observed to grow. This value was not computed, however, because the point at which the crack first grew on a macroscopic scale was often difficult to determine during testing. It was felt that the resultant error in the calculations would be too great for the data to provide useful information.

Table 3.1: Load and Displacement Used To Compute G_{Ic} 5%/Max Initiation Values

Panel	Specimens Which Used Intersection of 5% Compliance Offset	Specimens Which Used Point of Maximum Load
2		1,2,3,4,6,10
4	1,4,6,7,8	2,3,9
6	1,3,4,5,6,7,8	2,9,10
8	2,9	1,3,4,5,6,7,8,10

The average G_{Ic} values computed using the load and displacement that correspond to the onset of nonlinearity provide a lower limit for G_{Ic} initiation values. 5%/Max values have been found to be approximately 20% higher than the corresponding NL values[42]. ASTM D5528 recommended that NL values be used to determine failure criteria for durability and damage tolerance. The 5%/Max values were suggested as an additional means of quantitatively comparing the toughness of different materials, e.g., to compare the toughness of materials cooled at different rates.

A minimum of five specimens should generally be used to compute meaningful mean G_{Ic} values. It is known that propagation values from specimens which exhibit fiber bridging will be higher than propagation values from specimens which do not exhibit fiber bridging. It would be useful to verify that the initiation values are not also affected by fiber bridging. Consequently, the five specimens from each panel which exhibited the least fiber bridging during testing were grouped as "primary" specimens, while those with the most fiber bridging were grouped as "secondary" specimens. The mean values from these two groups would then be compared to determine whether there is a significant difference between the values for the two groups. Specimens in which the crack did not propagate down the middle of the specimen or which had anomalous loading curves were not included in either group. Table 3.2 lists the specimens included in the primary and secondary groups for each panel. There were only six specimens from the panel cooled at 2°C/min which did not have anomalous loading curves; therefore, this panel does not have a secondary group.

Table 3.2: Specimens Included in the Primary and Secondary Groups for Each Panel

Panel	Specimen Distribution	
	Primary	Secondary
2	1,2,4,6,10	
4	1,6,7,8,9	2,3,4
6	2,3,4,10	6,7,8,9
8	2,3,7,8,9	1,4,6,10

Only four specimens were included in the primary group for the panel cooled at 6°C/min. Specimens 6-6, 6-7, 6-8, and 6-9 exhibited very similar magnitudes of fiber bridging, so it was unjustifiable to select of one of these specimens over the others to include in the primary group. Similarly the loading curves for specimens 6-1 and 6-5 exhibited sufficient anomalous behavior that neither was included in either the primary or secondary group. For these reasons, only four specimens were included in the primary group for the panel cooled at 6°C/min.

3.2.1 - G_{Ic} Initiation Values for Primary Group Specimens

The calculated G_{Ic} NL and 5%/Max initiation values for each specimen in the primary groups and the resultant panel means, standard deviations, and coefficients of variations are reported in Tables 3.3 and 3.4. The mean values are plotted as a function of cooling rate in Figure 3.3. The error bars in this figure represent one standard deviation from the mean.

Table 3.3: G_{Ic} NL Initiation Values for Panel Primary Specimens

Panel	G_{Ic} Initiation Values - NL (J/m^2)					NL Mean	Standard Deviation	Coefficient of Variation
2	375	368	432	404	341	384	34.9	0.091
4	628	584	494	517	720	588	90.7	0.154
6	673	625	503	680		620	82.2	0.132
8	847	796	691	645	519	700	129	0.185

Table 3.4: G_{Ic} 5%/Max Initiation Values for Panel Primary Specimens

Panel	G_{Ic} Initiation Values - 5%/Max (J/m^2)					5% Mean	Standard Deviation	Coefficient of Variation
2	434	400	439	428	424	425	14.8	0.035
4	668	809	639	759	855	746	91.6	0.123
6	778	677	717	846		754	73.8	0.098
8	975	1039	852	889	829	917	88.2	0.096

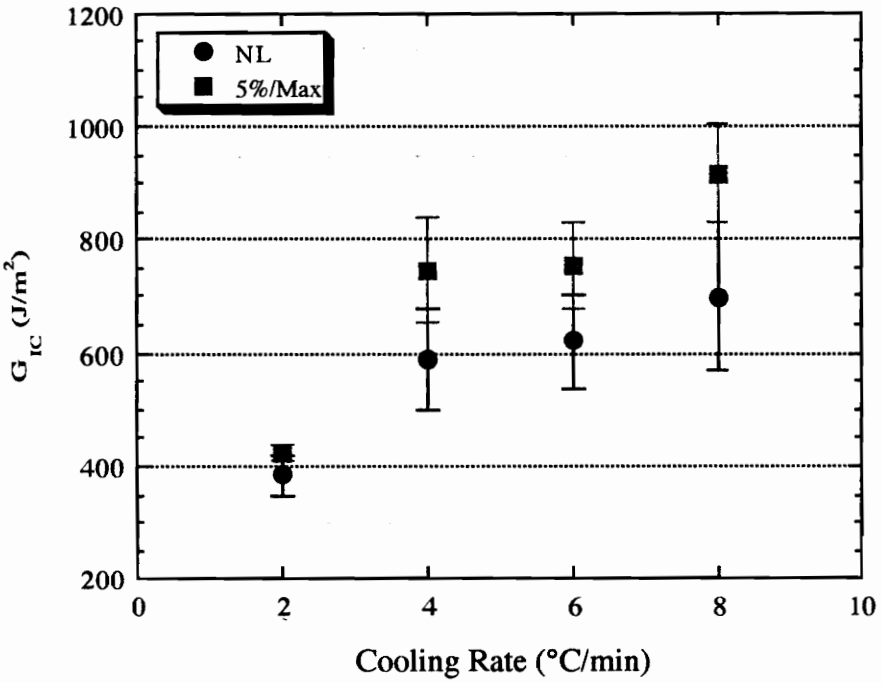

Figure 3.3: Primary Panel Mean G_{Ic} Initiation Values as a Function of Cooling Rate

Statistical analysis of the mean G_{Ic} values using a Duncan Multiple Range test[44]* showed that the G_{Ic} values for the panels cooled at 4°C/min, 6°C/min, and 8°C/min, are statistically equivalent. This means that there is not enough evidence to conclusively state that the toughness of a composite cooled at 8°C/min will consistently be greater than the toughness of a composite cooled at 6°C/min and so on. The statistical equivalence of the

* See Appendix C for a brief overview of the statistical tests used in this work.

experimental mean NL toughness values are illustrated in Figure 3.4. The panels are specified by cooling rate and are listed in order of increasing mean G_{Ic} values from left to right. A line underneath several panel designations indicates that the G_{Ic} values of the panels above the line are statistically equivalent.

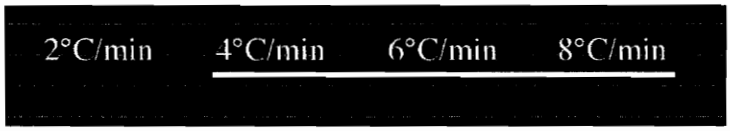

Figure 3.4: Grouping of Statistically Equivalent Primary NL G_{Ic} Initiation Values

Statistical analysis of the 5%/Max data using a Duncan Multiple Range test showed that the G_{Ic} initiation values for the panels cooled at 4°C/min and 6°C/min were the only statistically equivalent values. The mean 5%/Max G_{Ic} initiation values for the panel cooled at 2°C/min and 8°C/min could be identified as a statistically distinct values. The results of the statistical analysis are represented graphically in Figure 3.5.

Figure 3.5: Grouping of Statistically Equivalent Primary 5%/Max G_{Ic} Initiation Values

The results from the statistical analysis are not surprising considering the overlap of the data error bars seen in Figure 3.3. The plot shows no overlap between the error bars for the 2°C/min initiation values and the corresponding values for the other panels. The variances in the other three panels' NL values, however, are large enough that the range of values that each interval spans includes the values for the other panels. In contrast, the overlap between the lower standard deviation from the mean for the 8°C/min 5%/Max values and the upper standard deviation from the mean for the 4°C/min and 6°C/min 5%/Max values is relatively small. Consequently, it is not surprising that in this case the 5%/Max G_{Ic} value from the panel cooled at 8°C/min was found to be statistically distinct.

Comparison of the G_{Ic} values obtained from the NL computation to those obtained from the 5%/Max computation shows that the NL values are approximately 10%, 21%, 18%, and 24% lower than the corresponding 5%/Max values for the panels cooled at 2°C/min, 4°C/min, 6°C/min, and 8°C/min, respectively. The differences between the 4°C/min, 6°C/min, and 8°C/min panel data correspond well to the results from round robin testing of AS4/PEEK composites[42]. Testing in that study showed that NL values are generally about 20% lower than 5%/Max values. The 10% difference between the 2°C/min panel's NL and 5%/Max values was surprising since it is only half of the expected difference. The reason that this value was relatively unchanged for this panel is not clear.

3.2.2 - G_{Ic} Initiation Values for Secondary Group Specimens

The calculated NL and 5%/Max G_{Ic} initiation values for each specimen in each panels' secondary group and the resultant panel means, standard deviations, and coefficients of variation are reported in Tables 3.5 and 3.6. As mentioned earlier, there were only six viable specimens from the panel cooled at 2°C/min. A single specimen cannot be used as a group in statistical analysis; therefore, the panel cooled at 2°C/min does not have a secondary group.

Table 3.5: G_{Ic} NL Initiation Values for Panel Secondary Specimens

Panel	G_{Ic} Initiation Values - NL (J/m^2)				NL Mean	Standard Deviation	Coefficient of Variation
4	687	654	601		647	43.6	0.067
6	762	715	798	722	749	38.2	0.051
8	1087	551	954	571	790	271	0.343

Table 3.6: G_{Ic} 5%/Max Initiation Values for Panel Secondary Specimens

Panel	G_{Ic} Initiation Values - 5%/Max (J/m^2)				5% Mean	Standard Deviation	Coefficient of Variation
4	741	677	718		712	32.2	0.045
6	958	977	878	820	908	72.8	0.080
8	1120	1180	1020	1080	1100	66.5	0.061

The main issue surrounding or the secondary specimens is whether mean values from these specimens differ substantially from the mean values from the primary specimens. If the means do not differ, then this provides evidence that fiber bridging has little or no effect on initiation values. This finding would confirm that meaningful mean G_{Ic} initiation values can be computed using all the data from valid tests. This would be beneficial, since larger sample sizes generally reduce the impact of scatter in the data. DCB tests have historically been shown to have a significant amount of scatter in the data, so larger sample sizes generally produce more statistically significant results. The original division of available data into two groups, however, can indicate whether fiber bridging observed later in the test affects initial crack growth from the insert.

3.2.3 - Comparison of Primary and Secondary G_{Ic} Initiation Values

The mean G_{Ic} initiation values for primary and secondary groups were compared using either a pooled-variance t-test procedure or separate-variance t-test procedure depending upon the relative sample sizes and relative variances of the groups[44]. T-tests are similar to a Duncan Multiple Range test, except that only one pair of means are compared at a time. In this statistical analysis, fiber bridging was assumed to result in increased G_{Ic} initiation values; therefore, a 5% single-tailed rejection region was used in the analysis. The NL and 5%/Max values were both found to be equivalent for the panel cooled 4°C/min. The NL values were found to be equivalent for the panel cooled at 8°C/min, while the 5%/Max values were found to be statistically distinct. The NL and 5%/Max values were both found to be statistically distinct for the panel cooled at 6°C/min. These results are illustrated in Table 3.7. An "X" indicates that the G_{Ic} initiation values for panels with significant fiber bridging were found to be statistically larger than the values for panels with minor fiber bridging. The cell is empty if this was not found to be true.

Table 3.7: Results from T-Test Comparison of Primary and Secondary Specimen Means

Panel	Comparison of NL G_{Ic}	Comparison of 5%/Max G_{Ic}
4		
6	X	X
8		X

The results of this analysis are obviously not definitive. Half of the pairs were shown to be statistically equivalent while half were found to be statistically distinct. To further complicate the issue, in one case (the 4°C/min 5%/Max) the difference between the primary and secondary G_{Ic} means show that the primary specimens, not the secondary specimens, have higher average interlaminar fracture toughness. The inconclusive results of these comparisons suggest that only data from specimens with minor fiber bridging should be used to compute conservative "typical" G_{Ic} values for these composites. The resultant mean values for mode I interlaminar fracture toughness are shown with 5% confidence intervals in Table 3.8.

Table 3.8: Mode I Strain Energy Release Rates

Panel	2	4	6	8
NL Initiation G_{Ic} (J/m^2)	384 ± 43	588 ± 113	620 ± 131	700 ± 160
5%/Max Initiation G_{Ic} (J/m^2)	425 ± 18	746 ± 114	754 ± 117	917 ± 110

The mean G_{Ic} NL values for these carbon/PEKK composites range from 30% to 50% of the lower limit reported for carbon/PEEK composites. Although the magnitude of the decrease in toughness is larger than was anticipated, it is not surprising that carbon/PEKK composites have a lower toughness than carbon/PEEK composites. The mode I strain energy release rate for neat PEKK has been shown to be about half that of neat PEEK[31], but the composites in this study are only 40% polymer. Other factors which can affect the relative toughness of two materials include differences in crystallinity, differences in fiber-matrix adhesion, and differences in chain packing. Nevertheless, the values reported in Table 3.8 are believed to be reasonable values for the mode I strain energy release rate of carbon/PEKK composites.

3.3 - Examination of Additional Processing Variables

The four panels discussed in Section 3.2 all were made with polymer that had not previously been used in the towpreg fabrication system. These panels were also manufactured using a controlled cooling rate to cool the panel from the melt to room temperature. Two supplementary panels, however, were also manufactured: a panel that was annealed after being processed using the same cycle as the principal panel cooled at 8°C/min and a panel that was made with polymer that was recovered from the air cleaner. The manufacture of these two panels was discussed in Chapter 2.

In manufacturing, higher product throughput generally results in greater productivity and profitability. There is also often a considerable amount of time at some point in the manufacturing process during which parts are stored or simply sit in the plant before the next manufacturing step. Both of these factors could be taken advantage of through cooling a part quickly and then annealing it at a later time if this is shown to be beneficial. It was this premise that prompted manufacture and testing of an annealed panel.

Rather than simply throw away the polymer that accumulated in the dry powder prepregging facility's air cleaner during towpreg production, one would prefer to be able to reuse this polymer. Unfortunately, it is difficult to predict what effect fluidizing the polymer and subsequently drawing it through the air cleaner before using it in a composite might have on the polymer and composite properties. It was these two concerns that warranted manufacture of a panel using recovered polymer.

Double cantilever beam tests were carried out using specimens from the two additional panels. The load-displacement curves from DCB tests for each specimen are included in Appendix A along with the curves from the four principal panels. The annealed panel specimens are designated as 8A-X, while the specimens from the panel made with recovered polymer are designated as 4R-X. The panel fiber volume fractions are also provided in Appendix A. Similarly, each specimen's dimensions, initial crack length, and modified beam theory intercept value are cataloged in Appendix A.

As before, one of two pairs of load and displacement values could in the calculation of the 5%/Max initiation values: the load and displacement corresponding to the intersection of the load-displacement curve with a line drawn at 95% of the original compliance, or the

load and displacement corresponding to the point of maximum load. Table 3.9 lists whether the load and displacement used to calculate the 5%/Max initiation value corresponds to the 5% compliance intersection or the maximum load for each specimen in the supplementary panels.

Table 3.9: Load and Displacement Used To Compute G_{Ic} 5%/Max Initiation Values

Panel	Specimens Which Used Intersection of 5% Compliance Offset	Specimens Which Used Point of Maximum Load
8A	5	1,2,3,4,7,8,9,10
4R	2,3,8,9	1,4,5,6,7,10

The specimens from these two panels were also divided into primary and secondary groups based on the degree of fiber bridging observed during DCB testing. Table 3.10 indicates which specimens were included in the primary group and which were included in the secondary group for each of these two panels.

Table 3.10: Specimens Included in the Primary and Secondary Groups for the Supplementary Panels

Panel	Specimen Distribution	
	Primary	Secondary
8A	3,4,8,9,10	1,2,5
4R	2,3,6,7,10	1,4,5,8,9

3.3.1 - G_{Ic} Initiation Values for an Annealed Panel

A panel was processed using an 8°/min cooling rate and later annealed as described in Section 2.1.3. This panel was manufactured to investigate the effect of cooling a panel quickly and then annealing it on the material's toughness properties. This addition to the study was intended to indicate whether product throughput could be increased in a manufacturing situation without sacrificing a desired property by increasing the cooling rate used in the initial manufacturing process and then reheating the panel at a later time. The NL and 5%/Max G_{Ic} initiation values for each specimen in the primary and secondary groups are provided in Table 3.11. The mean, standard deviation, and coefficient of variation are also included in this table for the primary and secondary groups and for the combined group.

Table 3.11: G_{Ic} Initiation Values for the Annealed Panel

Value	Group	G_{Ic} Initiation Values (J/m^2)					Mean	Standard Deviation	Coefficient of Variation
NL	Primary	440	639	425	512	479	499	85.2	0.171
	Secondary	354	379	426			386	36.3	0.094
	All						457	89.0	0.195
5%/Max	Primary	970	696	780	969	710	825	136	0.165
	Secondary	879	713	721			771	93.3	0.121
	All						805	118	0.146

As mentioned in the overview, changing the processing conditions can change not only the configuration of the crystalline phase, but also the configuration of the amorphous phase. This means that the toughness of the annealed panel should only be compared to the toughness of the principal panel that was cooled at 8°C/min. The G_{Ic} values from these two panels are compared in Figure 3.6.

Statistical comparison of the values was completed using pooled-variance and separate-variance t-tests. In comparing these two panels, one would expect that the annealed panel had a higher level of crystallinity, and therefore a lower toughness, than the principal panel. As a result, a single-tailed, 5% rejection region is used to determine whether two values are equivalent or distinct. The result of the six comparisons are shown

in table form in Table 3.12. An X indicates that the mean G_{Ic} initiation value for the principal panel was shown to be statistically greater than the mean G_{Ic} initiation value from the annealed panel.

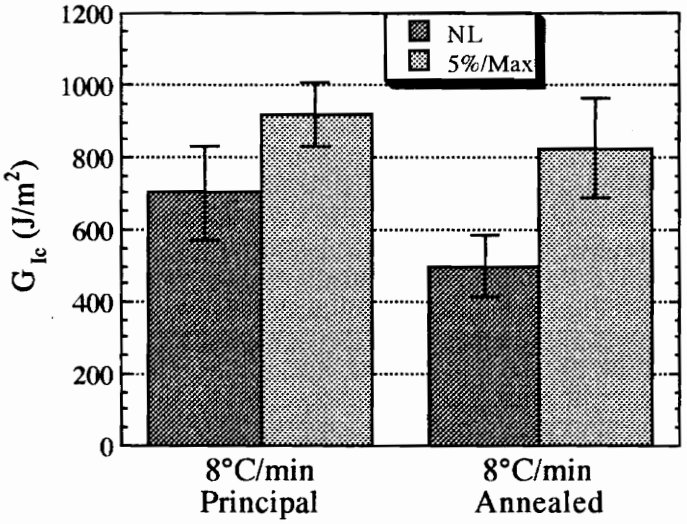

Figure 3.6: Comparison of the G_{Ic} Initiation Values for the Annealed Panel and the Principal Panel.

Table 3.12: Results from T-Test Comparison of Annealed Panel and Principal Panel Specimen Means

Group	Comparison of NL G_{Ic}	Comparison of 5%/Max G_{Ic}
Primary	X	
Secondary	X	X
All	X	X

As Table 3.12 illustrates, five of the six comparisons determined that the annealed panel has statistically lower toughness than the principal panel. The results shown in Table 3.12 are not surprising since the variance in the G_{Ic} 5%/Max values for the annealed panel primary specimens is very large. Large variance in a data set makes it difficult to identify statistically significant differences. Consequently, the results illustrated in Table 3.12 indicate that annealing a composite will decrease its mode I critical strain energy release rate.

3.3.2 - G_{Ic} Initiation Values for a Panel Made With Recovered Polymer

The polymer powder used to manufacture the towpreg used in this study had a median diameter of 27 μm. This small particle size resulted in large volumes of polymer being drawn into the air cleaner. Consequently, there was a significant amount of "waste" polymer collected in the air cleaner during manufacture of towpreg. The powder prepregging line was not operated in a clean room environment. As a result, the air drawn from the room by the system may have contained a significant number of dust particles and other contaminants which could have been combined with the polymer in the fluidization system. Although there were no visible contaminants in the powder reclaimed from the air cleaner, it is likely that some foreign matter accumulated in the polymer during it first pass through the fluidization system. The addition of contaminants is a concern because any foreign matter in the polymer can act as a heterogeneous nucleation site and influence the microstructure of the composite. The polymer was not tested to determine whether impurities existed in the reclaimed polymer, but instead was used to make one composite panel. A panel was manufactured and mechanically tested because the effect of foreign matter, rather than its presence, was the issue of concern.

NL and 5%/Max G_{Ic} initiation values for each specimen from this panel are listed in Table 3.13. As before, the mean, standard deviation, and coefficient of variance for the primary, secondary, and combined groups are included in this table.

Table 3.13: G_{Ic} Initiation Values for the Panel Made with Recovered Polymer

Value	Group	G_{Ic} Initiation Values (J/m^2)					Mean	Standard Deviation	Coefficient of Variation
NL	Primary	279	416	686	404	653	488	175	0.359
	Secondary	811	708	357	826	655	671	190	0.282
	All						580	197	0.341
5%/Max	Primary	613	547	828	752	888	725	144	0.198
	Secondary	973	821	788	994	891	893	90	0.101
	All						809	144	0.177

The G_{Ic} values from the panel made with recovered polymer were compared to the values from the principal panel that was cooled at 4°C/min to indicate whether there are significant differences between the toughness of the two panels. The mean G_{Ic} values from these two panels are plotted in Figure 3.7.

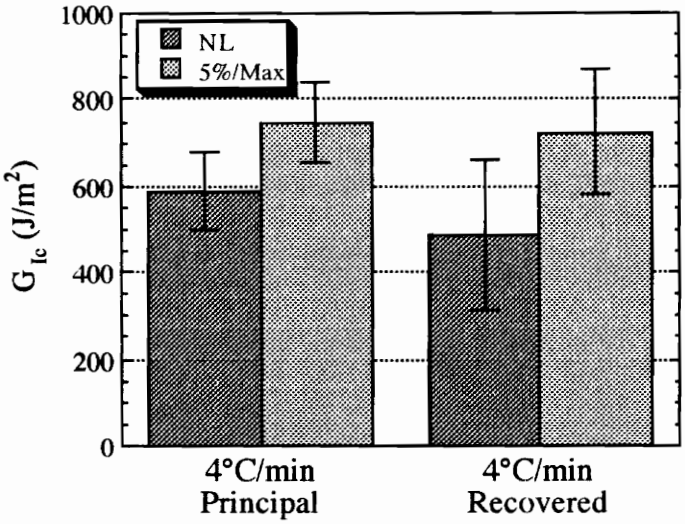

Figure 3.7: Comparison of G_{Ic} Initiation Values for the Panel Made with Recovered Polymer and the Principal Panel.

Statistical comparisons were completed using the pooled-variance t-tests and the separate-variance t-tests that were discussed in Section 3.2.3. In this analysis, however, there was no reason to assume that one panel will have a consistently higher toughness than the other panel. For this reason a two-tailed, 5% rejection region was used in the analysis. The six comparisons showed that only one pair, the 5%/Max secondary specimen values, was statistically distinct. The other five comparisons found no significant difference between the G_{Ic} values. These results are illustrated in Table 3.14.

Table 3.14: Results from T-Test Comparison of G_{Ic} Initiation Values from the Principal Panel and the Panel Made with Recovered Polymer.

Group	Comparison of NL G_{Ic}	Comparison of 5%/Max G_{Ic}
Primary		
Secondary		X
All		

Although the 5%/Max secondary specimen values were found to be statistically different, inclusion of these values into a larger group nullified the significance of the difference in the values. Increasing the sample size, however, generally increases the power of statistical tests, i.e. smaller differences become more statistically significant. This is the opposite of what occurred when the secondary specimens were combined with the primary specimens to calculate overall mean G_{Ic} values. Because the difference became insignificant when the sample size increased, the results from the primary specimen comparison and overall comparison are more likely to have characterized the actual relationship of the properties of these two panels than the single statistical dissimilarity seen in the 5%/Max secondary values. As a result, polymer that is reclaimed from the air cleaner reservoir, can be reused without causing significant discrepancies in mode I interlaminar fracture toughness properties.

3.6 - G_{Ic} Propagation Values

Double cantilever beam (DCB) testing also provides data for computing mode I propagation values in addition to the data that has been used to compute the initiation values. Mode I strain energy release rate propagation values are computed from values of load and displacement at several observed cracks lengths as specified in ASTM D5528. The G_{Ic} propagation values are then plotted with the initiation values to generate a

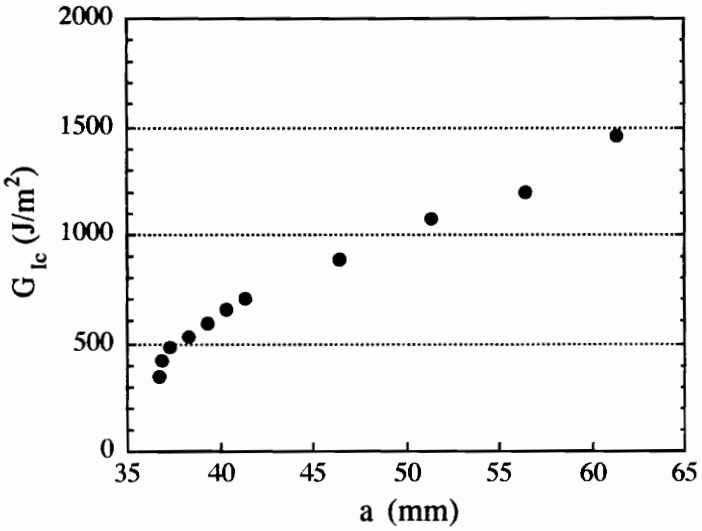

Figure 3.8: Delamination Resistance Curve for Specimen 2-10

delamination resistance curve. A typical delamination resistance curve is shown in Figure 3.8. The first two data points on this plot are the initiation values for the NL calculation and the 5%/Max calculation, respectively. The remaining nine points are propagation values calculated at crack propagation lengths of 1 mm, 2 mm, 3 mm, 4 mm, 5 mm, 10 mm, 15 mm, 20 mm, and 25 mm. Delamination resistance curves for all valid DCB specimens are presented in Appendix A.

G_{Ic} propagation values are not used for failure or fatigue analysis, but they do provide insight into a material's behavior. ASTM D5528 specifies that the apparent interlaminar toughness will increase after initiation, but then should stabilize at increasing crack lengths. Figure 3.8, however, shows that the apparent interlaminar toughness in these G30-500/ PEKK composites increases steadily as a function of crack length. This steady increase is a result of fiber bridging.

Since the apparent mode I toughness values continue to increase as the crack length increases, this indicates that the difference in degree of fiber bridging from one specimen to another should be evident in the delamination resistance curves. Specimens that exhibited significant fiber bridging are expected to have higher apparent interlaminar toughness propagation values than the specimens that exhibited only minor fiber bridging. Furthermore, comparison of the average propagation values from the primary specimens to those from the secondary specimens should show statistically significant differences in the G_{Ic} values at increasing crack lengths. Figures 3.9 graphically compare the average primary specimen G_{Ic} propagation values to the average secondary specimen G_{Ic} propagation values as a function of crack length for each panel. The standard deviation within each group is used to provide the error bars shown in these graphs.

Statistical analysis of the pairs of data that are graphically represented in Figures 3.9 was completed using a series of t-tests. A single-tailed, 5% rejection region was used in the analysis since the secondary specimens are expected to have higher propagation values as a result of increased fiber bridging. This analysis showed that although there are consistent and recognizable differences in all of the data when they are plotted, only the values from specimens in the panel cooled at 6°C/min were statistically distinct. The substantial variance in the data limited the power of the statistical analysis to conclusively prove that the trends seen in the G_{Ic} propagation values of these small groups of samples will occur consistently in future work. The trends evident in Figures 3.9 indicate, however, that increasing the degree of fiber bridging is likely to increase the apparent toughness of a composite as a crack propagates through the material. These plots also

indicate that the G_{Ic} propagation values observed in specimens that exhibit significant fiber bridging are likely to be higher than values in materials that do not exhibit fiber bridging.

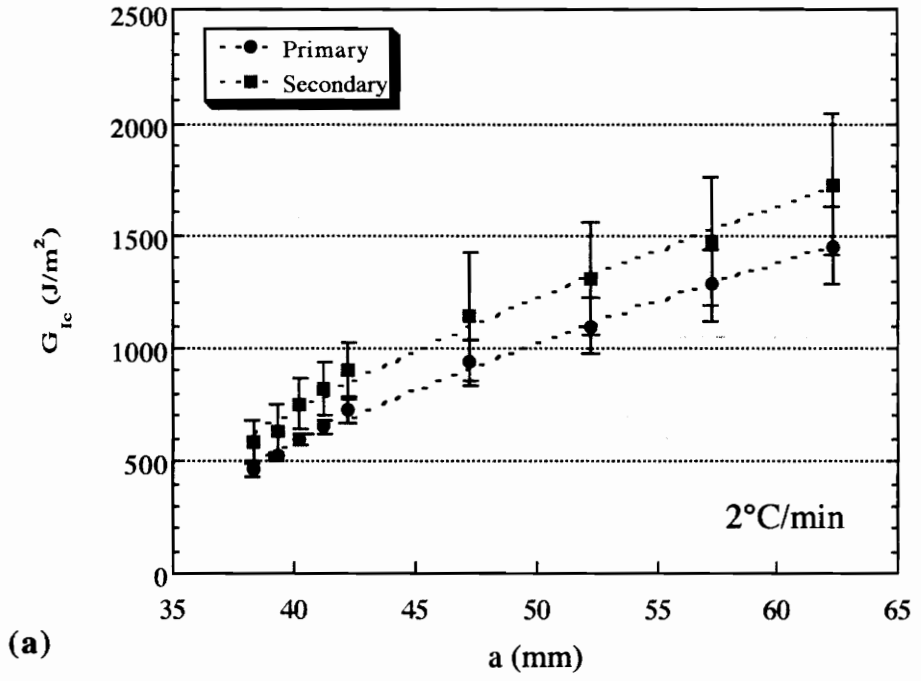

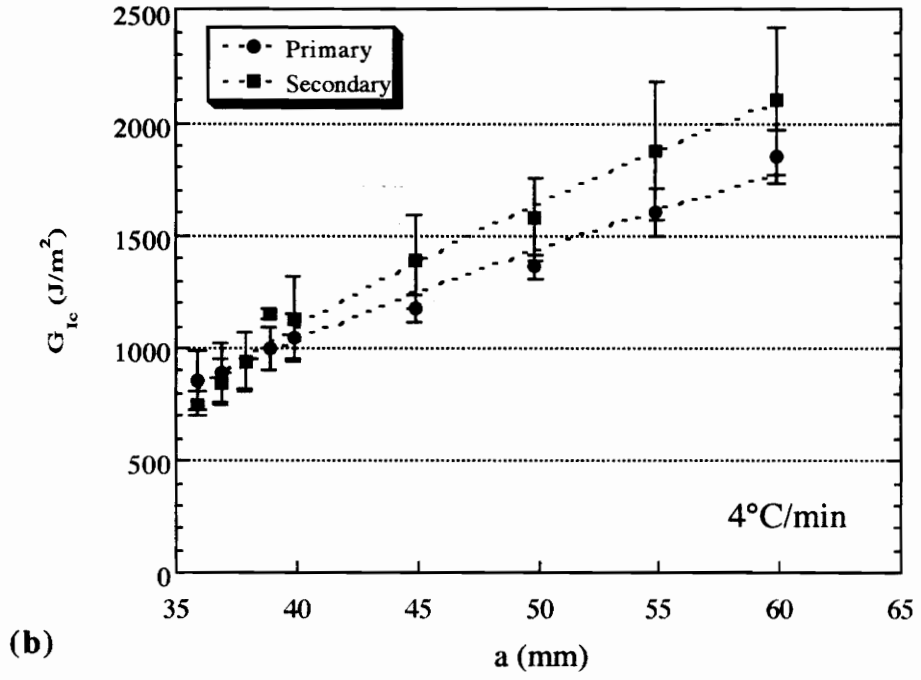

Figures 3.9: Comparison of Delamination Values for Primary and Secondary Groups (a) - Panel Cooled at 2°C/min and (b) - Panel Cooled at 4°C/min

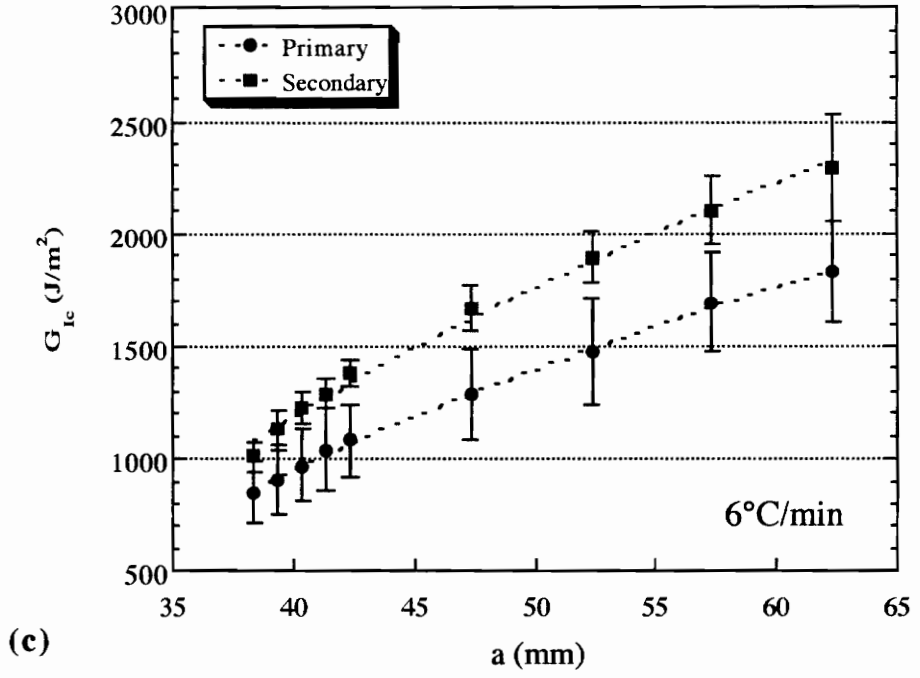

(c)

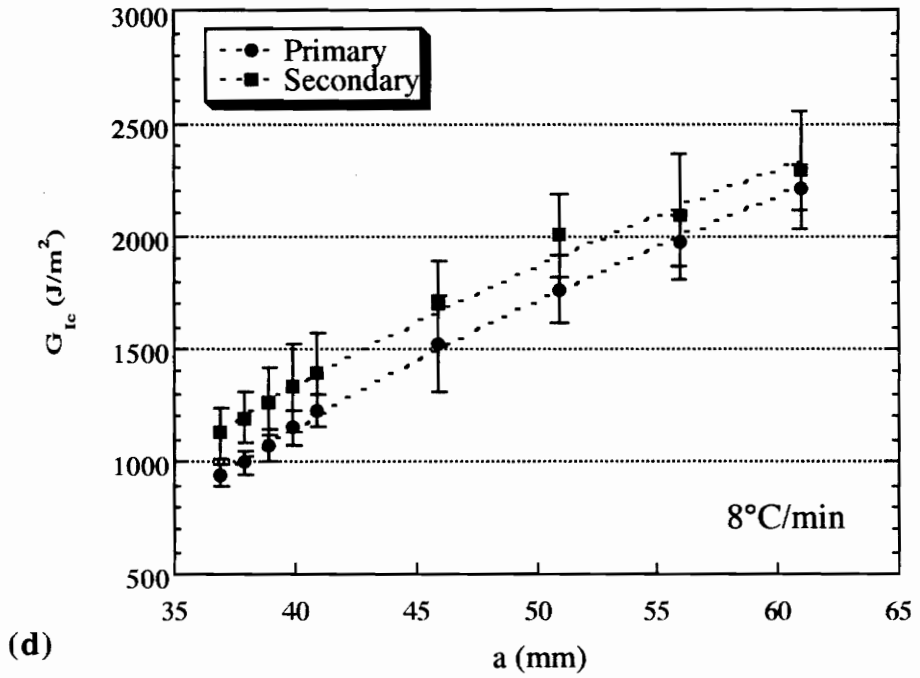

(d)

Figures 3.9 (Continued): Comparison of Delamination Values for Primary and Secondary Groups
(c) - Panel Cooled at 6°C/min and (d) - Panel Cooled at 8°C/min

Chapter 4 - Mode II Strain Energy Release Rate

End notch flexure tests are used to determine in-plane shear, i.e. mode II, strain energy release rates. Strain energy release rates, G_{IIc}, for carbon/poly(ether ketone ketone) (PEKK) matrix composites were not available from the literature. Moore and Seferis, however, reported a G_{IIc} value of 4930 J/m^2 for a carbon/poly(ether ether ketone) (PEEK) composite. PEEK and PEKK are both polymers in the poly(aryl ether ketone) family so they have similar properties. Russell and Street[45] found that strain energy release rates are generally three to four times greater in mode II fracture than in mode I fracture. As a result, an expected range for G_{IIc} values in carbon/PEKK matrix composites can be approximated from the range of mode I interlaminar fracture toughness values for carbon/PEEK composites that were reported by Moore and Seferis[1]. The approximation and single available data point indicated that carbon/PEKK G_{IIc} values should fall near the range of 4200 J/m^2 to 12800 J/m^2.

4.1 - G_{IIc} Initiation Values

There is no ASTM specification for end notch flexure (ENF) tests. The testing procedure and data analysis method that was used in this work is documented by Rau[43]. Rau's procedure is based upon the research of Russell and Street[45] and Whitney[46].

In ENF tests, three mode II initiation toughness values are to be calculated: onset of nonlinearity (NL), 5% compliance offset (5%), and point of maximum load (Max). These critical points are analogous to the critical points in double cantilever beam (DCB) testing. In ENF tests, however, separate 5% and Max initiation values, rather than a joint value, are calculated from the load and displacement at 5% compliance offset and at the point of maximum load. The three critical points are illustrated on a typical ENF load-displacement curve in Figure 4.1. Crack growth in mode II fracture is unstable, so mode II propagation values are not calculated from ENF data.

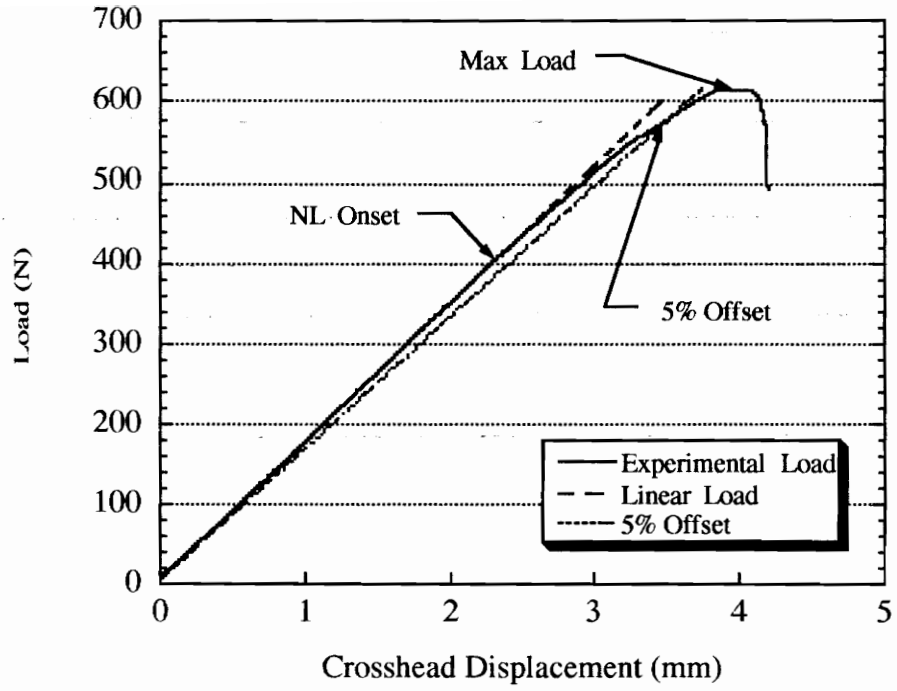

Figure 4.1: Representative Load-Displacement Curve from an ENF Test

The mode II strain energy release rate, G_{IIc}, is computed at each critical point using the local load, P_l, the local displacement, δ_l, and a modified crack length, a_{eq}, as shown in Equation 4.1.

$$G_{IIc} = \frac{9\, a_{eq}^2 P_l\, \delta_l}{2b\left(2L^3 + 3a_{eq}^3\right)} \tag{4.1}$$

In this equation L is the half span of the specimen and b is half of the specimen width. The modified crack length is calculated using the uncracked specimen modulus, E_x^b, and the local compliance, C_l, as shown in Equation 4.2.

$$a_{eq} = \left[\frac{16}{3} C_l\left(E_x^b b h^3\right) - \frac{2}{3}L^3\right]^{\frac{1}{3}} \tag{4.2}$$

In this equation h is half of the specimen thickness. The uncracked specimen modulus is computed using Equation 4.3, where C is the compliance of an uncracked region of the specimen.

$$E_x^b = \left(\frac{L^3}{8\,b\,h^3}\right)\frac{1}{C} \tag{4.3}$$

Fifty-three of the original sixty specimens were tested to obtain G_{IIc} data. The crack had progressed too far along the specimen during DCB testing to permit ENF testing in two of the excluded specimens. The other five excluded specimens were specimens in which the crack did not propagate along the centerline during DCB testing.

Unlike DCB testing, few anomalies were encountered during ENF testing. Furthermore, the few anomalies that did occur, occurred at the end of the test in the region of catastrophic failure. This was beyond the region used to determine G_{IIc} initiation values, so these abnormalities did not require the omission of the data from the G_{IIc} analysis.

A minimum of five specimens should be used in the calculation of mean G_{IIc} initiation values; therefore, the specimens were again grouped as primary and secondary specimens. There were two ways to divide the specimens into groups: significance of fiber bridging during crack initiation, i.e. during DCB testing, or conformance of experimental compliance values to theoretical compliances values. Grouping based on significance of fiber bridging would essentially be subjective, so the specimens were classified as primary or secondary based on the correlation of the measured compliance to the theoretical compliance at various crack length-to-half span ratios.

Compliance calibration, i.e. comparing measured compliance to theoretical compliance, has been suggested as a means to determine whether it is reasonable to assume that a specimen will provide reliable experimental data. The theoretical compliance is calculated using the measured stiffness of an uncracked region of the specimen, as shown in Equation 4.4, where a is the crack length.

$$C = \frac{2L^3 + 3a^3}{16\,E_x^b\,b\,h^3} \tag{4.4}$$

Compliance calibration plots depict the relationship between the theoretical compliance curve and experimental compliances measured at discrete crack lengths. A typical plot is shown in Figure 4.2. The plot for each specimen is provided in Appendix B. Appendix B also presents the load-displacement curve from catastrophic testing of each specimen.

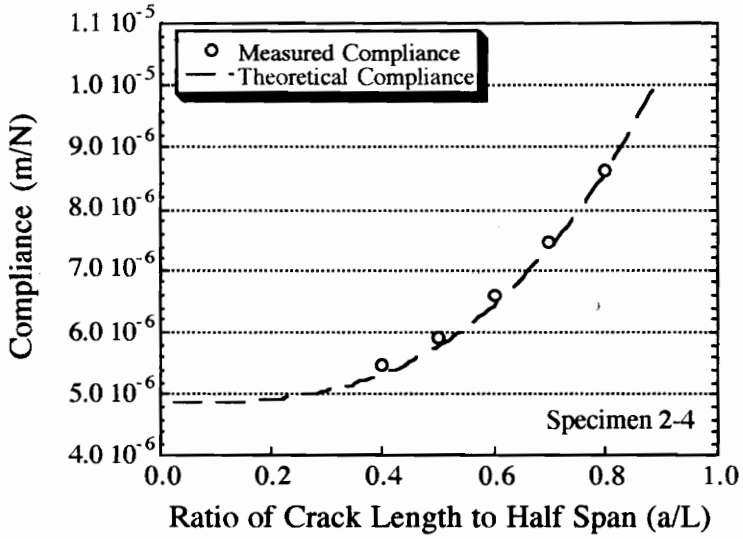

Figure 4.2: Compliance Calibration Curve for Specimen 2-4.

Figure 4.2 shows a typical compliance calibration curve. The theoretical compliance, as calculated using Equation 4.4, is shown as a continuous function of crack length-to-half span ratio. The experimental compliance was measured at crack length-to-half span ratios of 0.4, 0.5, 0.6, 0.7, and 0.8. Each experimentally measured value is shown as a discrete point in the compliance calibration plot. Figure 4.2 illustrates the remarkably good correlation that can be seen between measured and theoretical compliance values. Measured values do not necessarily have to correspond with the theoretical values to the extent shown in Figure 4.2. Poor correlation between measured and theoretical values could indicate that there was excessive friction between crack faces. Friction between the crack faces during mode II testing is a concern in these specimens because of the fiber bridging that occurred during DCB testing. Compliance calibration plots in this study, however, show that the measured values are generally within 5% of the theoretical values.

To verify that fiber bridging in some specimens did not have a strong influence on the measured G_{IIc} values, the specimens were again divided into two groups. The five specimens for the primary group are chosen based on fit of the experimental compliance values to the theoretical values. Specimens with the best apparent match are classified as primary specimens. Specimens included in the primary and secondary groups are specified in Table 4.1. Only six specimens were tested from the panel cooled at 2°C/min. Consequently, this panel again does not have a secondary group.

Table 4.1: Specimens Included in the Primary and Secondary Groups for Each Panel

Panel	Specimen Distribution	
	Primary	Secondary
2	2,4,6,8,10	
4	4,6,7,8,10	1,2,3,9
6	1,2,4,7,8	3,6,9,10
8	1,3,4,6,7	2,5,8,9,10

4.1.1 - G_{IIc} Initiation Values for Primary Group Specimens

The G_{IIc} initiation values calculated from onset of non-linearity, 5% compliance offset, and maximum load are reported in Tables 4.2 - 4.4, respectively, for each specimen in the primary groups. The mean, standard deviation, and coefficient of variation for each panel are also included in these tables. The mean values are plotted as a function of cooling rate in Figure 4.3. The error bars in this figure represent one standard deviation from the mean.

Table 4.2: G_{IIc} NL Initiation Values for Panel Primary Specimens

Panel	G_{IIc} Initiation Values - Onset of Non-linearity					NL Mean	Standard Deviation	Coefficient of Variation
2	1390	1470	1260	1550	1140	1360	165	0.121
4	1410	1690	1950	1900	1590	1710	221	0.130
6	1550	1670	1700	1520	1770	1640	103	0.063
8	1600	1420	1760	1860	1440	1620	195	0.121

Table 4.3: G_{IIc} 5% Initiation Values for Panel Primary Specimens

Panel	G_{IIc} Initiation Values - 5% Compliance Offset					5% Mean	Standard Deviation	Coefficient of Variation
2	4060	4500	3880	4550	4450	4290	300	0.070
4	4810	5880	5350	4170	4690	4980	655	0.132
6	3740	4180	4840	5210	5560	4700	744	0.158
8	4550	6030	5280	6750	5460	5620	826	0.147

Table 4.4:. G_{IIc} Max Initiation Values for Panel Primary Specimens

Panel	G_{IIc} Initiation Values - Maximum Load					Max Mean	Standard Deviation	Coefficient of Variation
2	4980	4330	3810	5790	3780	4540	852	0.189
4	5140	6350	6070	4120	4880	5310	906	0.171
6	5270	5300	5090	5490	6930	5610	749	0.133
8	5410	5220	5340	7070	3790	5370	1160	0.216

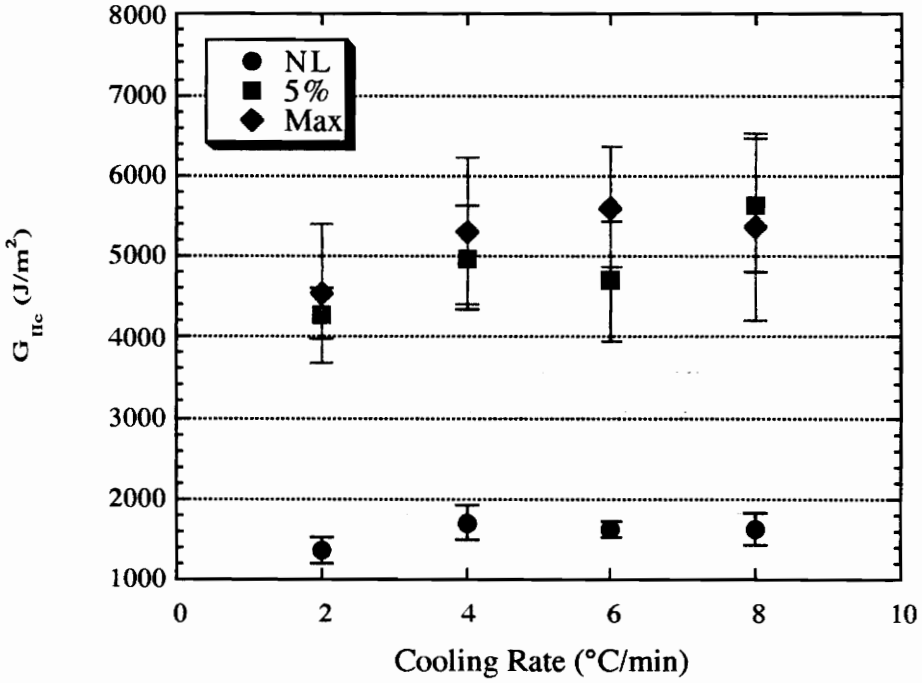

Figure 4.3: Primary Panel Mean G_{IIc} Initiation Values as a Function of Cooling Rate

The mean G_{IIc} values from the four panels were compared for each initiation value using a Duncan Multiple Range test[44]. Unfortunately the variance within the data from each panel was too great to draw many conclusions. Comparison of the initiation values showed that the NL initiation value of the panel cooled at 2°C/min is statistically lower than the NL values for the other three panels. On the contrary, in the 5% and Max cases, the

mean G_{IIc} value for the panel cooled at 2°C/min could only be shown to be statistically different from the panel mean G_{IIc} value for the panel cooled at 8°C/min. In the comparisons of all three initiation values, there was not enough difference between the mean values for the panels cooled at 4°C/min, 6°C/min, and 8°C/min to identify any mean as statistically distinct. Figures 4.4 - 4.6 illustrate the results from the statistical analysis. The panels are specified by cooling rate and are listed in order of increasing mean G_{IIc} value from left to right. Each line underneath the panel designations indicates that the G_{IIc} values of the panels above it are statistically equivalent.

Figure 4.4: Grouping of Statistically Equivalent Primary NL G_{IIc} Initiation Values

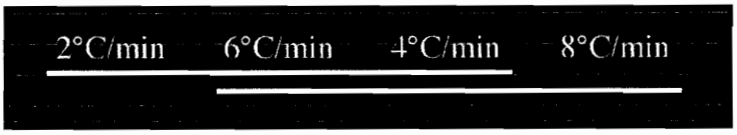

Figure 4.5: Grouping of Statistically Equivalent Primary 5% G_{IIc} Initiation Values

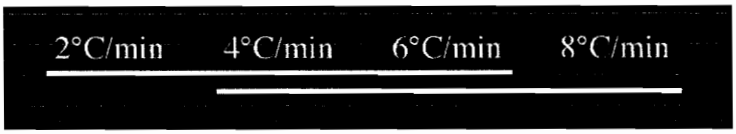

Figure 4.6: Grouping of Statistically Equivalent Primary Max G_{IIc} Initiation Values

In cases when there is not enough data to conclusively show that a value "A" will be larger than a value "B" in 95% of future tests, trends can still be identified from the ranked order of the mean data if there are two or more related sets of data. In order to draw conclusions from the ranking of the means, the ranking must be consistent between the sets of data. Unfortunately, in these data sets the rank of a panel mean varied for three of the four panels between the three sets of G_{IIc} initiation values. The panel cooled at 2°C/min had the lowest toughness for all three initiation values, but the relative rank for the other panels was not consistent. This does not, however, necessarily indicate that there was a problem

in data acquisition or analysis. The means for the three panels in question were shown to be statistically equivalent for all three initiation values; therefore, their relative ranking is, in effect, irrelevant. Since the order of the mean values changed between initiation values, the only trend that can be identified from analysis of the primary groups is that composites cooled at 2°C/min are likely to have a lower toughness than panels that are cooled at a rate of at least 4°C/min.

4.1.2 - G_{IIc} Initiation Values for Secondary Group Specimens

Tables 4.5 - 4.7 provide the three G_{IIc} initiation values for each specimen in the secondary groups. As before, the mean, standard deviation, and coefficient of variation for each panel are also included in these tables. As mentioned earlier, only six specimens were tested from the panel cooled at 2°C/min. The single remaining specimen from this panel was not included in the secondary group analysis.

The available specimens were separated into primary and secondary groups to determine whether the degree of correlation between the measured and theoretical compliance values had a significant effect on the G_{IIc} initiation values in these specimens. Severe differences between the primary and secondary group means would indicate that the fiber bridging seen in mode I testing of these specimens also affected the mode II results.

Table 4.5: G_{IIc} NL Initiation Values for Panel Secondary Specimens

Panel	G_{IIc} Initiation Values - Onset of Non-linearity					NL Mean	Standard Deviation	Coefficient of Variation
4	1400	1550	1620	1570		1530	94.2	0.061
6	1600	1780	2680	1960		2010	471	0.235
8	1570	1440	1470	1610	1480	1510	69.0	0.046

Table 4.6: G_{IIc} 5% Initiation Values for Panel Secondary Specimens

Panel	G_{IIc} Initiation Values - 5% Compliance Offset					5% Mean	Standard Deviation	Coefficient of Variation
4	4770	5120	6020	4750		5170	595	0.115
6	6150	6940	6840	4940		6220	923	0.148
8	5050	5650	5270	7890	5380	5850	1160	0.199

Table 4.7: G_{IIc} Max Initiation Values for Panel Secondary Specimens

Panel	G_{IIc} Initiation Values - Maximum Load					Max Mean	Standard Deviation	Coefficient of Variation
4	5490	5860	7440	5190		5990	1000	0.167
6	7470	6860	6830	6080		6810	568	0.083
8	6160	6570	6440	7920	6230	6660	722	0.108

If there was no statistically significance difference between the primary and secondary group means, then one can assume that the tendency of fibers in these composites to bridge the crack influenced the measured mode II strain energy release rate to the same extent in all of the specimens. This would allow all of the available data to be used to calculate mean G_{IIc} initiation values. The larger sample size should then yield more statistically significant differences between panels and/or improved correspondence of the ranking of panel means between the NL, 5%, and Max values.

4.1.3 - Comparison of Primary and Secondary G_{IIc} Initiation Values

Comparisons of primary and secondary group means were made using the pooled-variance t-tests and separate-variance t-tests. It was not expected that the differences in compliance calibration seen in these specimens were great enough to significantly effect the measured G_{IIc} initiation values. Consequently, these t-tests were completed using a two-tailed, 5% rejection region. Primary and secondary groups were compared for only the panels cooled at 4°C/min, 6°C/min, and 8°C/min since there was not a secondary group for the panel cooled at 2°C/min. The results from the nine comparisons are illustrated in Table 4.8. An "S" indicates that the secondary specimen mean was found to be statistically larger than the primary specimen mean. The cell is empty if the two values were found to be statistically equivalent.

Table 4.8: Statistically Inequivalent Primary Specimen and Secondary Specimen Means

Panel	Comparison of NL G_{IIc}	Comparison of 5% G_{IIc}	Comparison of Max G_{IIc}
4			
6		S	S
8			

In nearly eighty percent of the comparisons, the primary and secondary groups were shown to have statistically equivalent G_{IIc} initiation values. This should not be surprising, however, since there was significant variance within the data for each panel. There were several pairs which showed a considerable difference, but not a statistically significant difference, between the primary and secondary means; therefore, it is difficult to determine whether these differences are influenced by the large variance in the data. Additionally, in some of the pairs which were notably different, the primary specimen mean was larger than the secondary specimen mean. This implies that the differences in the means are simply a result of scatter in the data. There was simply not enough evidence to prove that a specimen will have a higher mode II strain energy release rate when the measured compliance does not correlate well to the theoretical compliance. The results of this analysis indicate that data from all the available specimens could be used to compute G_{IIc} initiation values with as much validity as the smaller group of primary specimens.

4.1.4 - Comparison of G_{IIc} Initiation Values Using All Available Data

Since comparison of primary means to secondary means showed no consistent trend between the two groups, mean G_{IIc} initiation values were calculated using all the data from the fifty-three ENF specimens. This inclusion of all available data differs from an analogous G_{Ic} calculation because in this case there was no reason to believe that data may be biased. Neither the compliance calibration curves in Appendix B nor the comparisons of the data from primary and secondary groups indicated that there were severe deviations from expected behavior in any of the data. The mean G_{IIc} initiation values calculated using data from all the primary and secondary specimens are provided with 5% confidence intervals for each panel in Table 4.9. The mean values are plotted as a function of cooling rate in Figure 4.7. The error bars in these plots represent one standard deviation from the mean.

Table 4.9: G_{IIc} Initiation Values Computed Using Data from All Available Specimens

Panel	2°C/min	4°C/min	6°C/min	8°C/min
NL Initiation G_{IIc} (J/m^2)	1360 ± 168	1630 ± 176	1800 ± 328	1570 ± 130
5% Initiation G_{IIc} (J/m^2)	4600 ± 923	5060 ± 553	5380 ± 1030	5730 ± 842
Max Initiation G_{IIc} (J/m^2)	4830 ± 1180	5610 ± 885	6150 ± 828	6270 ± 729

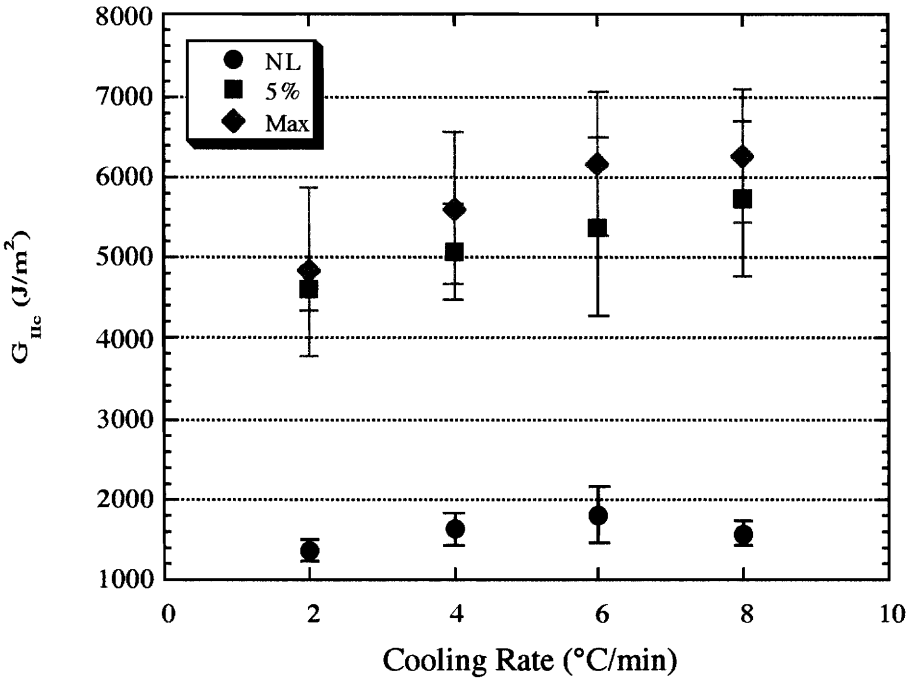

Figure 4.7: Combined Group Mean G_{IIc} Initiation Values as a Function of Cooling Rate

Duncan Multiple Range tests[44] using a 5% rejection region were completed to identify statistically significant differences between the means within each initiation value. Figures 4.8 - 4.10 graphically present the results of these statistical tests.

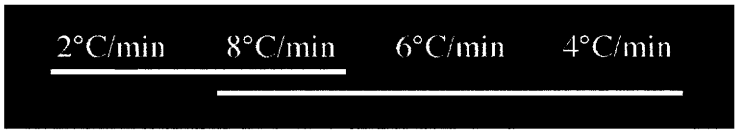

Figure 4.8: Grouping of Statistically Equivalent NL G_{IIc} Initiation Values Calculated Using All Available Data

Figure 4.9: Grouping of Statistically Equivalent 5% G_{IIc} Initiation Values Calculated Using All Available Data

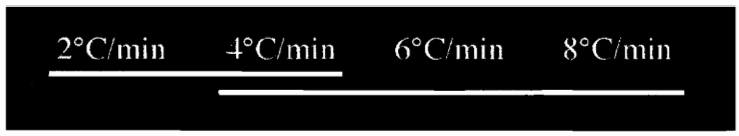

Figure 4.10: Grouping of Statistically Equivalent Max G_{IIc} Initiation Values Calculated Using All Available Data

Statistical analysis of the mean values calculated using all of the available data resulted in relatively few changes in the ranking of statistically equivalent groups in comparison to the rankings illustrated in Figures 4.4 - 4.6. There is now, however, improved consistency in the relative rankings of panel means between the three initiation values. Figures 4.8 - 4.10 show the ranking from the lowest mean to the highest mean was consistent between all three initiation values except for the shift in placement of the panel cooled at 8°C/min. This panel's NL initiation value was the second lowest of the NL values, but was the highest 5% and Max initiation values. It is unclear why the NL data for this panel were unexpectedly low. Although including all available data in the calculation of panel mean values provided only small improvements in the consistency of panel ranking, this improved consistency implies a trend of increasing G_{IIc} fracture toughness with increasing cooling rate. The improved consistency is important because it may indicate a trend in the data even though the differences between toughness values as a function of cooling rate are not necessarily statistically significant.

Comparison of the experimentally measured G_{IIc} values for carbon/PEKK composites to the range projected from carbon/PEEK values shows that the measured values are much lower than the projected range. The difference between PEKK and PEEK G_{IIc} values corresponds to the difference between the projected and measured G_{Ic} values that was discussed in Chapter 3. In the analysis of G_{Ic} values, PEKK G_{Ic} NL values were found to be 30% to 50% of the lower limit for PEEK G_{Ic} NL values. In this analysis, PEKK G_{IIc} values were found to be 30% to 45% of the approximated lower limit for PEEK G_{IIc} values. This equality of the differences between the two materials' values for both fracture toughness measurements was not expected, but suggests that the toughness values measured in this study are representative for this composite.

4.2 - Examination of Additional Processing Variables

The two additional panels, the annealed panel and the panel made from recovered polymer, were also tested for mode II interlaminar fracture toughness. The load-displacement curve and compliance calibration curve for each specimen from these panels are provided in Appendix B with the curves from the four principle panels. The annealed panel specimens are again designated as 8A-X, while the specimens from the panel made with recovered polymer are designated as 4R-X. Although all specimens from the principal panels were eventually used to compute G_{IIc} mean values, the specimens from these two panels are also divided into primary and secondary groups. This is to verify that the degree of compliance correlation does not affect the toughness of these two materials more than it affected the measured toughness of the principal panels. The specimens included in the primary and secondary groups for these two panels are listed in Table 4.10.

Table 4.10: Specimens Included in the Primary and Secondary Groups for the Additional Panels

Panel	Specimen Distribution	
	Primary	Secondary
8A	2,5,7,9,10	1,3,4,8
4R	1,2,3,9,10	4,5,6,7,8

Evaluation of G_{IIc} values for the two panels provides a second measure of the equivalence or difference in the materials as a result of the change in processing or material constituent. This second comparison is important because it could either corroborate the conclusions from mode I testing or indicate that there are differences in the materials that do not affect tensile fracture, but do affect in-plane shear fracture. Comparisons in the following two sections will indicate which conclusion is true for each of the two panels.

4.2.1 - G_{IIc} Initiation Values for an Annealed Panel

The three calculated G_{IIc} initiation values for the annealed panel are provided in Table 4.11 for both the primary and secondary group specimens. This table also includes the means, standard deviations, and coefficients of variance for the primary, secondary, and combined groups.

Table 4.11: G_{IIc} Initiation Values for the Annealed Panel

Value	Group	G_{IIc} Initiation Values (J/m^2)					Mean	Standard Deviation	Coefficient of Variation
NL	Primary	1570	2800	1500	1480	1620	1790	565	0.315
	Secondary	2300	1840	1850	1850		1960	228	0.117
	All						1870	430	0.230
5%	Primary	4840	5450	4460	6240	6100	5420	773	0.143
	Secondary	6270	6500	5190	6470		6110	623	0.102
	All						5720	760	0.133
Max	Primary	4830	5540	5660	6660	6790	5900	821	0.139
	Secondary	6180	6860	5960	7030		6510	519	0.080
	All						6170	740	0.120

Separate-variance t-tests[44] were used to compare the primary group means to the secondary group means. The comparison of principal panel primary and secondary groups showed that the mean G_{IIc} values of specimens with good correlation between measured and theoretical compliance values are equivalent to the mean values for specimens with poor correlation between measured and theoretical compliance values. There is no reason to believe that a different result would be seen in the comparison of the annealed panel primary and secondary groups, so a two-tailed, 5% rejection region was used in this analysis. In all three cases the primary and secondary group means were found to be statistically equivalent. This corroborates the finding in the principal panels.

The data from this panel can be compared to the data from the principal panel that was cooled at 8°C/min to determine what affect annealing had on the material's mode II toughness. The combined mean G_{IIc} initiation values from the two panels are compared in Figure 4.11. The error bars in this plot represent one standard deviation from the mean.

Statistical comparison of the two panels was completed using pooled-variance and separate-variance t-tests. As stated in the G_{Ic} analysis, a single-tailed, 5% rejection region was used since one would expect the annealed panel to have a higher crystallinity, and therefore a lower toughness. The data was statistically compared as primary, secondary, and combined groups for each initiation value. In this data, the initiation values of the principal panel cooled at 8°C/min were never shown to be statistically larger than the values for the annealed panel. In fact, in two of the nine comparisons (the NL secondary means and NL overall means) the initiation values for the annealed would have been shown to be statistically larger than the values for the principal panel had this been the tested hypothesis. This result was unexpected and will be discussed more fully in conjunction with the comparison of degree of crystallinity in the two panels.

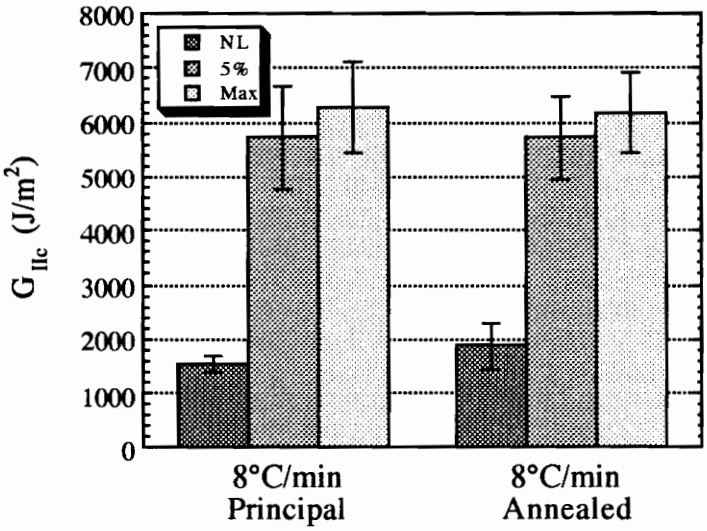

Figure 4.11: Comparison of G_{IIc} Initiation Values for the Annealed Panel and the Principal Panel.

4.2.2 - G_{IIc} Initiation Values for a Panel Made with Recovered Polymer

G_{IIc} initiation values calculated at the onset of non-linearity (NL), at the intersection of the load-displacement curve and a line drawn at 95% of the initial compliance (5%), and at the point of maximum load (Max) for this panel are listed in Table 4.12 for each specimen. To conform to the established format, the mean, standard deviation, and coefficient of variance for each group are also included in this table.

Pooled-variance t-tests[44] were used to compare the primary group means to the secondary group means. A two-tailed, 5% rejection region was used in this analysis just as it was used in the analyses for the other five panels. In all three cases, the two group means for this panel were found to be statistically equivalent. This also corroborates previous findings.

The data from this panel can be compared to the data from the principal panel that was cooled at 4°C/min to determine what affect using polymer recovered from the dry powder prepregging facility's air cleaner might have on the composite's mode II toughness. The combined mean G_{IIc} initiation values from the principal panel cooled at 4°C/min and the recovered polymer panel are plotted in Figure 4.12. The error bars in this plot represent one standard deviation from the mean.

Table 4.12: G_{IIc} Initiation Values for the Panel Made with Recovered Polymer

Value	Group	G_{IIc} Initiation Values (J/m^2)					Mean	Standard Deviation	Coefficient of Variation
NL	Primary	1310	1380	1470	1510	1700	1470	151	0.102
	Secondary	1770	1360	1620	1430	1390	1500	200	0.134
	All						1480	167	0.113
5%	Primary	3770	4140	4320	4990	4110	4270	449	0.105
	Secondary	3830	4240	4950	4620	3970	4320	463	0.107
	All						4290	431	0.100
Max	Primary	4190	4980	4410	5170	3860	4520	544	0.120
	Secondary	4020	4900	5140	4680	4540	4650	422	0.091
	All						4590	464	0.101

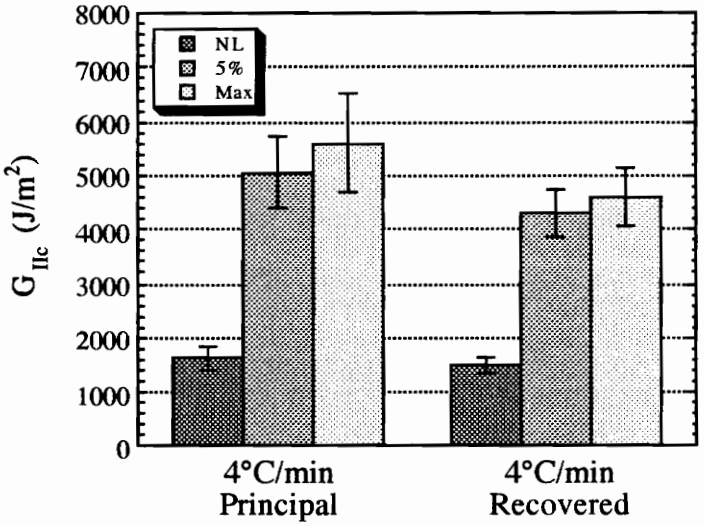

Figure 4.12: Comparison of G_{IIc} Initiation Values
from the Panel Made with Recovered Polymer and the Principal Panel.

The values for specimens from the panel made with recovered polymer were compared to the values for specimens from the principal panel cooled at 4°C/min using pooled-variance and separate-variance t-tests[44]. These comparisons were analogous to the comparisons completed for G_{Ic} values. Once again there was no reason to assume that one panel would have consistently higher toughness than the other panel, so a two-tailed, 5% rejection region was used in the analysis. The mean initiation values from the two panels were compared as primary groups, secondary groups and as a combined group. The nine comparisons showed that only one pair, the combined G_{IIc} Max means, were statistically dissimilar. Several of the other comparisons, however, showed notable differences between the panel mean values even though there was not enough data to conclusively prove that the two values were statistically unequal. If there had been some physical justification that would have allowed one to assume that values from the principal panel would be consistently larger than values from the recovered polymer panel, then a single-tailed rejection region could have been used in the statistical analysis. If this had been the case, the differences that do exist would have been found to be statistically significant.

This was true for all of the comparisons between 5% values, and the primary specimen NL and the secondary specimen Max comparisons. These results are illustrated in Table 4.13. An "X" indicates that the specimens from the principal panel were shown to have a statistically higher mode II interlaminar fracture toughness than specimens from the panel made with recovered polymer. An "x" indicates that the principal panel specimens had a notably higher G_{IIc} initiation value, but that there was not quite enough data to conclusively prove that similar composites will consistently have higher G_{IIc} values. A cell is empty if the two G_{IIc} values were effectively equal.

Table 4.13: Results from T-Test Comparison of G_{IIc} Initiation Values from the Principal Panel and the Panel Made with Recovered Polymer

Panel	Comparison of NL G_{Ic}	Comparison of 5% G_{Ic}	Comparison of Max G_{Ic}
Primary	x	x	
Secondary		x	x
Overall		x	X

Although the panel made with first use polymer cannot be conclusively shown to have higher mode II interlaminar fracture toughness than the panel made with recovered polymer, Table 4.13 indicates that further testing could show a statistically significant difference between these two materials' in-plane shear strain energy release rates. This result was not expected. This result will be discussed more fully in conjunction with the discussion of the degree of crystallinity measured in each panel.

Chapter 5 - Correlation of Crystallinity and Toughness

A main objective of this study was to determine whether a correlation exists between crystallinity and toughness in carbon/poly(ether ketone ketone) (PEKK) composites. Statistical analysis of the toughness data to this point has been able to show only a few statistically significant differences between the measured toughness values in these composites. The degree of crystallinity in the four principal panels as a function of cooling rate will now be analyzed. Analysis of the crystallinity in the panels will attempt to show that the ranking of the panels from lowest crystallinity to highest crystallinity is associated to the ranking of the panels from highest toughness to lowest toughness. Additionally, plots of toughness as a function of crystallinity will illustrate the strength of the dependency of toughness on crystallinity in these composites. The dependence of toughness of crystallinity will then be compared to the dependence of toughness on cooling rate.

5.1 - Effect of Cooling Rate on Crystallinity

The degree of crystallinity in a material is primarily dependent upon its thermal history, but it can also be affected by a number of other factors. In general, slower cooling rates result in higher crystallinity[6]. Nevertheless, the exact relationship can be affected by the type of fiber[22], the molecular weight of the polymer[11], or other processing variables[1,13]. This study is primarily concerned with the effect of cooling rate on crystallinity, but differences due to quickly cooling and then annealing the composite or due to possibly increasing the number of heterogeneous nucleation sites are also examined.

5.1.1 - Measured Degree of Crystallinity

The crystallinity in the composites was determined from the heat of formation of the crystalline phase as measured by differential scanning calorimeter (DSC). Representative DSC curves from each of the six panels are provided in Figures 5.1.

The accuracy of DSC measurement of crystallinity is controversial. As a general rule of thumb, the degree of crystallinity as measured by DSC is considered to be accurate to within six or seven percent. The main source of error is the subjective way in which the baseline must be drawn. The location of the assumed baseline affects the calculated heat flow, and therefore the calculated crystallinity. Since it is difficult to determine the baseline definitively, this is a source of error in the crystallinity computation that cannot be

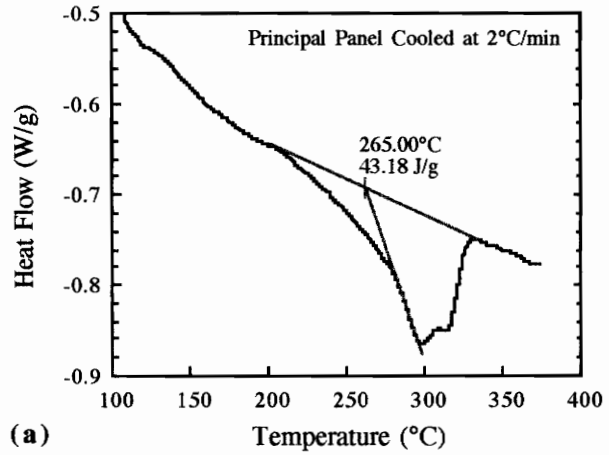

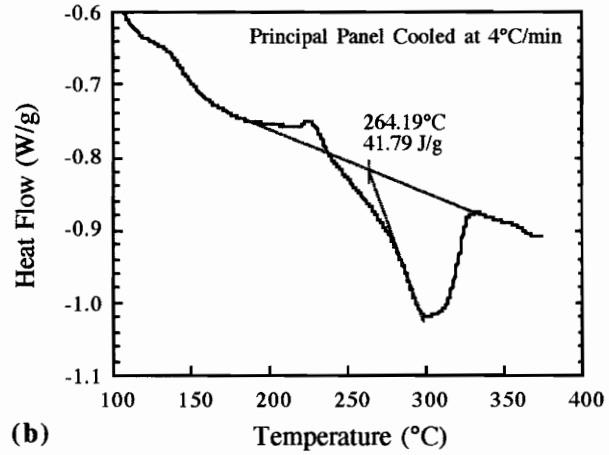

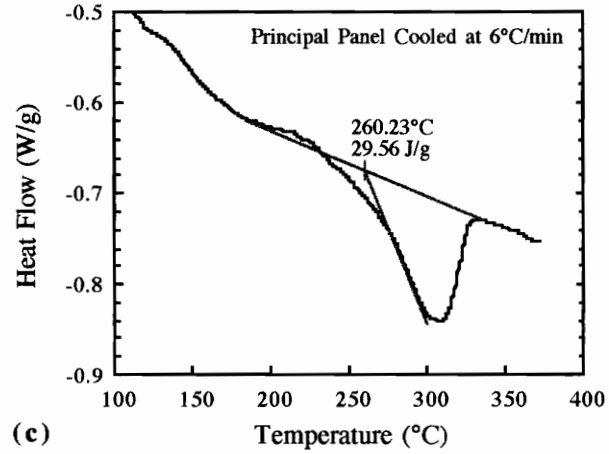

Figures 5.1: Representative DSC Scans for Each Panel
a) Panel Cooled at 2°C/min, b) Panel Cooled at 4°C/min, c) Panel Cooled at 6°C/min

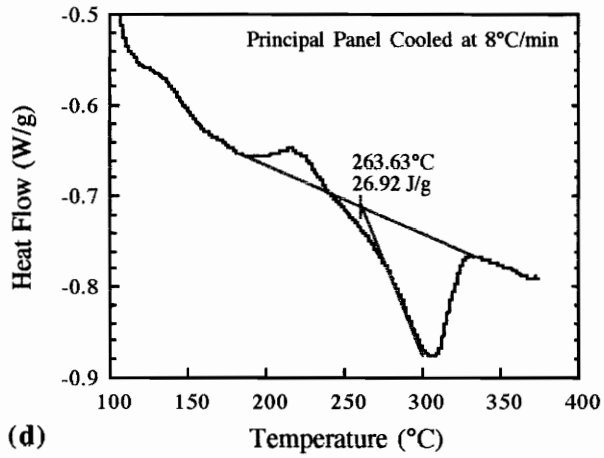

(d)

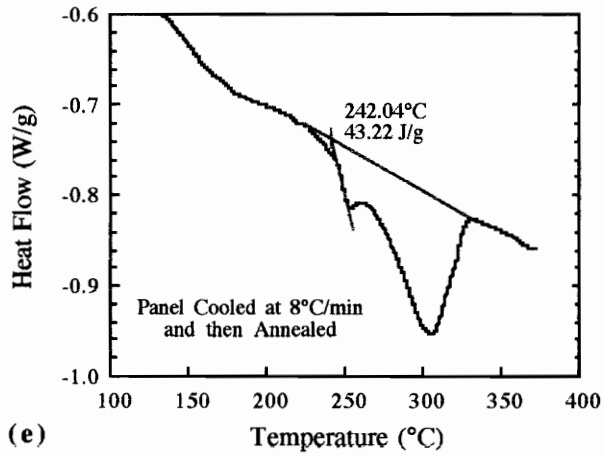

(e)

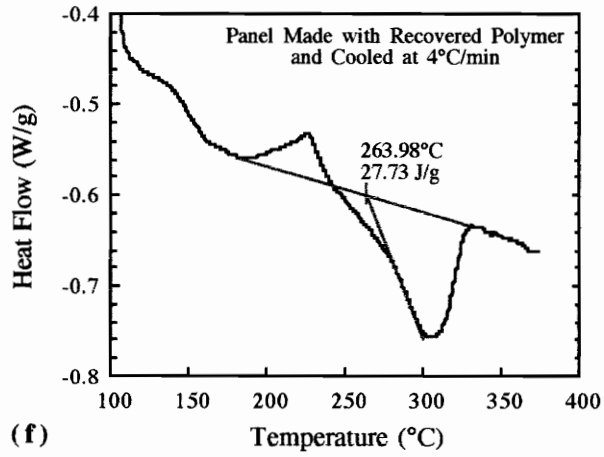

(f)

Figures 5.1 (cont): Representative DSC Scans for Each Panel
d) Panel Cooled at 8°C/min, e) Panel Initially Cooled at 8°C/min and then Annealed,
f) Panel Made with Recovered Polymer and Cooled at 4°C/min

eliminated. In composites, there is also an error introduced due to the determination of the exact amount of polymer in a sample. The exact fiber volume fraction, and therefore the exact mass of polymer in the sample, is difficult to determine precisely for small samples because of local variations within the composite. In this study, however, we are primarily interested in the difference between the degree of crystallinity in each panel rather than the absolute level of crystallinity. Consequently, the crystallinity will be discussed as an apparent, rather than exact, value.

The apparent degree of crystallinity was measured for five samples from each panel. These values and the mean crystallinity, standard deviation, and coefficient of variation for each panel are provided in Table 5.1. The mean crystallinities for the four principal panels, the panels denoted 2, 4, 6, and 8 in Table 5.1, are plotted as a function of cooling rate in Figure 5.2. Error bars in this plot represent one standard deviation from the mean. The reader should note, however, that the experimental error in this data could be more than twice the statistical error.

Table 5.1: Percent Crystallinity in Each Panel

Panel	Percent Crystallinity for Each Specimen					Mean	Standard Deviation	Coefficient of Variation
2	33%	29%	38%	34%	33%	33%	3.0%	0.09
4	24%	27%	32%	23%	28%	27%	3.7%	0.14
6	28%	29%	22%	23%	18%	24%	4.5%	0.19
8	29%	27%	21%	18%	21%	23%	4.5%	0.20
8A	30%	31%	30%	28%	33%	30%	2.1%	0.07
4R	25%	30%	21%	30%	22%	26%	4.3%	0.17

All of the values in Table 5.1 are calculated assuming that each sample contained exactly 60% fiber by volume. The precise mass of polymer in each DSC sample is critical because the energy released during a DSC scan is dependent upon the amount of polymer in the sample. A brief evaluation of the dependence of calculated heat of fusion, ΔH_f, on fiber volume fraction showed that a 4% error between the actual fiber volume fraction and the assumed fiber volume fraction can result in up to an 8% change in the apparent degree of crystallinity. This relationship is illustrated in Table 5.2.

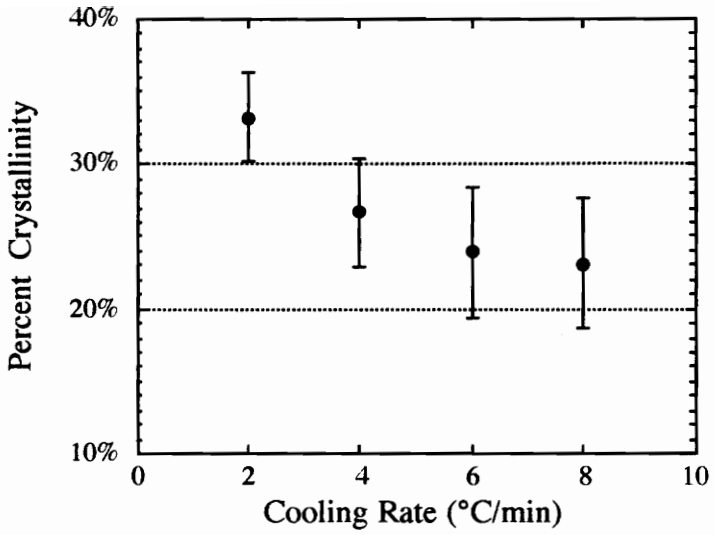

Figure 5.2: Crystallinity as a Function of Cooling Rate for the Principal Panels

Table 5.2: Illustration of the Effect of Assumed FVF on Percent Crystallinity

Assumed FVF	Sample Mass	Calculated ΔH_f	Apparent % Crystallinity
57.7%	9.7988	40.75	31%
60%	9.1975	43.22	33%
62.5%	8.5558	47.04	36%

The data in Table 5.2 illustrates the importance of the assumed fiber volume fraction. The assumed FVF determines the mass of polymer in the sample and the mass of the polymer in the sample determines the calculated heat of fusion. The degree of crystallinity in the sample is calculated by dividing the heat of fusion of the sample by the heat of fusion for a purely crystalline sample. The error quoted earlier is computed for the situation where the actual fiber volume fraction is 4% higher or lower than the assumed fiber volume fraction of 60%. Although inaccuracies in the actual FVF are an additional source of error, the potential error is not factored into the reported values or the statistical analysis.

The effect of local variations can be reduced by increasing the number of samples taken from each panel. Since five samples from each panel were evaluated, the majority of the change in apparent crystallinity due solely to variation in local fiber volume fraction should be minimized. Furthermore, it is unlikely that any one panel would have more local

variation in fiber volume fraction than any other panel. Consequently, local variations in fiber volume fraction should affect the apparent degree of crystallinity to the same extent in all six panels. These considerations suggest that differences in the FVF of each panel or errors in the assumed fiber volume fraction should not have resulted in significant bias in the apparent crystallinity for any particular panel.

The two methods used to calculate the global fiber volume fraction in each panel were presented in Section 2.6. Both calculated values for each panel are presented in Appendix A. The fiber volume fractions as calculated by either method were found to differ by less than 1.8% in the six panels. This difference could result in a bias of some of the calculated crystallinities, but the resultant error in the apparent crystallinity will not be larger than 4% percent. Table 5.1 shows that the statistical variance of the data within each principal panel is at least 10% of the value of the crystallinity. This indicates that variation in the apparent degree of crystallinity as a result of variation in fiber volume fraction between panels will be less of a factor than the variation that results from variation in the crystallinity within the panel and the variation due to experimental error in DSC measurements.

One reason that there is a significant amount of scatter in the apparent crystallinity of each panel is that some DSC samples were taken from the outer edges of the panels while other specimens were taken from interior points within the panels. Although these panels were relatively small, there would have been a temperature gradient across the panel during cooling. This temperature gradient would have resulted in the outer edges of the panel cooling faster than the inner regions of the panel. As a result, there is in a variation in crystallinity across the panel. Specimens were taken from a variety of locations in the panel to obtain an average degree of crystallinity for the panel. This does, however, result in another source of variation between individual measurements within a particular panel.

5.1.2 - Comparison of the Degree of Crystallinity in the Principal Panels

The mean degree of crystallinity from the four principal panels were compared using a Duncan Multiple Range test[44]. In the statistical analysis, the statistical error was used to identify equivalent values. The results of the analysis are illustrated in Figure 5.3. The panels are specified by cooling rate and listed from left to right in order of increasing mean crystallinity. Each line underneath the panel designation indicates that the apparent crystallinity of the panels above it were found to be statistically equivalent. The ability of this test to differentiate between the degree of crystallinity in each panel was similar to the

results seen in the toughness comparisons. The panel cooled at 2°C/min was shown to have a statistically higher toughness than the other three principal panels. Although the mean degree of crystallinity increased as the cooling rate decreased from 8°C/min to 6°C/min to 4°C/min, the differences between individual values were not statistically significant. These results would not change if an experimental error of six percent was used to identify equivalent values.

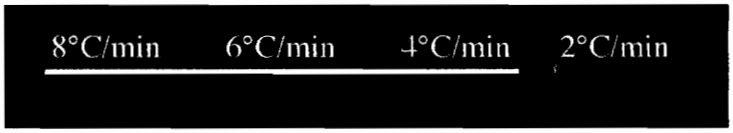

Figure 5.3: Grouping of Statistically Equivalent Crystallinities

Even though the degree of crystallinity in the panels cooled at 4°C/min, 6°C/min, and 8°C/min were found to be statistically equivalent, the mean values are ordered in a logical and expected sequence. Increasing the cooling rate decreases the amount of time that polymer chains are mobile enough to reorganize into crystalline structures. As a result, the degree of crystallinity in a polymeric materials decreases with increasing cooling rate. It would have been advantageous to have seen more statistically significant differences in the degree of crystallinity between cooling rates, but there is a large amount of scatter in the data. The reasons for the variance in the data have been discussed. Unfortunately the large variance in the data reduces the probability that statistical comparison will identify statistically significant differences.

Fortunately, the grouping of statistically similar crystallinities is identical to the grouping of statistically equivalent NL primary G_{Ic} values, NL combined G_{Ic} values, and NL primary G_{IIc} values. This grouping and ordering is also quite similar to the grouping and ordering of 5% combined G_{IIc} values and Max combined G_{IIc} values. The implications of the trend in crystallinity as a function of cooling rate when compared with trends seen in toughness values will be discussed in Section 5.2.

5.1.3 - Comparison of the Crystallinity in Panels Initially Cooled at 8°C/min

The degree of crystallinity in the panel that was initially cooled at 8°C/min and then annealed in an oven at 250°C for two hours can be compared to the degree of crystallinity of the principal panel cooled at 8°C/min. In this comparison, the annealed panel was expected to have a higher crystallinity that the principal panel. Lamellar thickening[8] and development of imperfect crystals[10] have been shown to occur during the annealing of polymers. Both processes will increase the degree of crystallinity in the composite. The apparent degree of crystallinity for each panel is compared graphically in Figure 5.4. The error bars represent one standard deviation from the mean.

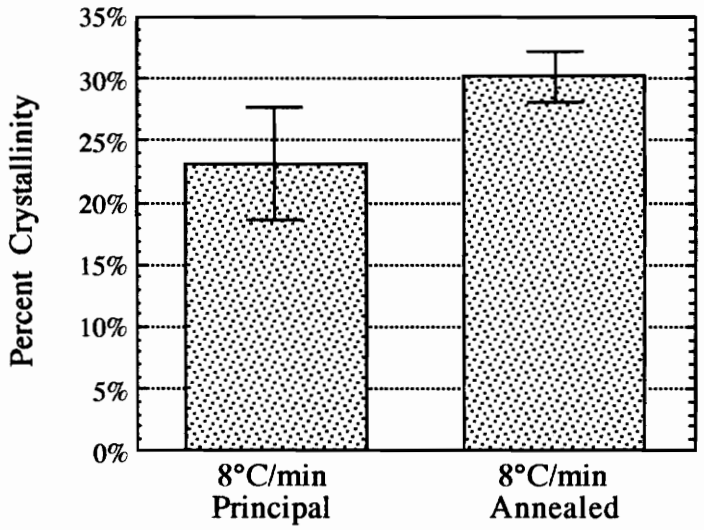

Figure 5.4: Comparison of the Crystallinity for the Panels Initially Cooled at 8°C/min

Examination of Figure 5.4 indicates that statistical comparison is essentially unnecessary. In this figure, the error bars do not overlap; therefore, it is not surprising that the t-test comparison using a single-tailed, 5% rejection region showed that the annealed panel has a statistically higher degree of crystallinity that the corresponding principal panel.

5.1.4 - Comparison of the Crystallinity in the Panels Cooled at 4°C/min

The apparent crystallinity of the two panels cooled at 4°C/min were compared to determine if there was a significant difference between the degree of crystallinity in these composites. The two panels were expected to have a similar, if not equal, degree of crystallinity. There was a possibility that polymer recovered from the dry powder prepregging facility's air cleaner would contain more impurities than new polymer. These additional impurities could act as heterogeneous nucleation sites in the polymer and change both the crystalline structure and the degree of crystallinity of the composite. The crystallinity was not, however, expected to be substantially different between the two panels. The apparent degrees of crystallinity from the two panels are compared graphically in Figure 5.5. The error bars in this plot represent one standard deviation from the mean.

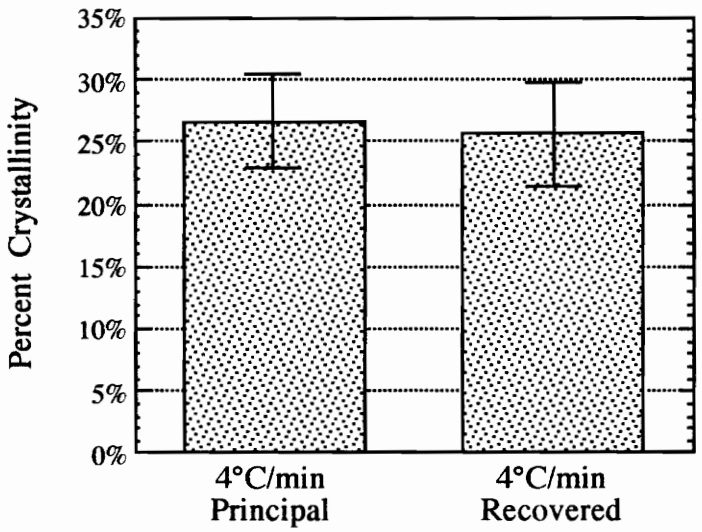

Figure 5.5: Comparison of the Crystallinity for the Two Panels Cooled at 4°C/min

Plotting the two mean values with error bars again nearly eliminates the need to perform a statistical test. In this case, however, Figure 5.5 indicates that the two panels have essentially equal degrees of crystallinity. The crystallinity in the two panels were compared using a pooled-variance t-test with a two-tailed, 5% rejection region[44]. The t-test showed that there is very little statistical difference between the degree of crystallinity in the two panels. This cannot be assumed to mean that the microstructures are necessarily equivalent, but only that the degree of crystallinity is equivalent. Microscopy could be used to determine the degree of microstructural similarity in the two composites.

5.2 - Correlation of Toughness and Crystallinity in the Principal Panels

Crystalline regions in PEEK have been shown to have a higher strength and stiffness but lower strain-to-failure than amorphous regions[1]; therefore, the PEKK composites in this study are expected to show decreasing interlaminar fracture toughness with increasing crystallinity. This study was designed so that both crystallinity and toughness could be measured as a function of cooling rate and then compared to determine what, if any, correlation exists between the two experimentally measured values.

Toughness in polymer matrix composites is generally considered to be affected by the degree of crystallinity in the polymer, the energy state of the amorphous phase, and the residual stresses in the composite. The mean strain energy release rates will be plotted as a function of crystallinity to show whether a direct relationship exists between these two values. If a direct relationship does not exist, this would indicate that the differences in toughness are more likely to be a result of differences in the state of the amorphous phase or differences in the residual stress state of the composites. These panels are, however, relatively thin, so it is unlikely that cooling rates used in this study resulted in major differences in the residual stresses in the panels. Furthermore, differences in the amorphous phases of the materials are also unlikely to be extremely influential since the cooling rates used in processing are of the same order of magnitude. It is difficult to clearly ascertain which of the three possible factors is the primary source of the differences in toughness simply through examination of the experimental data that is presently available. Nevertheless, comparison of the trends in toughness as a function of crystallinity to the trends in toughness as a function of cooling rate should indicate whether the correlation between toughness and cooling rate can be justified by the changes in the degree in crystallinity. If there is no correspondence between toughness and crystallinity, this would indicate that the changes in toughness with cooling rate must be attributed to some other cooling rate dependent factor. Conversely, if there is a strong correlation between toughness and crystallinity, this would indicate that the degree of crystallinity is likely to be the primary factor which determines the toughness in these composites. In addition to comparing plots of toughness as a function of crystallinity to plots of toughness as a function of cooling rate, the results from statistical analyses of toughness and crystallinity as functions of cooling rate will also be compared to further explore relationships between the two modes of toughness and the crystallinity.

5.2.1 - Correlation between G_{Ic} Values and Crystallinity

The two G_{Ic} initiation values are plotted as a function of crystallinity in Figures 5.6. Error bars are included for both crystallinity and toughness and represent one standard deviation from the mean.

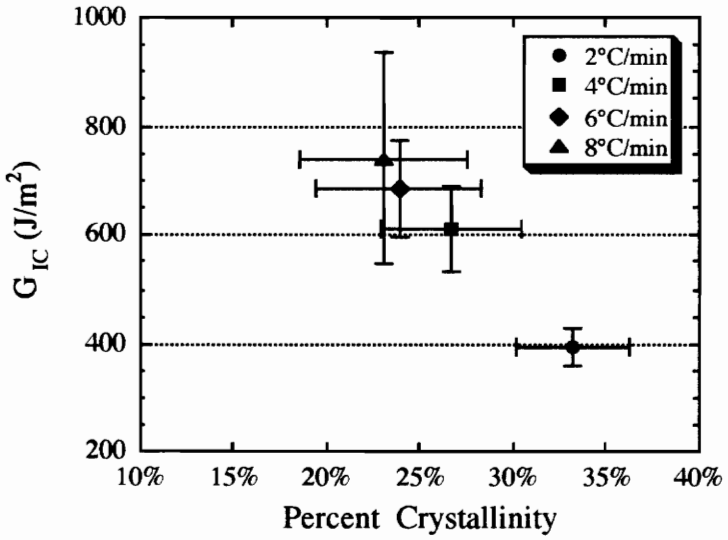

Figure 5.6a: Mean NL G_{Ic} Initiation Values as a Function of Crystallinity

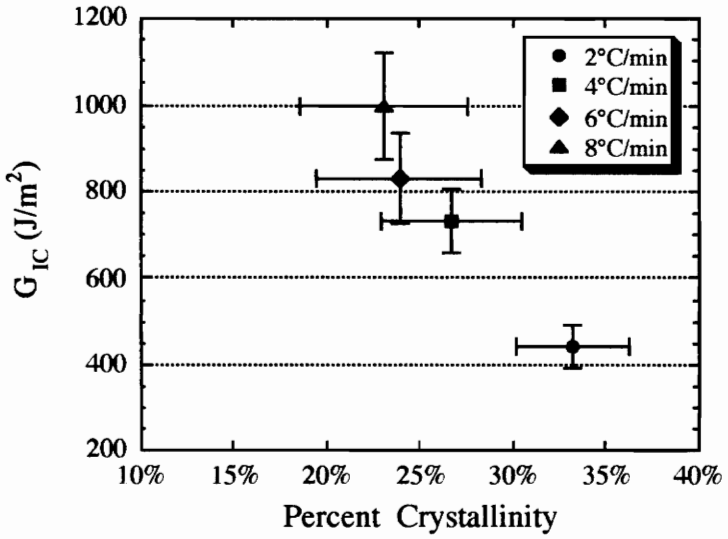

Figure 5.6b: Mean 5%/Max G_{Ic} Initiation Values as a Function of Crystallinity

These plots show that, although there is a considerable amount of scatter in the data, when the data are plotted as a function of crystallinity rather than a function of cooling rate the mean values still fall along a nearly linear path. Figures 5.7 compare the correlation of mode I toughness to crystallinity to the correlation of mode I toughness to cooling rate. These plots do not show the appropriate error bars so that the linear fit to the mean values can be more easily seen. Although the scales of crystallinity and cooling rate are not necessarily equivalent, linear least square curve fits through the data indicate that the correlation of toughness to crystallinity is at least equivalent to the correlation of toughness to cooling rate. This supports the conclusion that it is the crystallinity, rather than some other factor, that is the source of the increase in mode I strain energy release rate with increasing cooling rate. The differences between individual values may not be statistically significant, but the linear relationship between the mean toughness values as a function of crystallinity implies that there is a direct relationship between crystallinity and G_{Ic}.

If the results from the statistical analyses are now compared by comparing Figures 3.4 and 3.5 to Figure 5.3, the order of panel mean G_{Ic} values from smallest to largest is nearly opposite the order of panel mean degree of crystallinity. As mentioned earlier, this is the expected relationship. The order of the panel mean values is the same regardless of which initiation value is considered or whether all available data or only a subset of the data are

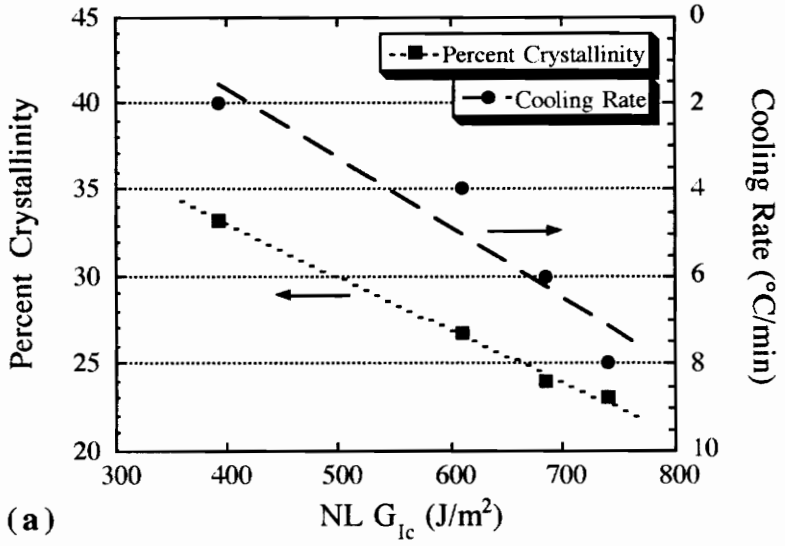

Figure 5.7a: Comparison of the Correlation of NL G_{Ic} Values to Crystallinity to the Correlation of NL G_{Ic} Values to Cooling Rate

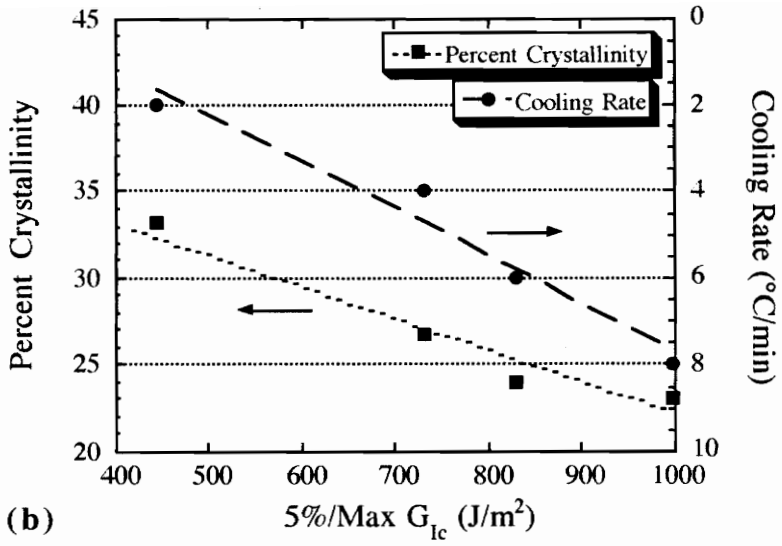

Figure 5.7b: Comparison of the Correlation of 5%/Max G_{Ic} Values to Crystallinity to the Correlation of 5%/Max G_{Ic} Values to Cooling Rate

considered. Unfortunately, the order of the mean values in any of the data sets is not necessarily relevant because many panels were found to have either statistically equivalent crystallinity or statistically equivalent toughness.

Since many values were found to be statistically equivalent, the grouping of statistically equivalent values can also be compared to verify the plausibility of a direct correlation between crystallinity and mode I toughness in these composites. If the differences between crystallinity are not statistically significant and the mode I toughness values are directly dependent upon the crystallinity, then one might expect that the toughness values should also be identified as statistically equivalent. This was the case for both the primary and overall NL G_{Ic} initiation values. Comparison of the groups of equivalent mean NL G_{Ic} initiation values shows that the panels cooled at 4°C/min, 6°C/min, and 8°C/min have both statistically equivalent toughness and statistically equivalent crystallinity.

Unfortunately, even though the groups of equivalent NL G_{Ic} values are identical to the groups of equivalent crystallinities, the same degree of correlation does not exist for the 5%/Max initiation values. The mean primary 5%/Max G_{Ic} value for the panel that was cooled at 8°C/min is statistically larger than the values for the panels cooled at 4°C/min and 6°C/min.

5.2.2 - Correlation between G_{IIc} Values and Crystallinity

The three G_{IIc} initiation values are plotted as a function of crystallinity in Figures 5.8. These plots again show error bars in the form of one standard deviation from the mean for both toughness and crystallinity.

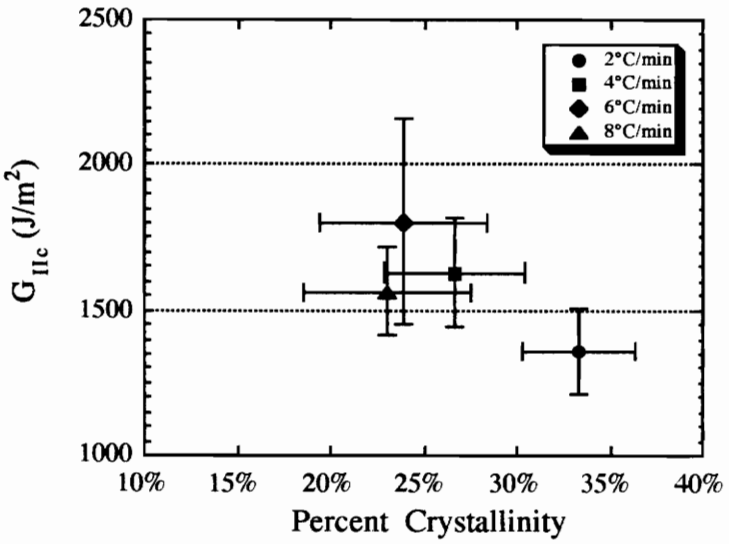

Figure 5.8a: Mean NL G_{IIc} Initiation Values as a Function of Crystallinity

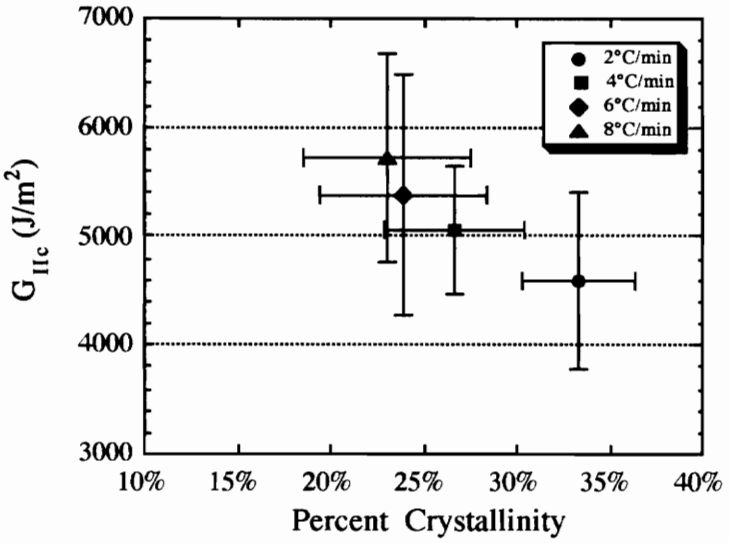

Figure 5.8b: Mean 5% G_{IIc} Initiation Values as a Function of Crystallinity

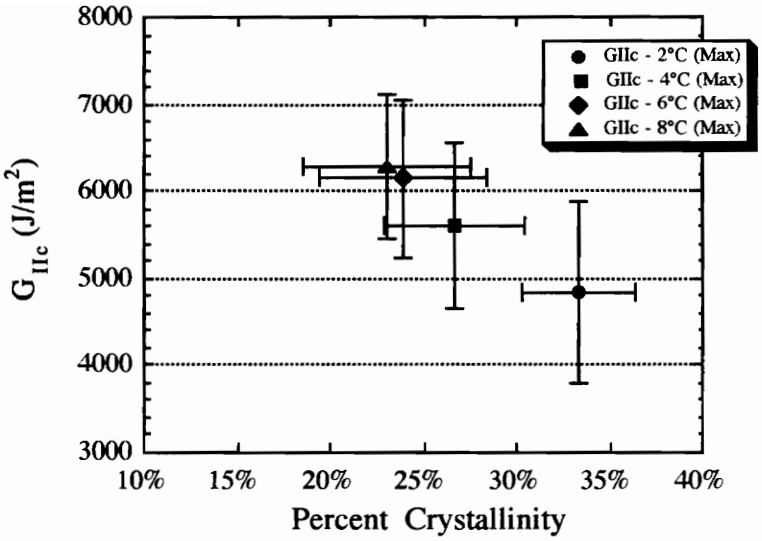

Figure 5.8c: Mean Max G_{IIc} Initiation Values as a Function of Crystallinity

Figures 5.9 compare the correlation of mode II toughness values to crystallinity with the correlation of mode II toughness values to cooling rate. The appropriate error bars are not shown in Figure 5.9b and Figure 5.9c to allow the reader to more easily see the fit of the linear least squares curve through the mean values. The error bars are shown in Figure 5.9a to show that, although a linear fit is not necessarily a good fit in either case, a linear least square curve fit passes through the error bars of all four data points when mode II toughness is plotted as a function of crystallinity. This is not true when the mode II toughness values are plotted as a function of cooling rate. In this case, the linear least squares curve falls beyond the error bars for the NL G_{IIc} value of the panel cooled at 8°C/min.

As mentioned in the discussion of mode I toughness correlation, the scales for crystallinity and cooling rate in these plots are not necessarily equivalent. Nevertheless, linear least square curve fits through the data implies that the relationship between toughness and crystallinity is as least as strong as that between toughness and cooling rate. Even the NL linear data with the seemingly anomalous value for the panel cooled at 8°C/min still supports the trend since the linear fit through the data when plotted as a function of crystallinity is significantly better than the liner fit through the data when plotted as a function of cooling rate.

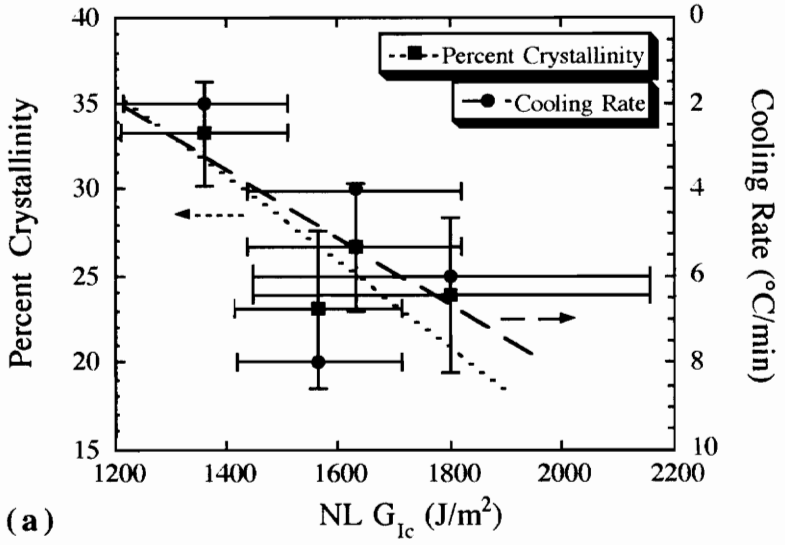

Figure 5.9a: Comparison of the Correlation of NL G_{IIc} Values to Crystallinity to the Correlation of NL G_{IIc} Values to Cooling Rate

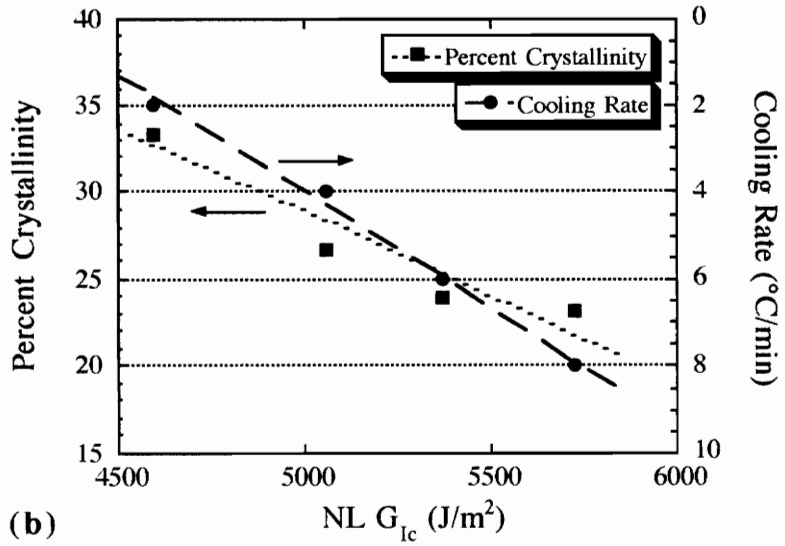

Figure 5.9b: Comparison of the Correlation of 5% G_{IIc} Values to Crystallinity to the Correlation of 5% G_{IIc} Values to Cooling Rate

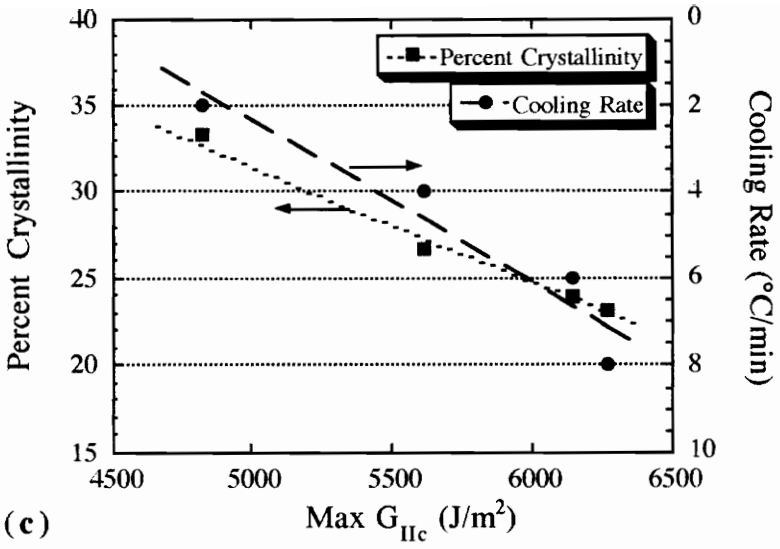

Figure 5.9c: Comparison of the Correlation of Max G_{IIc} Values to Crystallinity to the Correlation of Max G_{IIc} Values to Cooling Rate

The results of the statistical analysis of G_{IIc} values as a function of cooling rate and of crystallinity as a function of cooling rate can again be compared by comparing Figures 4.8, 4.9. and 4.10 to Figure 5.3. This comparison shows that, in general, the order of mean toughness values from smallest to largest are opposite of the order of increasing mean degree of crystallinity. The order of the mean NL G_{IIc} initiation values from smallest to largest when compared to the order of the mean crystallinity values does not follow this trend, but this is the only deviation from the expected sequence. As before, however, the order is not necessarily relevant since many values were shown to be statistically equivalent.

The grouping of statistically equivalent NL data shows that when the panels cooled at 2°C/min and 8°C/min were compared using a multiple range test, these two panels found to have statistically equivalent NL values. If these two values are instead compared individually using a single-tailed t-test, the values are found to be statistically distinct. This discrepancy between the results of the individual comparison and the group comparison is due to the very large standard deviation in the data from the panel cooled at 6°C/min. The individual t-test indicates that even though the multiple range test found the panels cooled at 2°C/min and 8°C/min to have statistically equivalent NL mode II toughness, these values may, in reality, be statistically distinct. This discrepancy between results of the multiple range test and individual t-tests was not repeated for any other grouping.

If the remaining groups of equivalent mean G_{IIc} values are now compared to the group of statistically equivalent crystallinities, the values for the panels cooled at 4°C/min, 6°C/min, and 8°C/min are seen to be equivalent in all cases. In addition, however, the 5% G_{IIc} values for the panels cooled at 2°C/min, 4°C/min, and 6°C/min and the Max G_{IIc} values for the panels cooled at 2°C/min and 4°C/min were also found to be equivalent. This is not surprising since ENF measurements generally result in large amounts of scatter in the data. When there is a large amount of scatter in the data, statistical analysis will identify fewer statistically significant differences. It is encouraging, however, that the panels cooled at 4°C/min, 6°C/min, and 8°C/min were found to be statistically equivalent in all cases. If other panels were found to be statistically equivalent, but these were not, this would indicate that mode II toughness is not necessarily dependent upon crystallinity. Exact correlation of groups of equivalent data can support a theory, but cannot prove it; therefore, the lack of exact correlation in these groups may not corroborate the theory that G_{IIc} is dependent upon crystallinity, but it also does not necessarily disprove the theory.

5.3 - Toughness and Crystallinity in the Panels Initially Cooled at 8°C/min

Statistical comparison of the degree of crystallinity in annealed panel to that in the principal panel cooled at 8°C/min showed that the crystallinity and the mode I strain energy release rates from these two panels were statistically distinct. Mode II strain energy release rates, on the other hand, were found to be statistically equivalent. In the discussion of the principal panels, the toughness was shown to be directly dependent upon the crystallinity. It is apparent that in these two materials the degree of crystallinity was not the only factor which affected their relative toughness.

Figures 5.10 and 5.11 illustrate the differences in mode I toughness and mode II toughness, respectively, as a function of the degree of crystallinity in the two composites. The error bars, as is the convention, represent one standard deviation from the mean for each measured value.

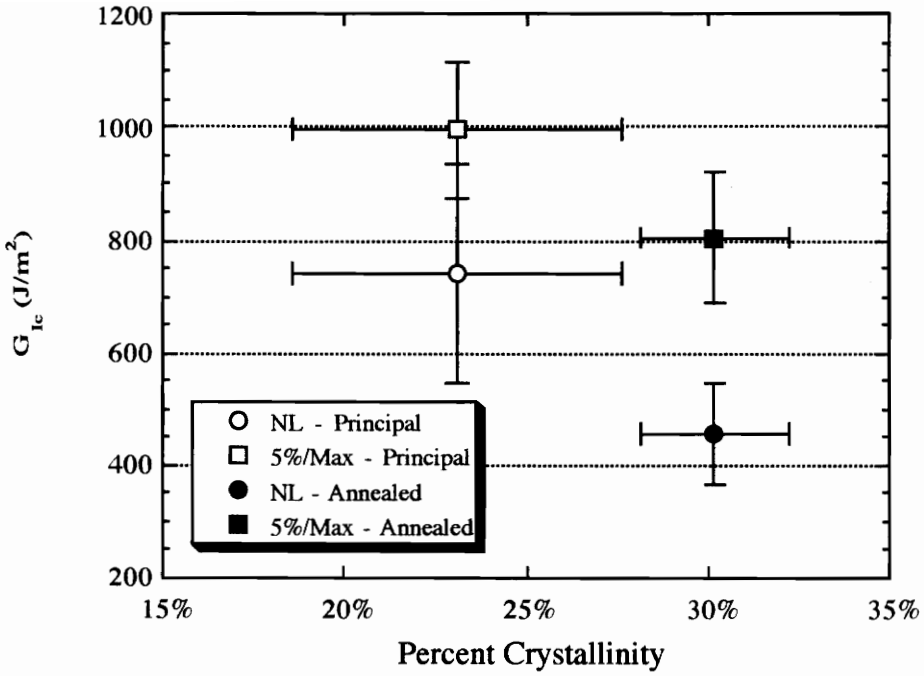

Figure 5.10: Mean G_{Ic} Initiation Values as a Function of Crystallinity for the Two Panels Initially Cooled at 8°C/min

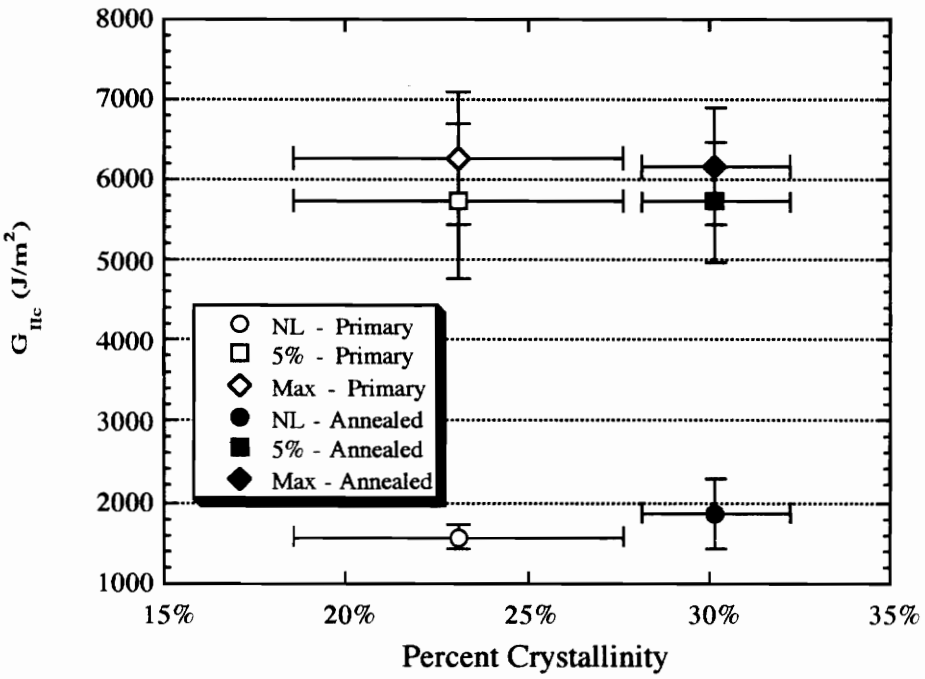

Figure 5.11: Mean G_{IIc} Initiation Values as a Function of Crystallinity for the Two Panels Initially Cooled at 8°C/min

Figure 5.10 indicates that the mode I toughness values decrease as the degree of crystallinity increases, as was expected. The mode II toughness values shown in Figure 5.11, however, do not decrease with increasing crystallinity, even though there is a significant difference in the degree of crystallinity in the two materials. This is in direct contradiction of the trends seen in the data from the principal panels. These two plots imply that there are other factors which are important to the mode II strain energy release rate in annealed PEKK composites.

As mentioned earlier, the three main influences on toughness are degree of crystallinity, state of the amorphous phase, and residual stresses. The degree of crystallinity in the annealed panel and in the principal panel cooled at 2°C/min are statistically equivalent. Consequently, if the degree of crystallinity was wholly responsible for the toughness of the annealed panel, one would expect that the G_{IIc} initiation values from these two panels would also be statistically equivalent. This is not the case. Residual stresses are also unlikely to explain the similarity in mode II toughness of the two panels initially cooled at 8°C/min because the panels are relatively thin and the cooling rates at which both panels were cooled, even after annealing, are on the same order of magnitude. This leaves the state of the amorphous phase of the polymer as a possible source of the greater than expected mode II toughness in the annealed panel.

The state of the amorphous phase of a polymer is largely dependent upon the amount of time that the polymer chains have to attain an equilibrium state. Chain mobility is not significantly restricted until the temperature drops below T_g[26]. Furthermore, the amorphous phase can maintain an equilibrium state for longer periods of time at slower cooling rates[31]. In the annealed panel, the polymer was held above T_g for about 90 minutes. This gave the amorphous regions time to relax and attain a lower energy state before the panel was cooled to room temperature the second time. As a result, it is likely that the energy state of the amorphous phase in the annealed panel would be closer to equilibrium than that of the amorphous material in the corresponding principal panel. Furthermore, the cooling rate progressively decreased after annealing and had reached about 2°C/min by the time the temperature had reached T_g. This would also have allowed more time for the molecules to rearrange before the polymer reached a glassy state in comparison to the time available for the molecules in the principal panel. Consequently, the amorphous material in the annealed panel will have a reduced free volume with respect to the amorphous material in the principal panel[31]. Amorphous material with a lower free

volume will be more brittle than material with a higher free volume[31]. This is not the result seen in this data. As a result, the energy state of the amorphous phase also does not seem capable of explaining the unexpectedly high mode II toughness in the annealed panel.

Although not generally considered as a main factor in the determination of a material's toughness, the microstructure of a composite could be responsible for the higher than expected mode II toughness in the annealed composite. Differences in the microstructure of these two panels are implied by their respective DSC curves. The annealed panel DSC scans show a secondary melting peak that occurs at a temperature below the larger primary peak. This is illustrated in the representative DSC curve provided as Figure 5.1e. Other work has shown that this peak could be due to a small population of imperfect crystals which will melt just above their formation temperature[10]. Formation of crystals with a low melting point is typical during annealing of polymers[38]. The existence of a cold crystallization peak in the DSC curve for a specimen from the principal panel cooled at 8°C/min as shown in Figure 5.1d supports the premise that the PEKK will crystallize during an annealing stage. The existence of the cold crystallization peak indicates that the amorphous polymer in a panel cooled at 8°C/min can readily crystallize once the polymer reaches a high enough energy state.

Results reported in the literature support the theory that there are microstructural differences between the principal panel and the annealed panel. In PEKK, the type of unit cell structure that is formed is dependent upon the whether the polymer is melt crystallized or cold crystallized[14]. The unit cell structure that forms during cold crystallization is a less stable structure[14] and has been shown to result in high levels of disorder in the resulting spherulites[12]. Highly disordered spherulites and imperfect crystals between spherulitic lamella would both act to decrease the stiffness and, therefore, increase the toughness of the polymer. Nevertheless, annealing also causes crystallites to thicken[8]. Thicker lamella and larger spherulites result in low strain-to-failure and lower toughness. The data would, however, seem to indicate that lamellar thickening is not a concern in these materials, but there is no data to support this supposition. These conflicting microstructural effects do not yield a clear indication of the underlying dependence of mode II toughness on microstructure. Consequently, further investigation will be necessary to determine what factor is responsible for the annealed panel and cooled-only panel having equivalent mode II toughness with different degrees of crystallinity.

5.4 - Toughness and Crystallinity in the Panels Cooled at 4°C/min

Statistical comparison of the principal panel cooled at 4°C/min and the panel made with recovered polymer showed that the degree of crystallinity and the mode I interlaminar fracture toughness values were statistically equivalent. The mode II interlaminar fracture toughness values of these two panels were found to be nearly statistically distinct. This is similar to the results found in the comparison of the principal panel that was cooled at 8°C/min and the annealed panel. In this case, however, the panel made from recovered polymer had lower than expected mode II toughness. Once again it appears as though the degree of crystallinity is not the only factor which controls the relative mode II toughness in PEKK composites.

Figures 5.12 and 5.13 illustrate the differences in mode I toughness and mode II toughness, respectively, with respect to the degree of crystallinity in the principal panel cooled at 4°C/min and the panel made with recovered polymer. The error bars represent one standard deviation from the mean for each measured value.

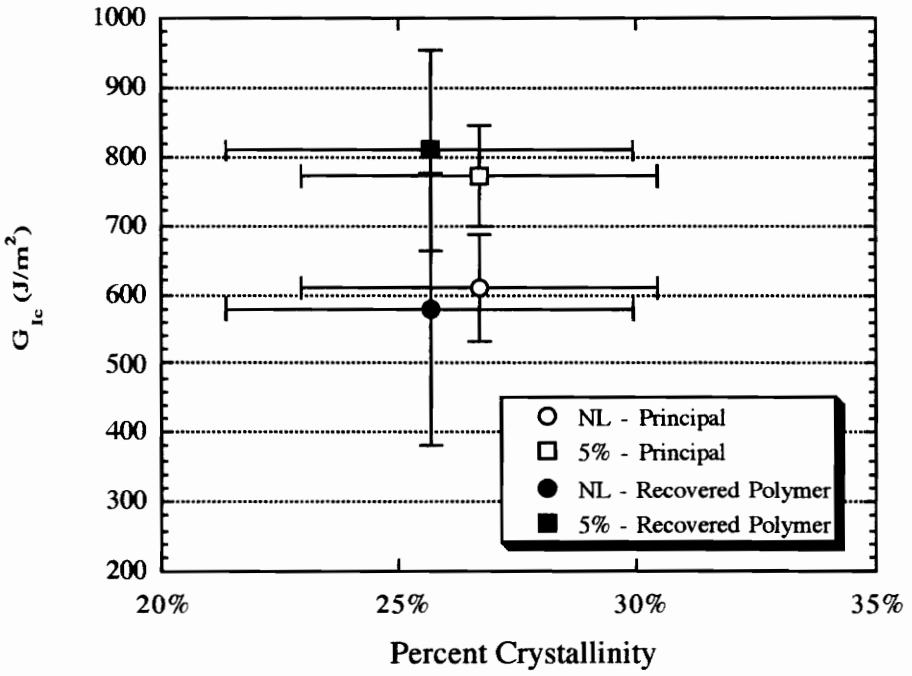

Figure 5.12: Mean G_{Ic} Initiation Values as a Function of Crystallinity for the Two Panels Cooled at 4°C/min

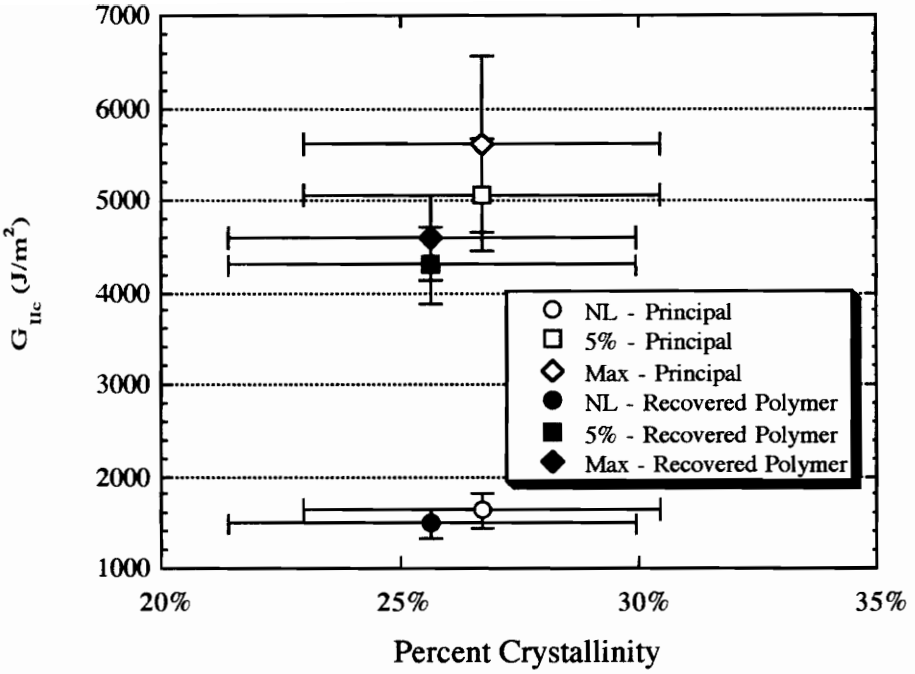

Figure 5.13: Mean G_{IIc} Initiation Values as a Function of Crystallinity for the Two Panels Cooled at 4°C/min

Any conclusions drawn from these two figures must take into consideration that the degree of crystallinity in these two panels is statistically equivalent. As a result, the toughness values, if those values were based entirely on the degree of crystallinity, should also be statistically equivalent. This is the case for the mode I values. The mode II toughness values from the panel made with recycled polymer, on the other hand, were considerably lower than the values from the corresponding principal panel. Although there was not quite enough data to conclusively prove that composites made with recovered polymer will consistently have a lower mode II toughness than composites made with new polymer, the difference that does exist should be acknowledged. If this difference could be verified, this would indicate that other factors besides the degree of crystallinity will affect the mode II toughness in composite made with the recovered polymer.

If the degree of crystallinity cannot completely account for the measured toughness of these two composites, then the other two other main influences, the state of the amorphous polymer and the residual stresses, should also be considered. As was discussed for the annealed panel, it is unlikely that residual stresses are the source of the substantial, but not

statistically significant, difference in mode II toughness of these two panels. All six panels are relatively thin and therefore the residual stresses in the composites should be relatively small. Furthermore, since both panels currently under consideration were cooled at the same cooling rate, the residual stresses and energy state of the amorphous phase should be nearly identical. As a result, none of the three main influences on toughness can explain entirely why composite made with polymer recovered from the air cleaner might have a lower mode II toughness than composite made with unused polymer.

This again leaves microstructural differences as a possible source for the differences in mode II toughness. If there is a higher heterogeneous nucleation density in the recovered polymer, this would result smaller spherulites[36]. Smaller spherulites have been shown to increase the modulus of the material[8]. This could explain the results seen in Figures 4.12 and 5.13. There is, however, no physical evidence to support this supposition. Consequently, further examination of both the mode II toughness and the microstructural characteristics of composites made with reused polymer powder as compared to composites made with previously unused polymer is warranted.

Chapter 6 - Conclusions and Recommendations

The main objectives of this research were to investigate mode I and mode II strain energy release rates for poly(ether ketone ketone) (PEKK)/carbon composites and to identify the relationship, if any, between crystallinity and toughness in these materials. Four principal panels were manufactured and tested to achieve these objectives. The panels were fabricated using dry powder impregnated towpreg. The panels were processed in a hot press and cooled at a controlled rate of either 2°C/min, 4°C/min, 6°C/min, or 8°C/min. Two additional panels were manufactured to investigate the affect of annealing the composite and the affect of reusing polymer that had collected in the air cleaner of the dry powder towpreg fabrication system. After processing each panel was cut into ten specimens and each specimen was tested as both a double cantilever beam specimen and as an end notch flexure specimen. Strain energy release rates for both mode I and mode II fracture were then calculated. A number of conclusions can be drawn from the available data, but there are also several areas which require further investigation.

6.1 - Conclusions from Present Work

Although fiber bridging did occur to some extent in all sixty specimens during double cantilever beam testing, the comparison of G_{Ic} initiation values from specimens which showed substantial fiber bridging to values from specimens which showed minor fiber bridging was inconclusive. As a result, more conservative G_{Ic} initiation values were calculated using only the specimens from each panel which exhibited minor fiber bridging. These values were reported with 5% confidence intervals in Table 3.8.

The degree of correlation between measured compliances and theoretical compliances in end notch flexure (ENF) testing was shown to have no affect on the measured mode II toughness. This indicated that inclusion of all available data in the computation of mean G_{IIc} initiation values would not result in bias of the values. Consequently, the values reported in Table 4.9 for G_{IIc} initiation values of G30-500/PEKK composites were calculated using all available ENF data.

Both mode I and mode II strain energy release rates from the four principal panels were found to be significantly lower than analogous values in poly(ether ether ketone) (PEEK) matrix composites. This was not surprising, however, since strain energy release

rates for neat PEKK have been shown to be about half of those for neat PEEK. Additionally, changes in many other factors, including molecular weight of the polymer, chain packing, fiber-matrix adhesion, and nucleation density of both the polymer and fiber, would alter the measured strain energy release rates. The G_{Ic} initiation values and the G_{IIc} initiation values in these G30-500/PEKK composites were found to be 30% to 50% of the analogous values in carbon/PEEK composites. As a result, it is reasonable to consider that the values reported in Table 3.8 and Table 4.9 are representative strain energy release rates for a 60% fiber volume fraction PAN-based carbon/PEKK composite.

Comparison of G_{Ic} and G_{IIc} values from the principal panels when plotted as a function of cooling rate to those same values when plotted as a function of crystallinity showed that the relationship between toughness and crystallinity is at least as strong as the relationship between toughness and cooling rate. This was true for both the G_{Ic} data and the G_{IIc} data. In many cases, however, the differences between the toughness or crystallinity of two or more panels could not be identified as statistically significant because there was a substantial amount of scatter in the data. Nonetheless, a trend of increasing toughness with decreasing crystallinity was evident. Although toughness in a polymer matrix composite can also be affected by residual stresses and the state of the amorphous material, the relatively small differences in cooling rates used in this study diminish the possibility that there are significant differences between the magnitudes of either of these two factors in the four principal panels. These considerations and the good correlation seen between toughness and crystallinity indicates that the differences in toughness were a result of the degree of crystallinity in the composites and not some other factor cooling rate dependent factor.

The degree of crystallinity appeared to have a more significant effect on mode I strain energy release rates than on mode II rates. When the cooling rate was increased by a factor of two from 2°C/min to 4°C/min, the mean degree of crystallinity decreased by 6.6%, the mean NL G_{Ic} initiation value increased by 204 J/m^2, and the mean 5%/Max G_{Ic} initiation value increased by 321 J/m^2. When the cooling rate was increased by another factor of two from 4°C/min to 8°C/min, the mean degree of crystallinity decreased by another 3.6%, the mean NL G_{Ic} initiation value increased by another 112 J/m^2, and the mean 5%/Max G_{Ic} initiation value increased by another 171 J/m^2. The change in each value when the cooling rate was increased from 4°C/min to 8°C/min was 54.5%, 56%, and 53%, respectively, of the change that occurred when the cooling rate was increased from 2°C/min to 4°C/min.

Although there is uncertainty in the mean values, the fact that the increase in mean toughness was proportional to the increase in mean crystallinity reinforces conclusion that mode I toughness was directly dependent on crystallinity. The increase in mode II toughness values was not, however, proportional to the increase in crystallinity, even though the mode II toughness values did appear to be directly dependent upon crystallinity when the data were plotted.

This implied stronger dependency of mode I toughness on crystallinity seems to be supported by the comparison of the principal panel cooled at 8°C/min to the annealed panel. The degree of crystallinity and mode I toughness values of these two panels were shown to be statistically distinct. The crystallinity in the annealed panel was much greater than the degree of crystallinity in the principal panel. Accordingly, both G_{Ic} initiation values from the annealed panel were much smaller than the G_{Ic} initiation values from the corresponding principal panel. The mode II toughness values from the two panels were, however, statistically equivalent. If the mode II toughness had the same degree of dependency on crystallinity as mode I toughness, then one would expect to see equivalent changes in G_{Ic} and G_{IIc} initiation values. Since the G_{IIc} values were equivalent for the two panels, while the G_{Ic} values were not, this indicates that some factor other than crystallinity was also important in determining mode II toughness.

The stronger dependency of mode I toughness on crystallinity also seems to be supported by the comparison of the principal panel cooled at 4°C/min to the panel made with polymer that was recovered from the dry powder prepreg fabrication system's air cleaner. In these two panels, both the degree of crystallinity and mode I toughness values were shown to be statistically equivalent. The mode II toughness values from the panel made with recovered polymer, however, were found to be substantially lower than the mode II values from the analogous principal panel. As mentioned earlier, if the two modes of toughness had the same degree of dependence on crystallinity, the comparison of the data from the two panels should either be equivalent or distinct for both modes. The fact that the mode I values of these two panels were found to be equivalent while the mode II values were found to be substantially different again suggested that different factors affect the two modes of toughness to different extents.

6.2 - Recommendations for Future Work

Although mode I toughness seemed to be more strongly dependent upon crystallinity than mode II toughness, there was no physical evidence to justify this difference in degree of dependency. Toughness can be dependent upon the composite residual stresses, but the geometry of these composites made residual stresses unlikely to be a major factor in this particular study. Even if the residual stresses could have been shown to have a significant effect on the toughness in these materials, the range of cooling rates used in this study was sufficiently small so the change in relative toughness of the six panels as a result of changes in residual stresses should have also been small. Two other factors which could have influenced the toughness of carbon/PEKK composites were the energy state of the amorphous phase and the microstructural characteristics of the polymer. There may also, however, have been other factors, such as chemical degradation or fiber/matrix adhesion, that could have been responsible for the trends in toughness that were found in this study, but only the two factors mentioned above were considered.

The issues of chemical degradation and fiber/matrix adhesion were not considered because they are not expected to have significantly affected the properties of these materials. If chemical degradation had occurred, one would expect that the crystallinity would have decreased in the panels cooled at a slow cooling rate, especially the panel cooled at 2°C/min, due to degradation of the chains. This, however, was not the case. Chemical analysis was not completed, so chemical degradation of the polymer cannot be conclusively ruled out. Nevertheless, the inferential evidence provided by the crystallinity indicates that it is unlikely that the polymer matrix was significantly degraded during processing. The only panel in which fiber/matrix adhesion could be expected to have changed significantly is the panel made with polymer that was recovered from the air cleaner of the towpreg manufacturing system. There is no reason to believe that the fiber/matrix adhesion would be different in the other panels simply because the panels were manufactured from effectively identical towpreg. Since the panel made from recovered polymer was manufactured primarily to verify whether using recovered polymer will affect the properties of the composite, changes in fiber/matrix adhesion were not addressed. These two concerns could be addressed in future work.

The effect of the energy state of the amorphous phase of the polymer could be examined through a more extensive study on the effect of annealing. Annealing changes the degree of deviation from equilibrium of the amorphous regions; therefore, a more comprehensive study would be beneficial to help discriminate between the various changes that can occur as a result of changes in the cooling rate. The cooling rate of the panel in this study was controlled during cooling from the melt, but was not controlled after annealing. This means that the state of the amorphous phase was coupled to the degree of crystallinity and the morphology of the crystalline phase. To better understand the effects of each factor, six panels could be manufactured at two different cooling rates, e.g. 2°C/min and 8°C/min. Four of those panels, two from each cooling rate, could then be annealed using controlled cooling rates of 2°C/min and 8°C/min. The six panels would then have thermal histories of 2°C/min, 2°/2°C/min, 2°/8°C/min, 8°C/min, 8°/2°C/min, and 8°/8°C/min, where the first rate specifies the rate at which the panel is cooled from the melt and the second rate, if any, specifies the rate at which the panel is cooled after annealing. In addition, it would be beneficial to perform ENF tests a second time after several months of physical aging at room temperature to determine whether the differences in toughness seen in these specimens are a permanent or transitory attribute of the composite.

The effect of differences in the microstructural characteristics of the crystalline phase of the polymer could be investigated through a combination of optical and electron microscopy. Optical microscopy using crossed polars would allow easy identification of the size of spherulites, while electron microscopy can identify the size of lamella within spherulites. A study of this type would work well in tandem with the study outlined above because the microstructure could be correlated to the thermal history.

Before any further investigation into the reason that the panel made with recovered polymer had substantially lower G_{IIc} values than the analogous composite made with previously unused polymer, a second set of panels should be manufactured and tested to verify the results from this study. In the analysis of a second set of panels, the panel made with recovered polymer could be assumed to have lower mode II interlaminar fracture toughness. If the mean values and the variance in the new data is equivalent to those values from this study, the differences then could be declared statistically significant.

If testing of a second set of panels made from unused and recovered polymer confirms the implied difference in mode II toughness shown in the analogous panels in this study, a study of the effect of microstructural characteristics on mode II toughness values would then also be warranted. Both the recovered polymer and the unused polymer should be tested for impurity content, since an increase in heterogeneous nucleation sites can significantly affect the microstructure of the composite. A combination of optical and electron microscopy, such as that discussed earlier, could then provide the evidence necessary to determine what microstructural differences might affect the toughness in the composite. If the difference in mode II toughness is substantiated, shown to be a result of increased population of heterogeneous nucleation sites, and determined to be undesirable, the polymer might still be able to be reused if an air purification system was added to the dry powder prepregging system. This, however, would be expensive and would add complexity to both the operation and maintenance of the system. This option should be avoided if possible.

Appendix A - Double Cantilever Beam Data

Panel Fiber Volume Fraction

Table A1: Panel Fiber Volume Fraction Calculations

Panel	2	4	6	8	8A	4R
FVF by Density Calculation	58.2%	58.3%	59.0%	57.2%	57.7%	58.5%
FVF by Areal Weight	61.7%	61.5%	63.0%	62.6%	61.2%	62.0%
Avg FVF	60.2%	59.9%	61.0%	59.9%	59.5%	60.2%

Specimen Dimensions

Table A2.1: Specimen Dimensions and Crack Length For the Panel Cooled at 2°C/min

Specimen	2-1	2-2	2-3	2-4	2-6	2-7	2-8	2-10
Avg Width (mm)	12.63	12.63	12.62	12.64	12.65	12.64	12.65	12.64
Avg Thickness (mm)	3.18	3.16	3.16	3.16	3.16	3.17	3.16	3.17
Avg Crack Length (mm)	39.52	36.68	39.26	37.05	36.47	36.44	36.20	36.38

Table A2.2: Specimen Dimensions and Crack Length For the Panel Cooled at 4°C/min

Specimen	4-1	4-2	4-3	4-4	4-6	4-7	4-8	4-9	4-10
Avg Width (mm)	12.64	12.65	12.66	12.64	12.66	12.66	12.64	12.66	12.66
Avg Thickness (mm)	3.22	3.21	3.20	3.19	3.18	3.18	3.17	3.17	3.16
Avg Crack Length (mm)	34.53	34.29	34.24	34.16	34.58	35.03	35.20	35.65	36.13

Table A2.3: Specimen Dimensions and Crack Lengths For the Panel Cooled at 6°C/min

Specimen	6-1	6-2	6-3	6-4	6-5	6-6	6-7	6-8	6-9	6-10
Avg Width (mm)	12.57	12.65	12.65	12.65	12.64	12.64	12.63	12.63	12.64	12.62
Avg Thickness (mm)	3.12	3.11	3.10	3.10	3.08	3.09	3.09	3.08	3.09	3.09
Avg Crack Length (mm)	37.76	37.44	37.61	37.57	37.69	37.63	37.35	36.69	36.85	37.06

Table A2.4: Specimen Dimensions and Crack Lengths For the Panel Cooled at 8°C/min

Specimen	8-1	8-2	8-3	8-4	8-5	8-6	8-7	8-8	8-9	8-10
Avg Width (mm)	12.62	12.62	12.62	12.63	12.63	12.63	12.64	12.64	12.64	12.62
Avg Thickness (mm)	3.15	3.14	3.14	3.12	3.11	3.10	3.09	3.08	3.09	3.08
Avg Crack Length (mm)	36.05	35.97	35.53	35.77	35.46	35.85	36.28	35.99	36.15	36.40

Table A2.5: Specimen Dimensions and Crack Lengths For the Panel Cooled at 8°C/min and Then Annealed

Specimen	8A-1	8A-2	8A-3	8A-4	8A-5	8A-6	8A-7	8A-8	8A-9	8A-10
Avg Width (mm)	12.63	12.65	12.64	12.65	12.65	12.63	12.64	12.64	12.63	12.64
Avg Thickness (mm)	3.25	3.23	3.20	3.21	3.18	3.19	3.18	3.19	3.18	3.19
Avg Crack Length (mm)	38.02	38.02	38.01	38.25	38.18	38.24	38.21	37.93	37.82	37.66

Table A2.6: Specimen Dimensions and Crack Lengths For the Panel Made With Recovered Polymer and Cooled at 4°C/min

Specimen	4R-1	4R-2	4R-3	4R-4	4R-5	4R-6	4R-7	4R-8	4R-9	4R-10
Avg Width (mm)	12.65	12.66	12.65	12.64	12.68	12.64	12.65	12.64	12.63	12.62
Avg Thickness (mm)	3.21	3.18	3.17	3.15	3.15	3.14	3.14	3.15	3.14	3.15
Avg Crack Length (mm)	35.24	35.52	35.53	35.63	36.19	36.00	36.07	36.32	36.39	36.76

Modified Beam Theory Intercept Values

Table A3: Intercept Values Calculated for Each Valid Specimen

Specimen	1 (mm)	2 (mm)	3 (mm)	4 (mm)	5 (mm)	6 (mm)	7 (mm)	8 (mm)	9 (mm)	10 (mm)
2°C/min	6.46	6.05	-0.39	3.71		5.27				2.15
4°C/min	0.94	-0.23	2.51	3.78		1.52	0.87	6.42	0.71	
6°C/min		-0.60	1.16	1.28		0.19	0.00	0.00	5.37	1.71
8°C/min	2.13	4.57	2.76	4.86		1.69	4.80	1.61	1.72	7.49
8°C/min (A)	1.27	3.45	-0.16	3.25	0.00			1.65	1.96	3.11
4°C/min (R)	2.80	1.05	0.13	0.00	1.36	0.12	1.01	0.00	0.00	1.84

Loading Curves

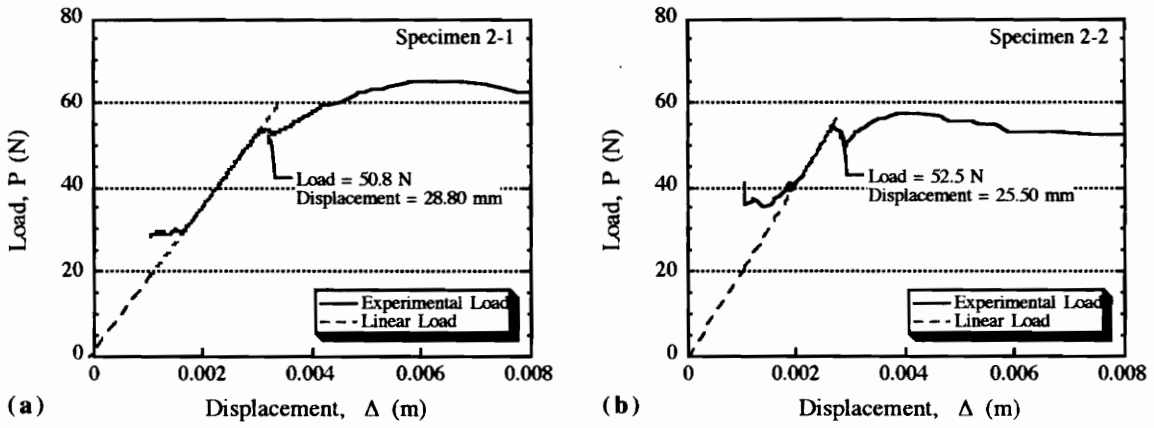

Figures A1.1: Load-Displacement Curves for Specimens from the Principal Panel Cooled at 2°C/min
a) Specimen 2-1, b) Specimen 2-2

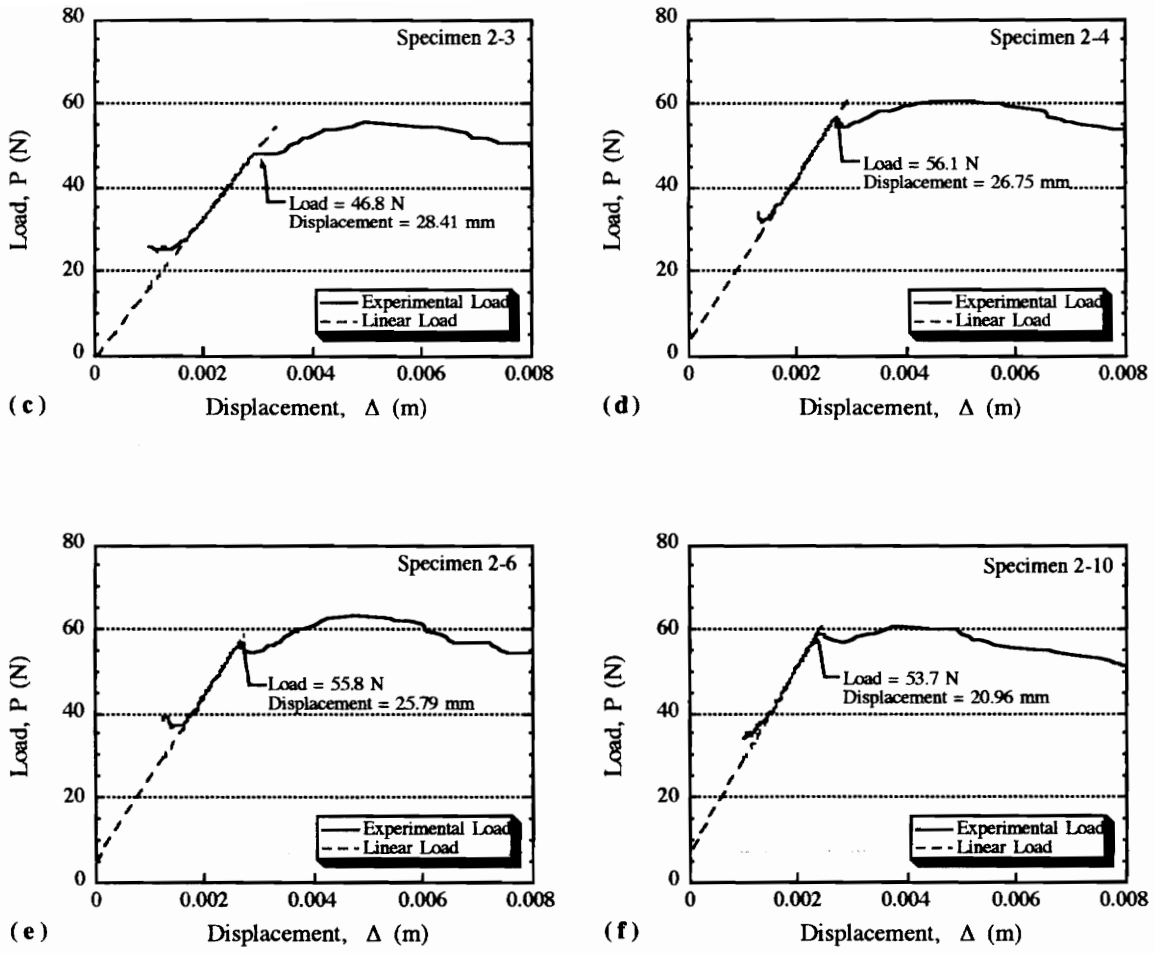

Figures A1.1 (continued) : Load-Displacement Curves for Specimens from the Principal Panel Cooled at 2°C/min
c) Specimen 2-3, d) Specimen 2-4,
e) Specimen 2-6, and f) Specimen 2-10

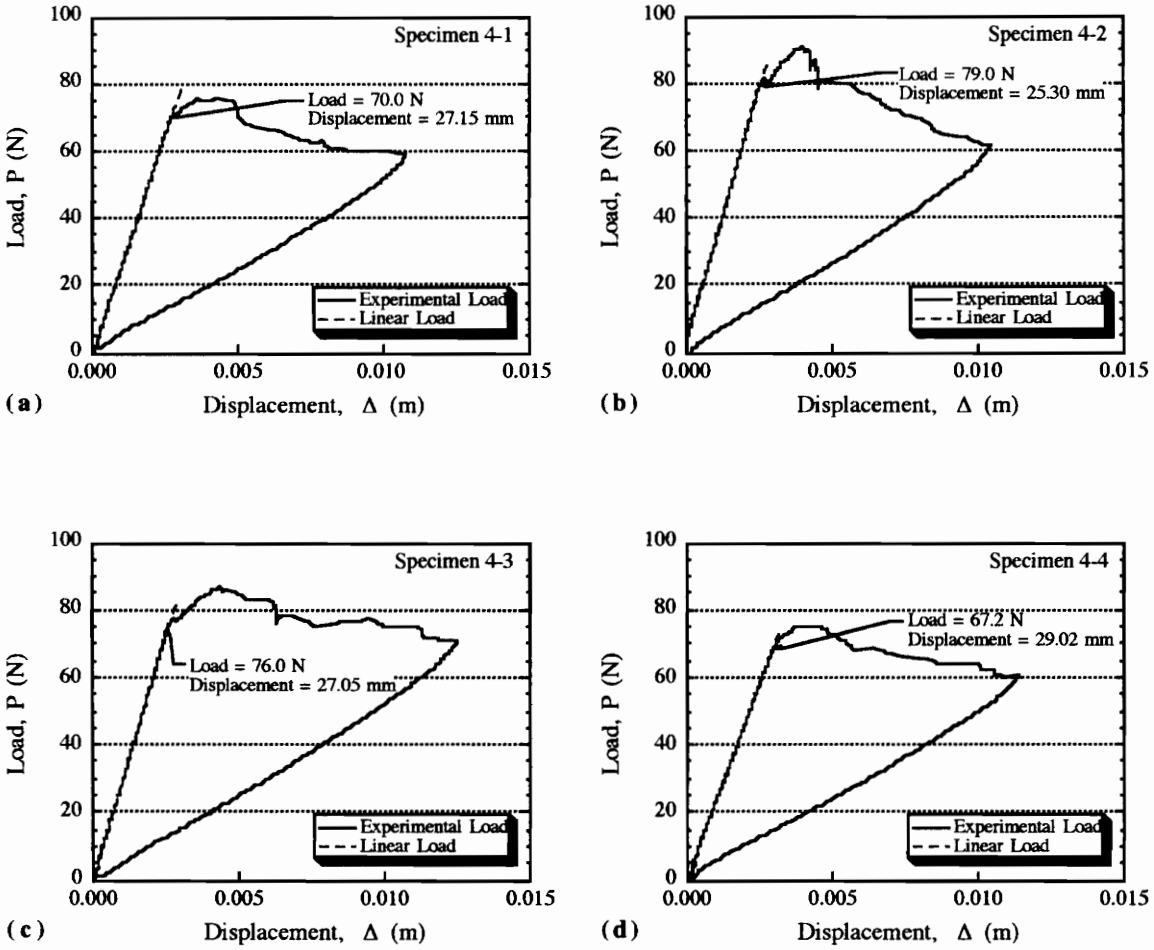

Figures A1.2: Load-Displacement Curves for Specimens from the Principal Panel Cooled at 4°C/min
a) Specimen 4-1, b) Specimen 4-2,
c) Specimen 4-3, and d) Specimen 4-4

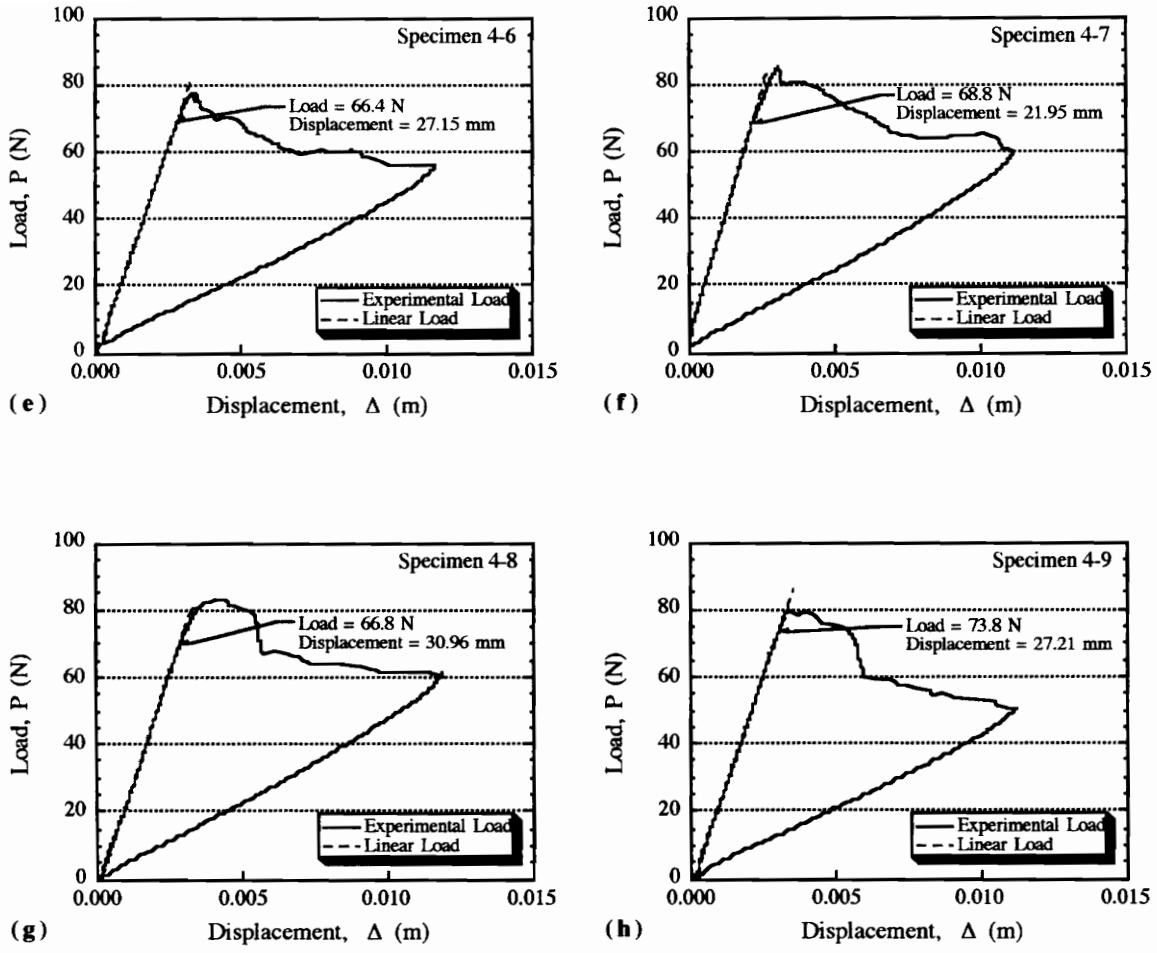

Figures A1.2 (continued): Load-Displacement Curves for Specimens from the Principal Panel Cooled at 4°C/min
e) Specimen 4-6, f) Specimen 4-7,
g) Specimen 4-8, and h) Specimen 4-9

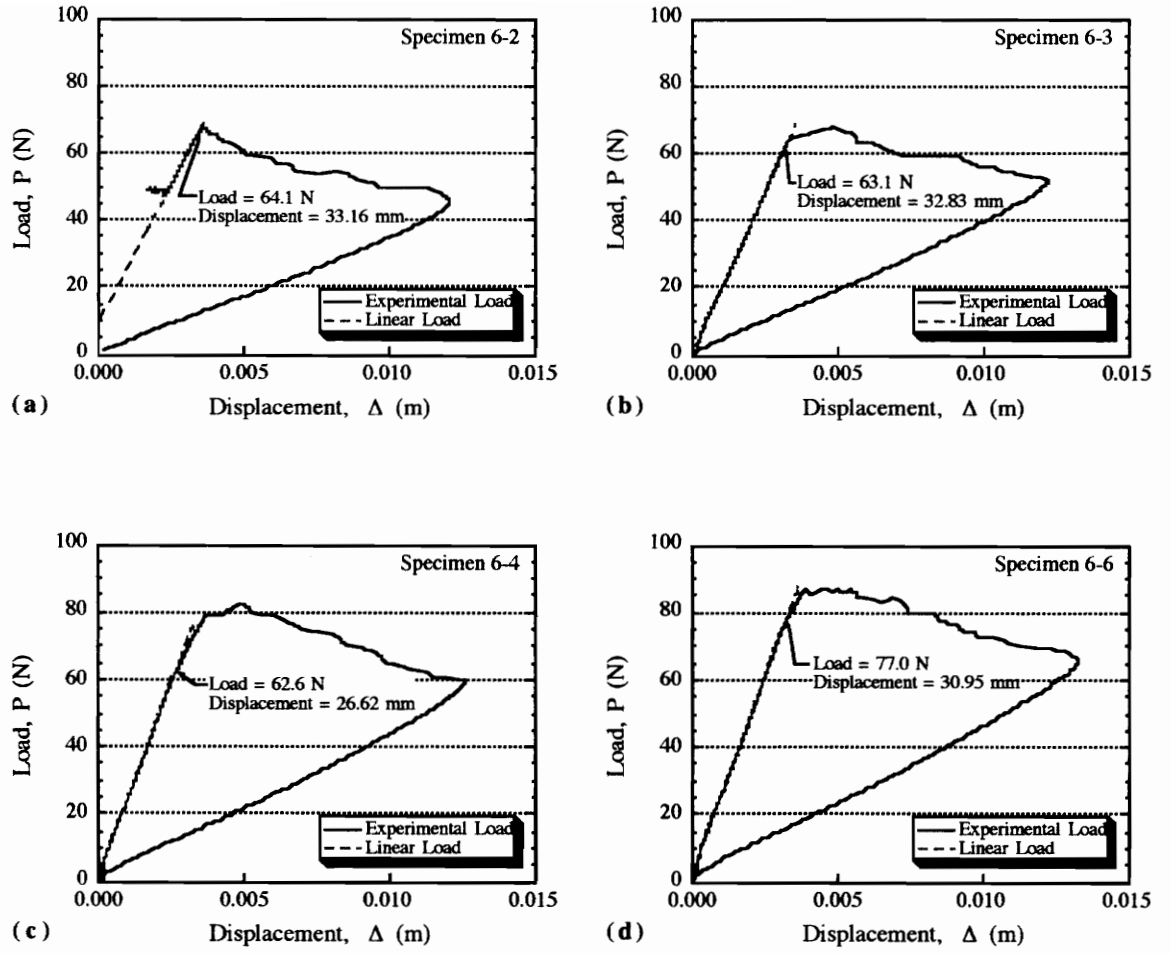

Figures A1.3: Load-Displacement Curves for Specimens from the Principal Panel Cooled at 6°C/min
a) Specimen 6-2, b) Specimen 6-3,
c) Specimen 6-4, and d) Specimen 6-4

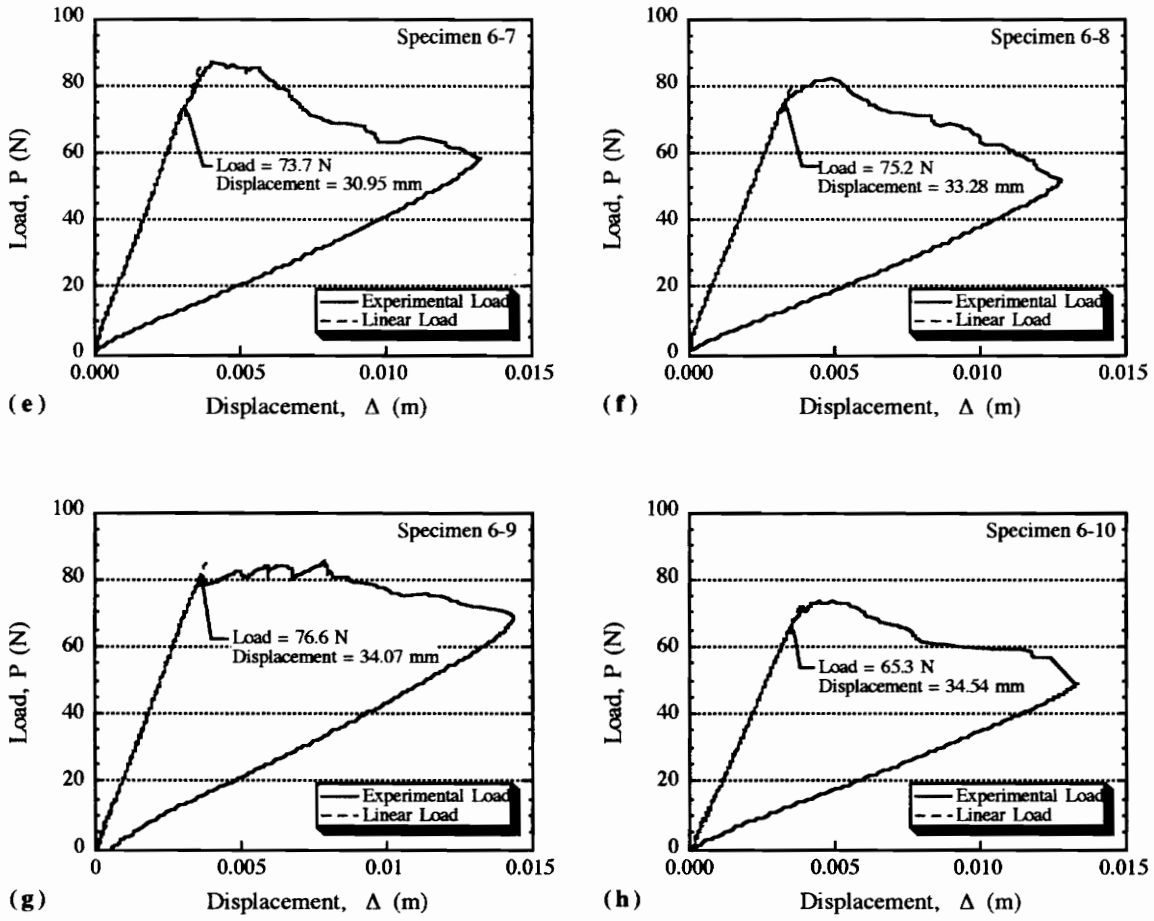

Figures A1.3 (continued): Load-Displacement Curves for Specimens from the Principal Panel Cooled at 6°C/min
e) Specimen 6-7, f) Specimen 6-8,
g) Specimen 6-9, and h) Specimen 6-10

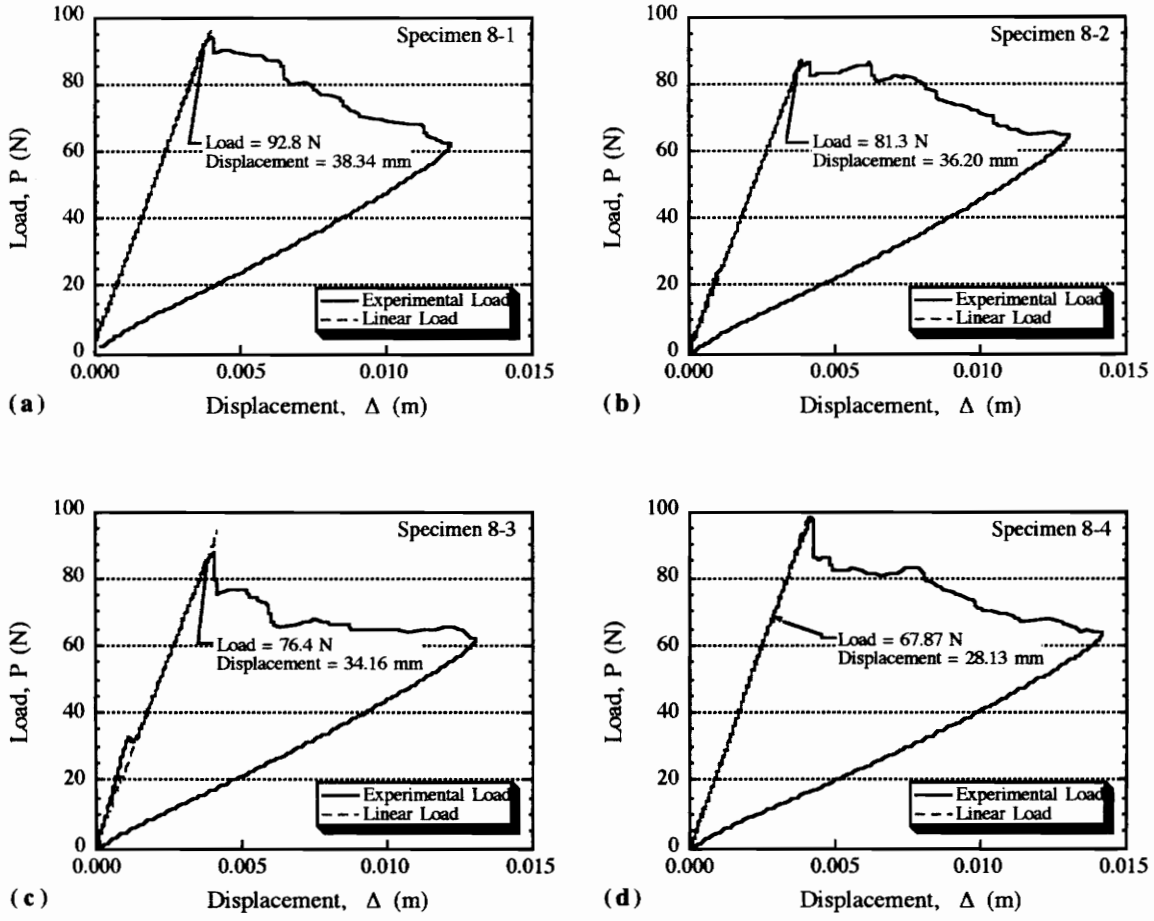

Figures A1.4: Load-Displacement Curves for Specimens from the Principal Panel Cooled at 8°C/min
a) Specimen 8-1, b) Specimen 8-2,
c) Specimen 8-3, and d) Specimen 8-4

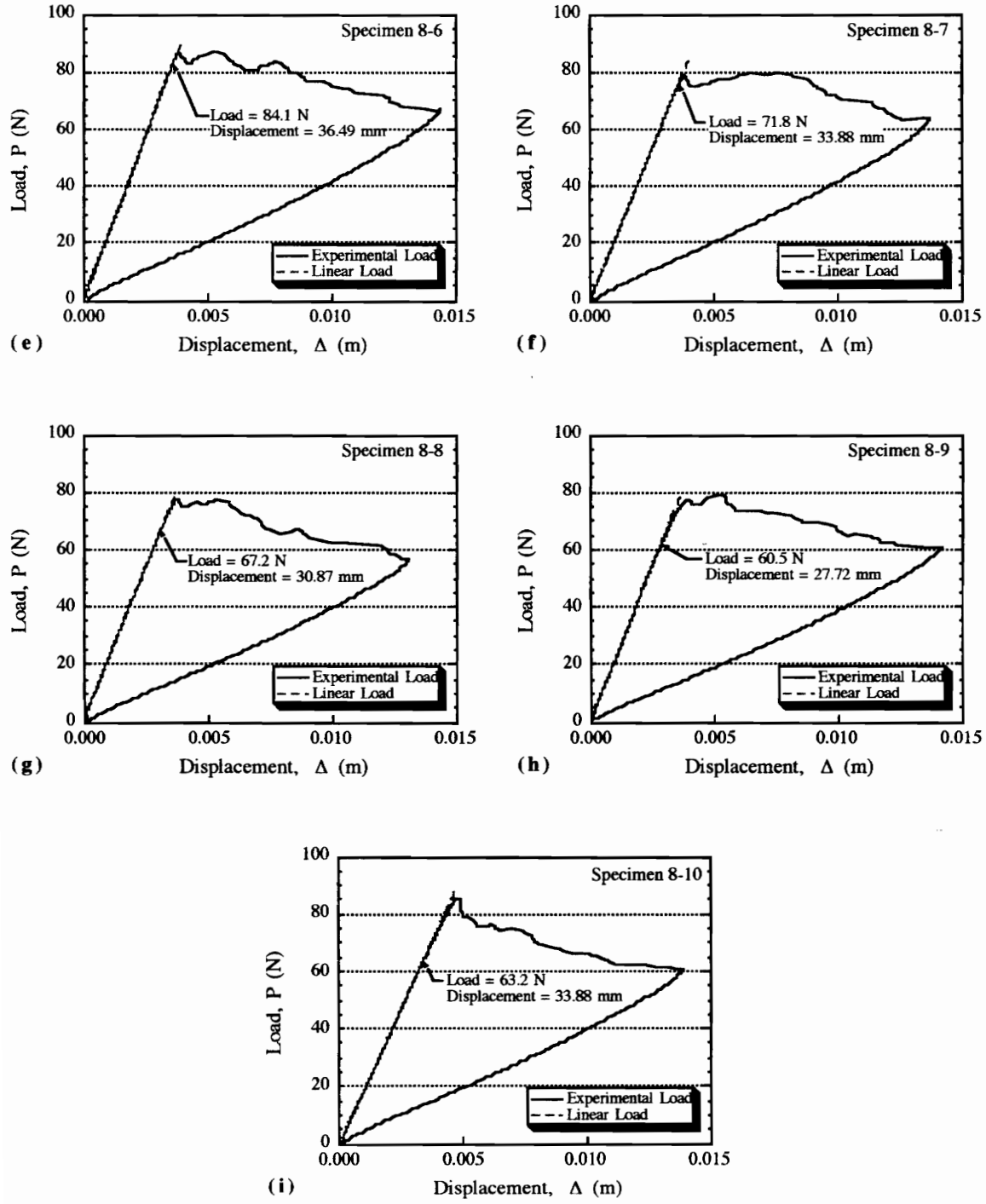

Figures A1.4 (continued): Load-Displacement Curves for Specimen from the Principal Panel Cooled at 8°C/min
e) Specimen 8-6, f) Specimen 8-7, g) Specimen 8-8,
h) Specimen 8-9, and i) Specimen 8-10

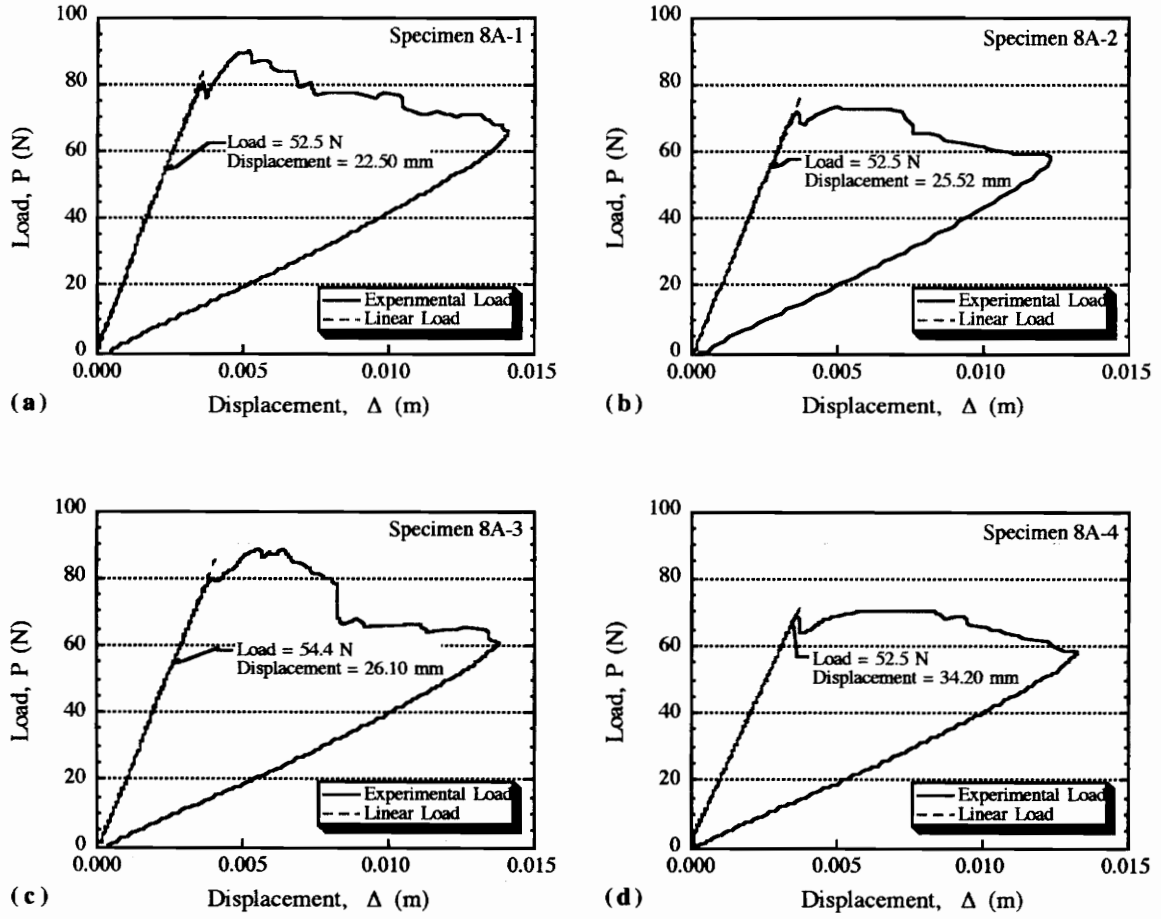

Figures A1.5: Load-Displacement Curves for Specimens from the Panel Cooled at 8°C/min and then Annealed a) Specimen 8A-1, b) Specimen 8A-2, c) Specimen 8A-3, and d) Specimen 8A-4

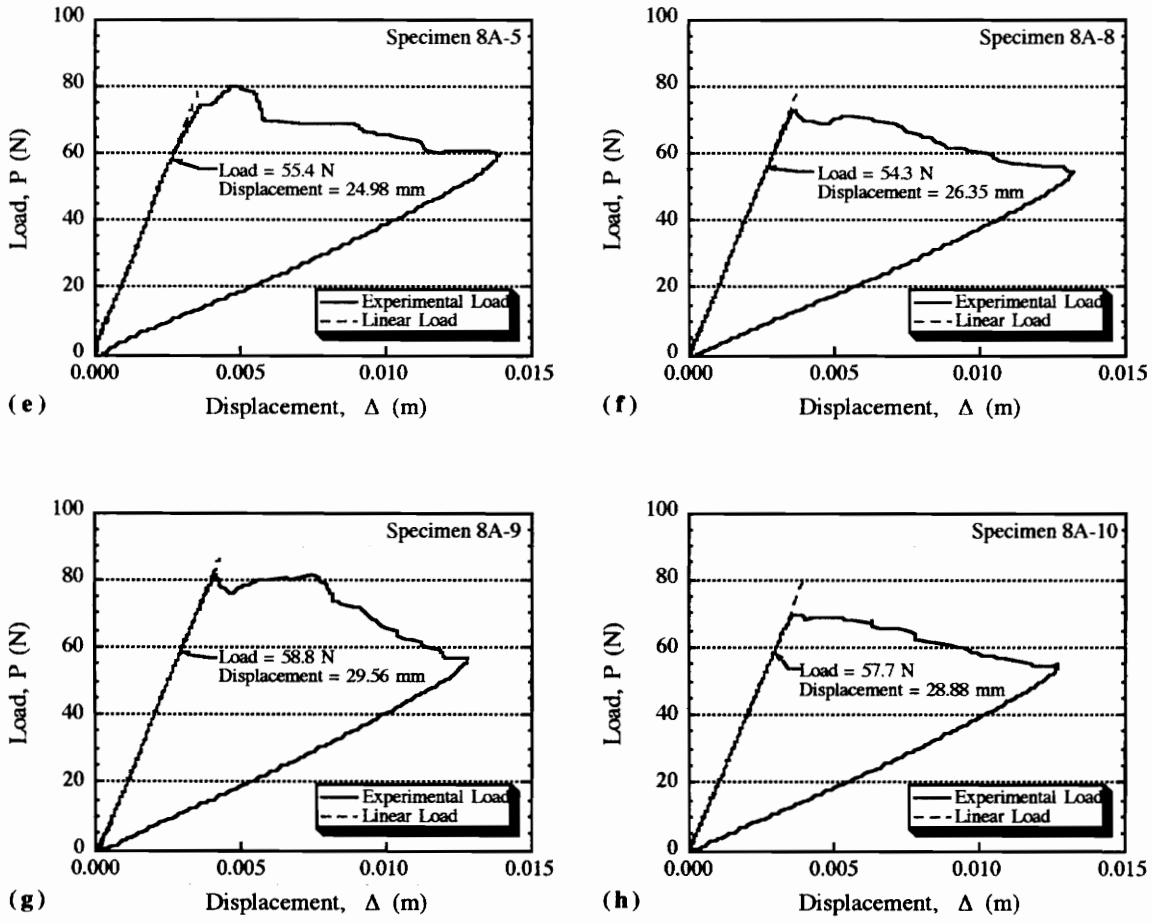

Figures A1.5 (continued): Load-Displacement Curves for Specimens from the Panel Cooled at 8°C/min and then Annealed
e) Specimen 8A-5, f) Specimen 8A-8,
g) Specimen 8A-9, and h) Specimen 8A-10

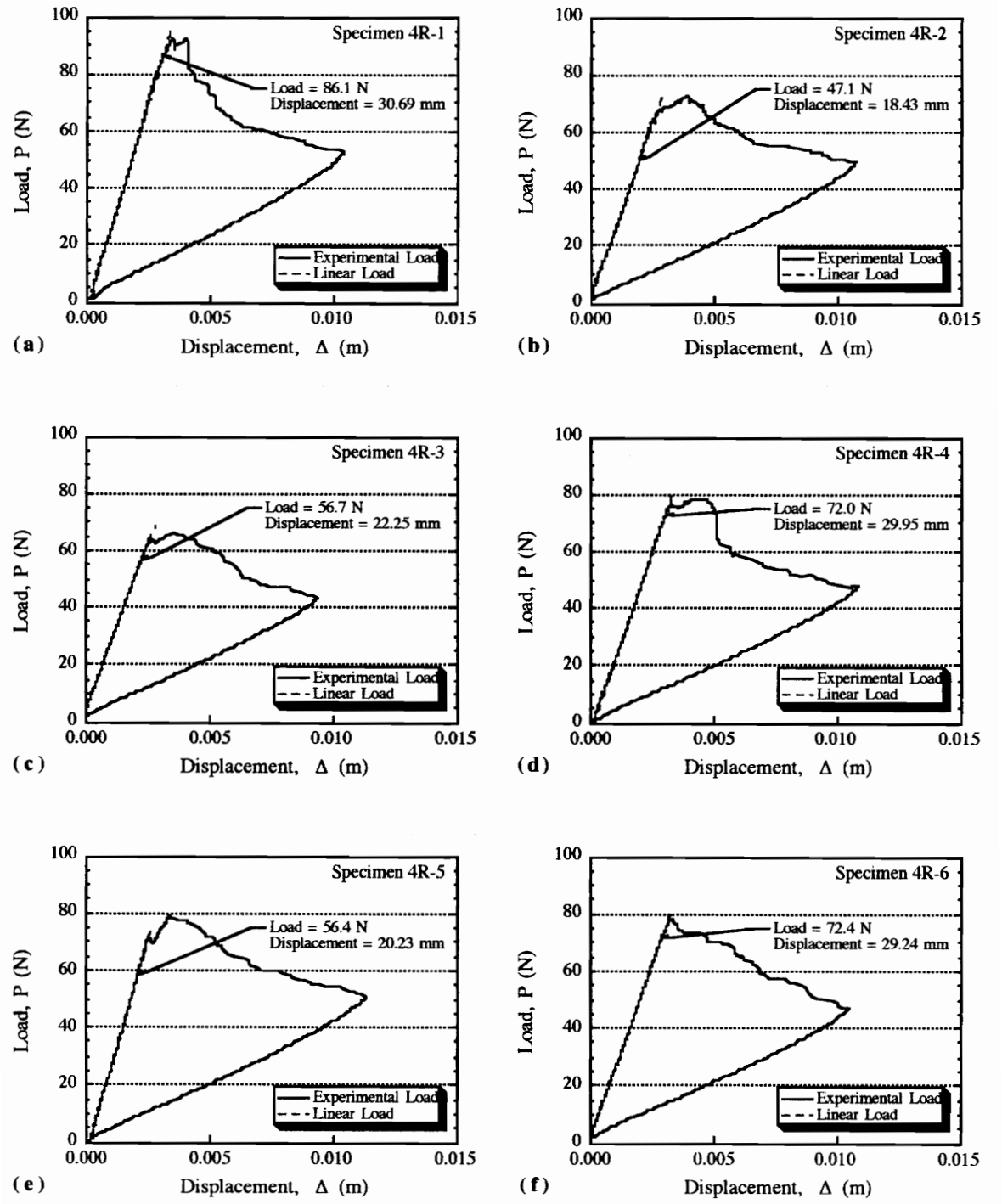

Figures A1.6: Load-Displacement Curves for Specimens from the Panel Made with Recovered Polymer and Cooled at 4°C/min a) Specimen 4R-1, b) Specimen 4R-2, c) Specimen 4R-3, d) Specimen 4R-4, e) Specimen 4R-5, and f)Specimen 4R-6

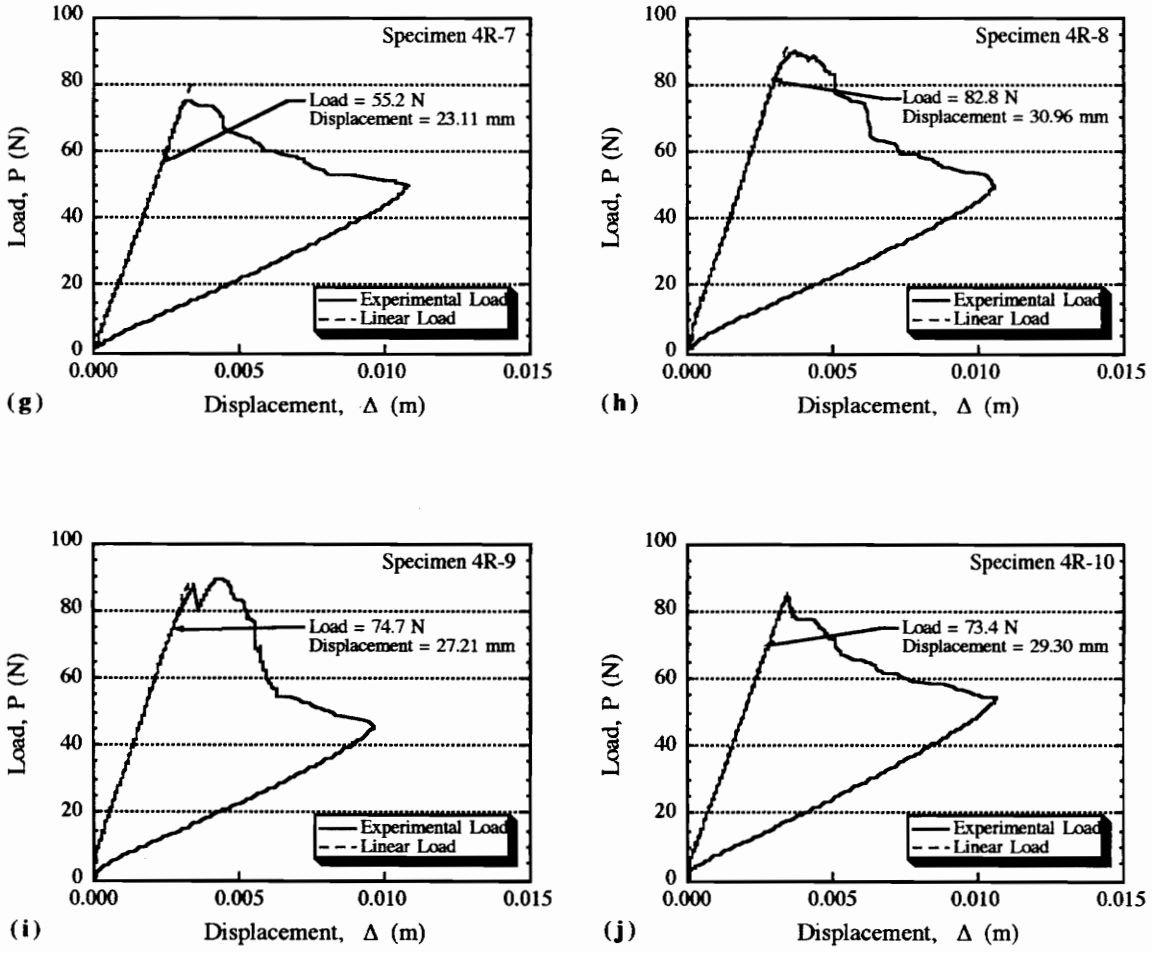

Figures A1.6 (continued): Load-Displacement Curves for Specimens from the Panel Made with Recovered Polymer and Cooled at 4°C/min
g) Specimen 4R-7, h) Specimen 4R-8,
i) Specimen 4R-9, and j) Specimen 4R-10

Delamination Resistance Curves

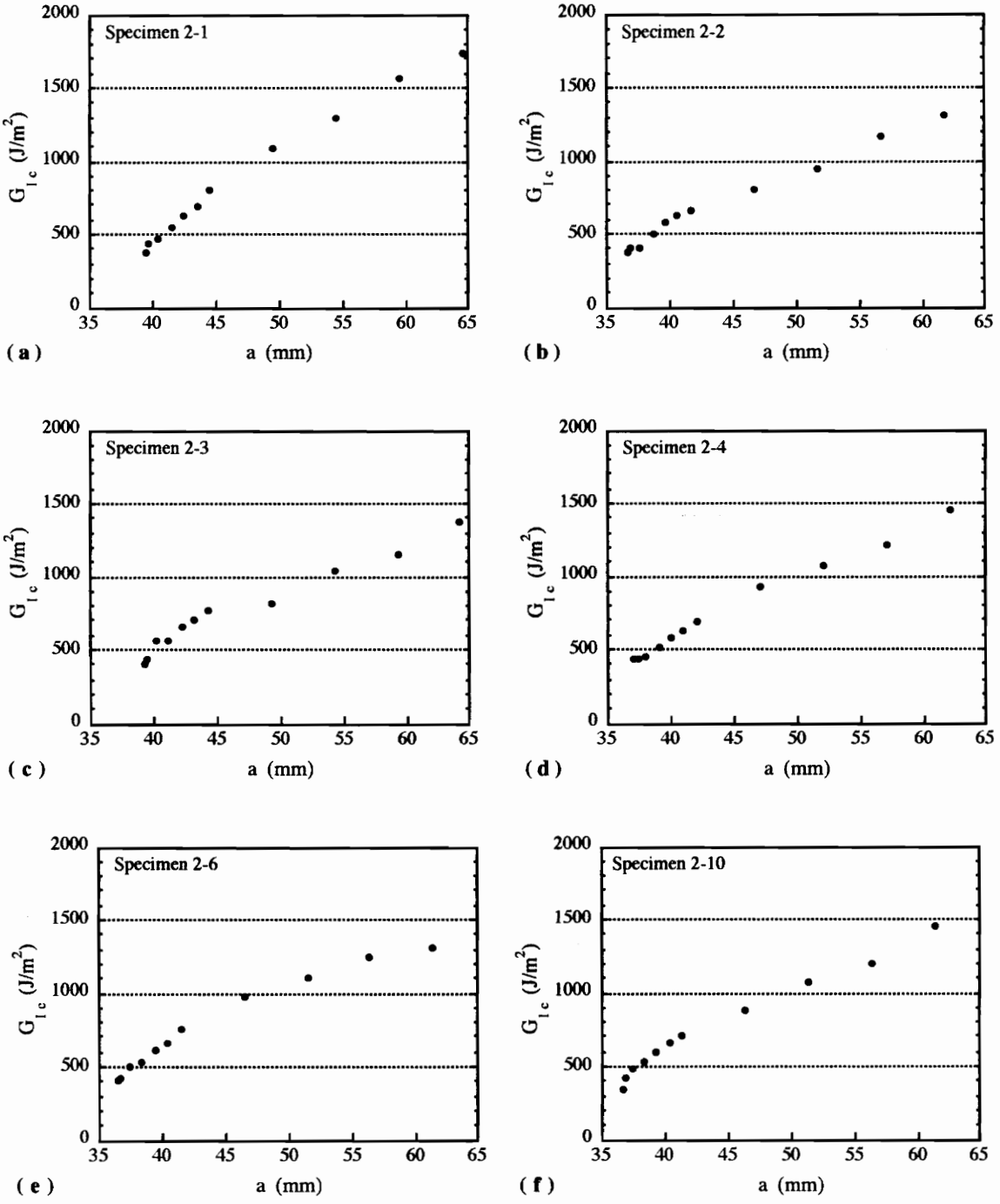

Figures A2.1: Delamination Resistance Curves for Specimens from the Principal Panel Cooled at 2°C/min
a) Specimen 2-1, b) Specimen 2-2, c) Specimen 2-3,
d) Specimen 2-4, e) Specimen 2-6, and f) Specimen 2-10

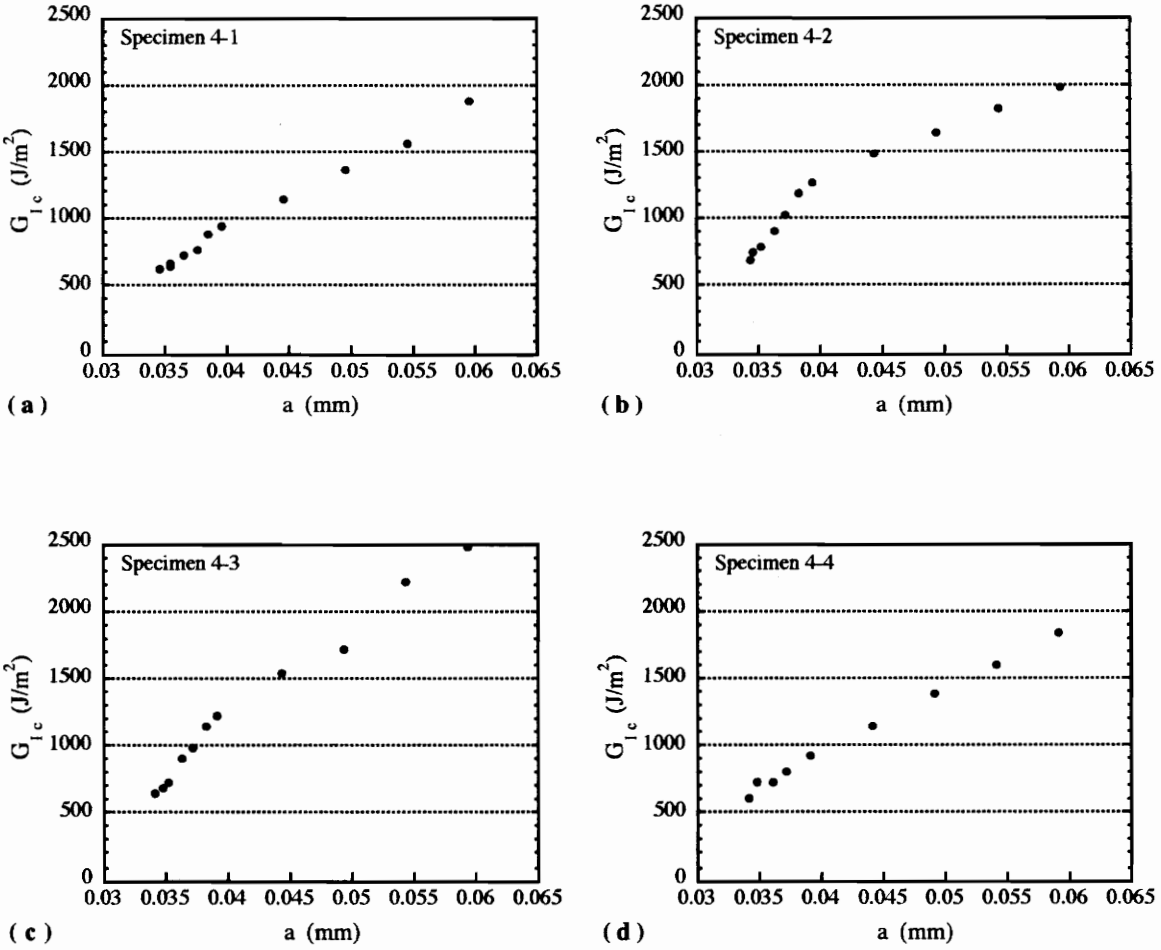

Figures A2.2: Delamination Resistance Curves for Specimens from the Principal Panel Cooled at 4°C/min
a) Specimen 4-1, b) Specimen 4-2,
c) Specimen 4-3, and d) Specimen 4-4

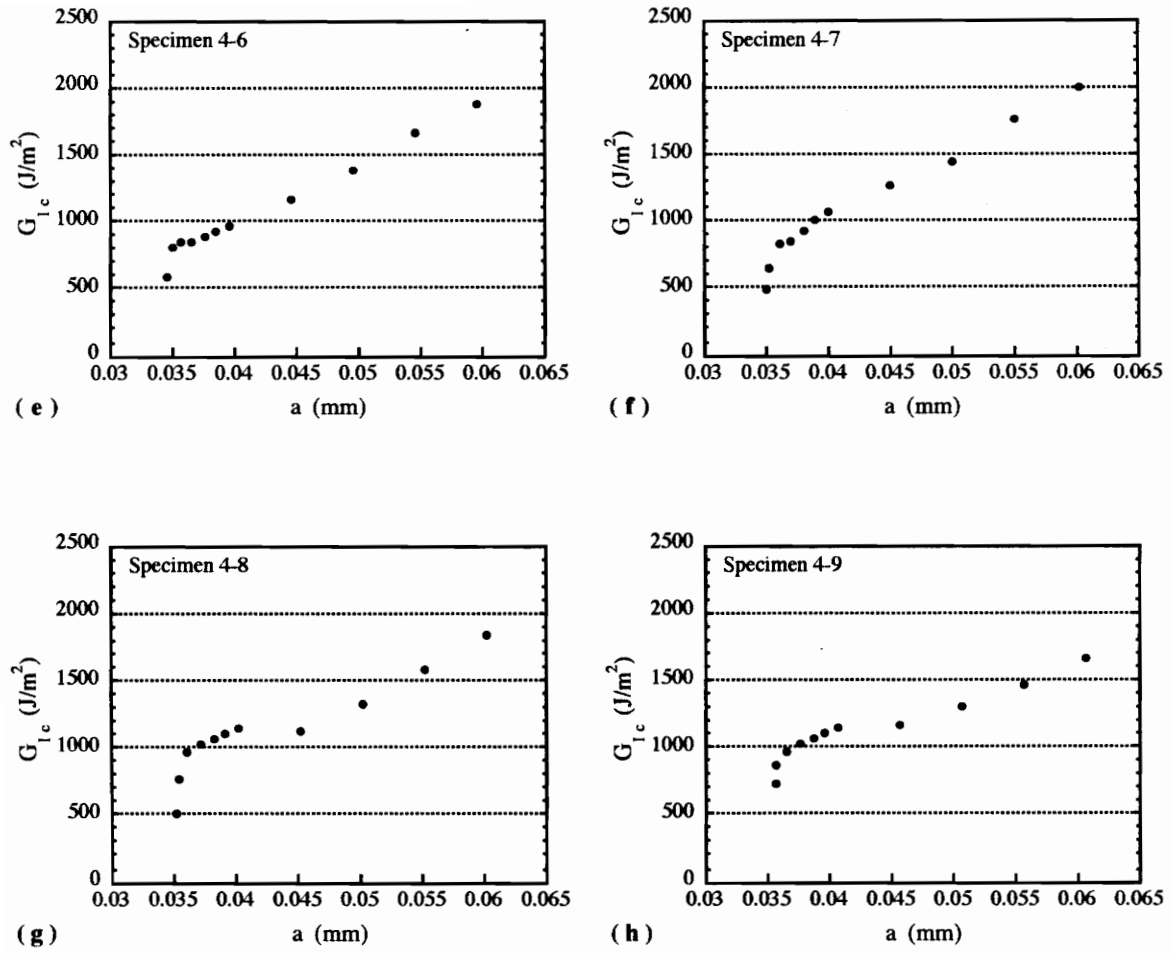

Figures A2.2 (continued): Delamination Resistance Curves
for Specimens from the Principal Panel Cooled at 4°C/min
e) Specimen 4-6, f) Specimen 4-7,
g) Specimen 4-8, and h) Specimen 4-9

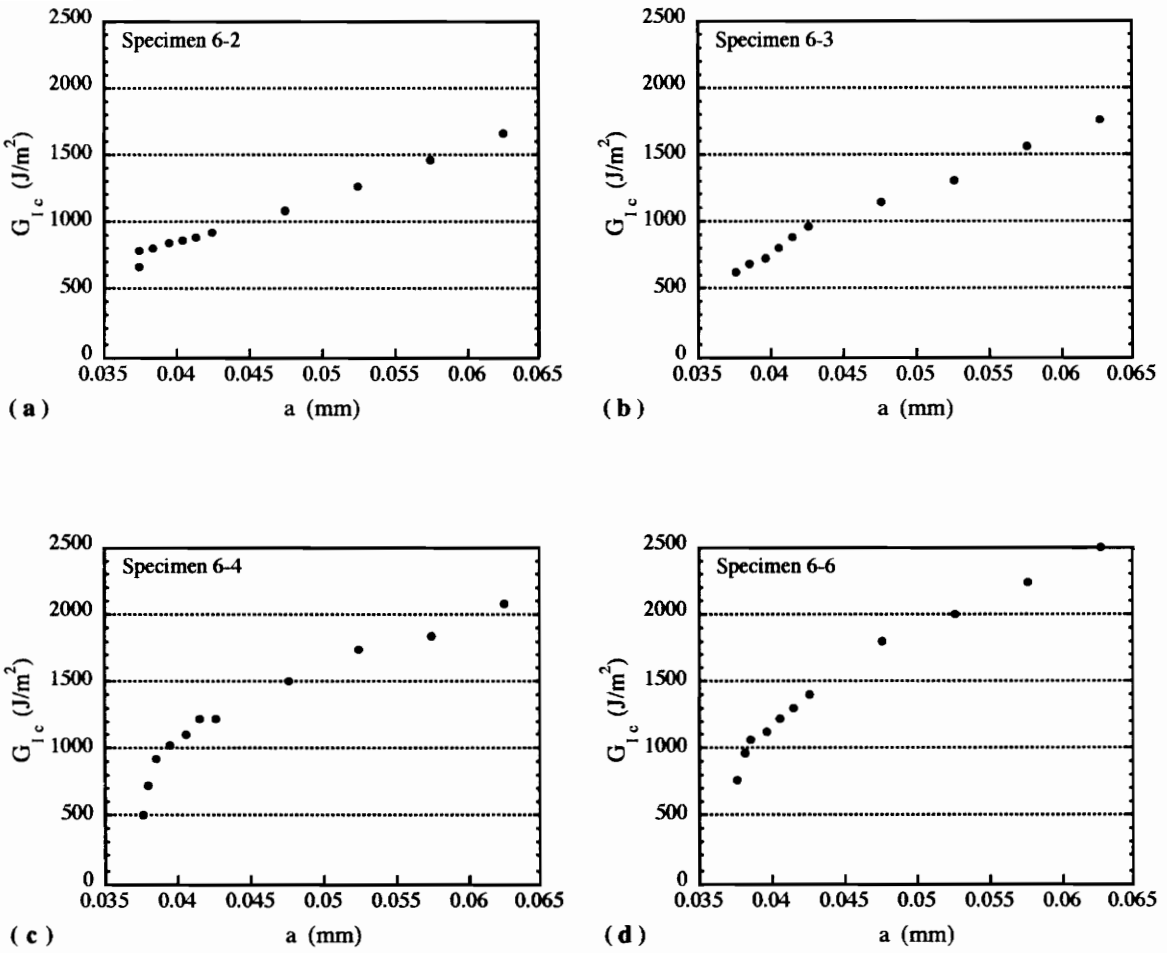

Figures A2.3: Delamination Resistance Curves for Specimens from the Principal Panel Cooled at 6°C/min
a) Specimen 6-2, b) Specimen 6-3,
c) Specimen 6-4, and d) Specimen 6-6

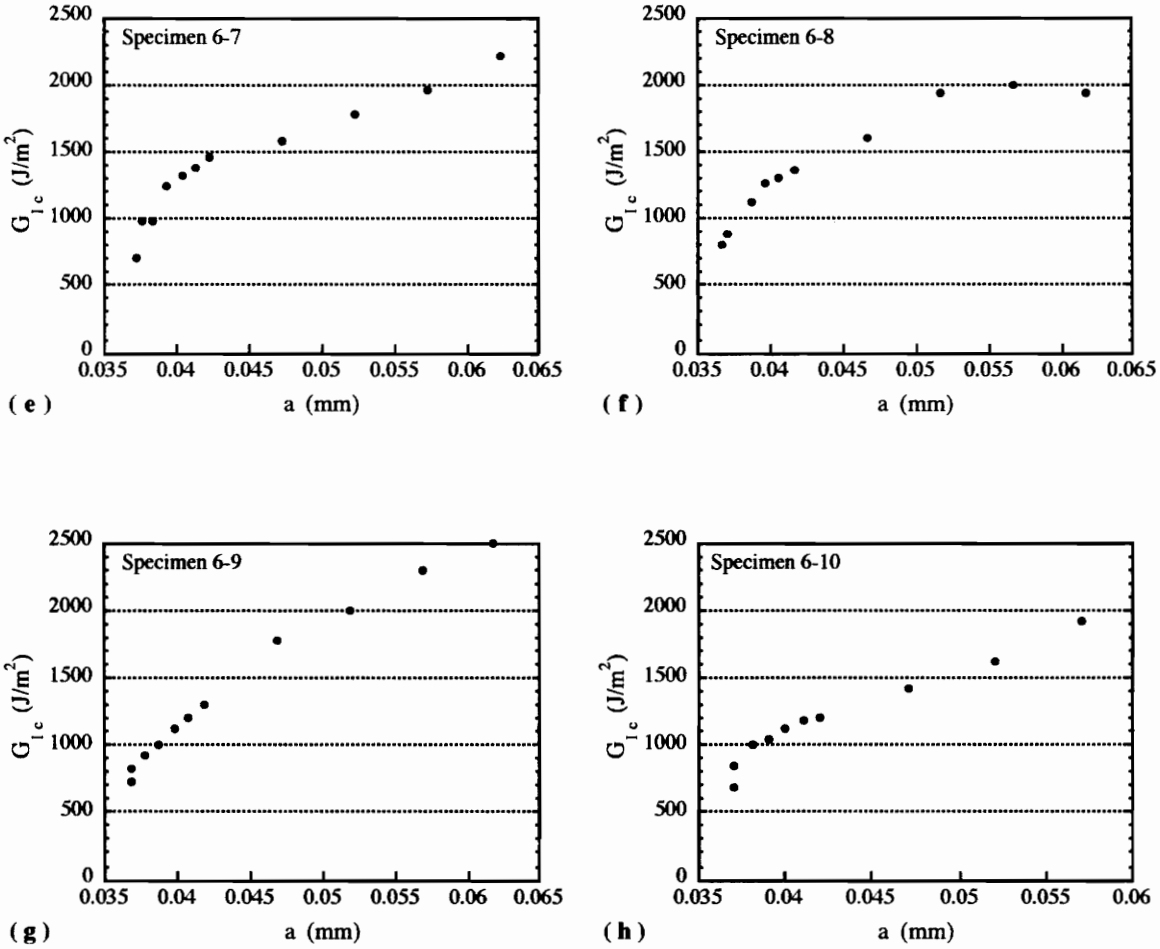

Figures A2.3 (continued): Delamination Resistance Curves
for Specimens from the Principal Panel Cooled at 6°C/min
e) Specimen 6-7, f) Specimen 6-8,
g) Specimen 6-9, and h) Specimen 6-10

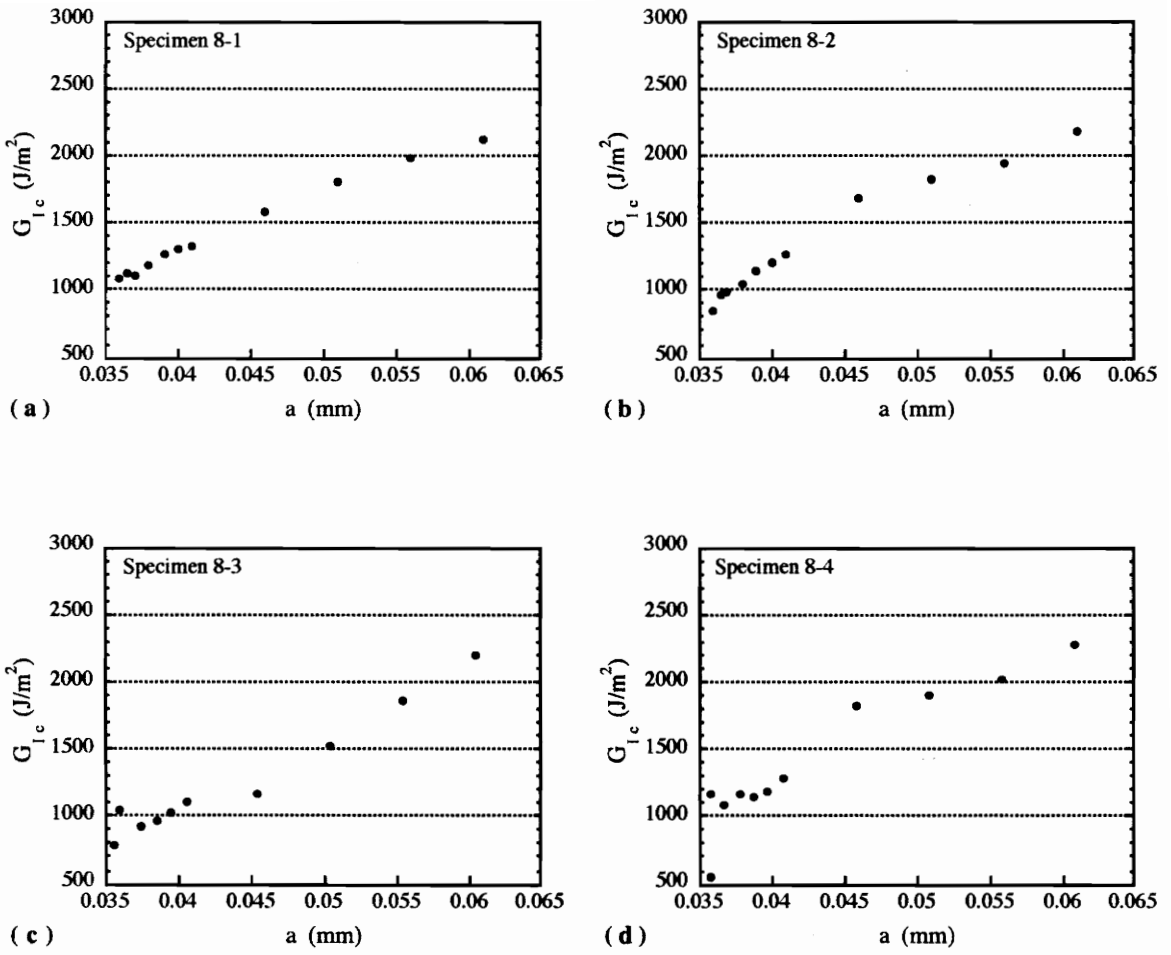

Figures A2.4: Delamination Resistance Curves for Specimens from the Principal Panel Cooled at 8°C/min
a) Specimen 8-1, b) Specimen 8-2,
c) Specimen 8-3, and d) Specimen 8-4

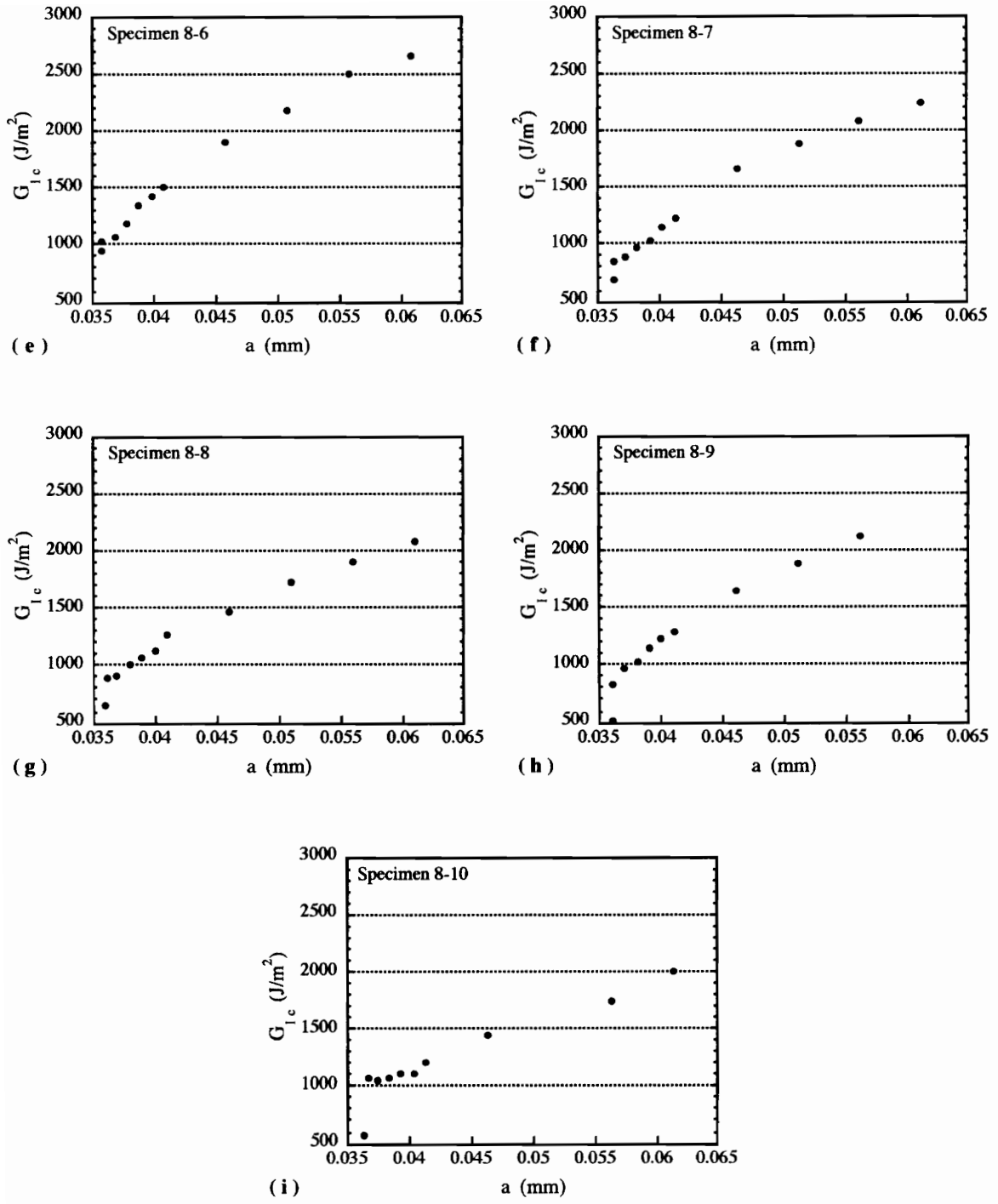

Figures A2.4 (continued): Delamination Resistance Curves for Specimens from the Principal Panel Cooled at 8°C/min
e) Specimen 8-6, f) Specimen 8-7,
g) Specimen 8-8, h) Specimen 8-8, and Specimen 8-10

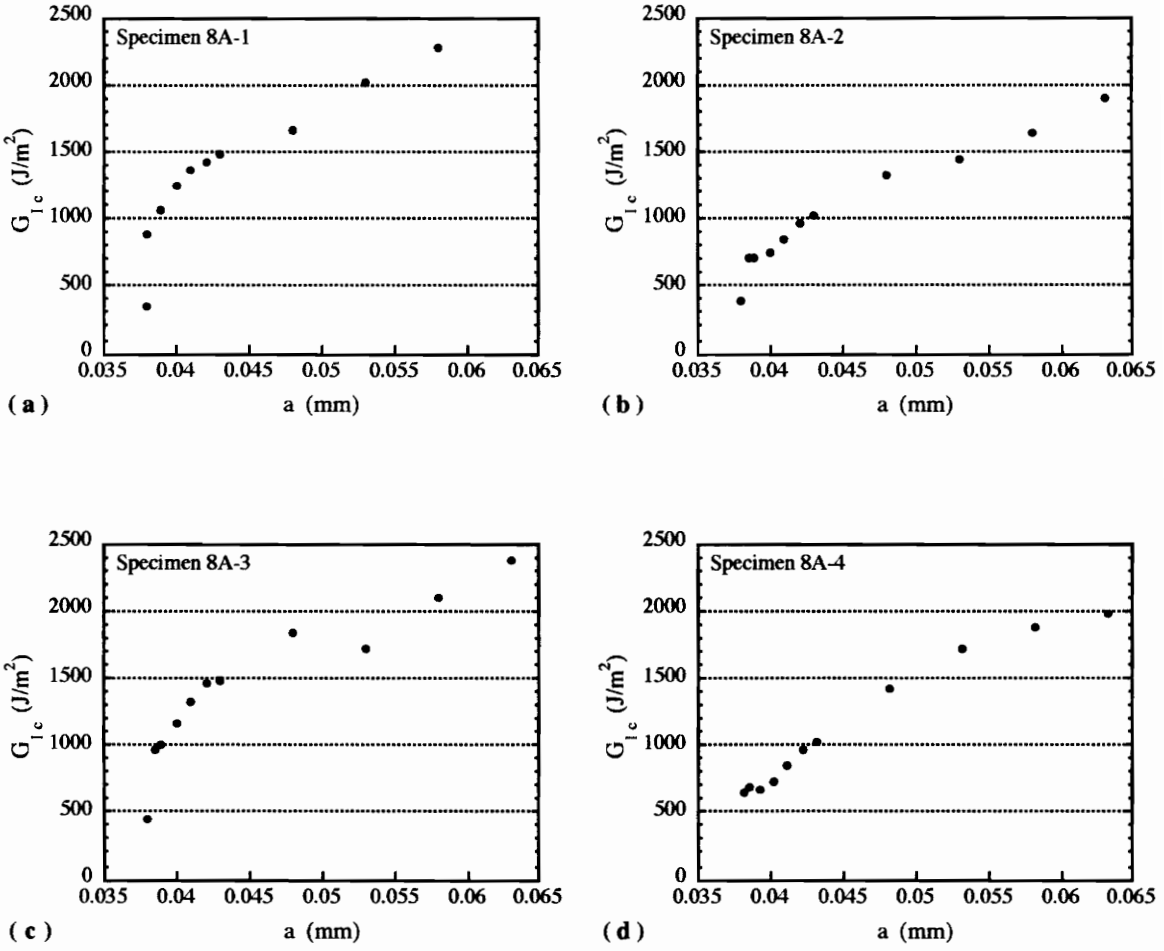

Figures A2.5: Delamination Resistance Curves for Specimens from the Panel Cooled at 8°C/min and then Annealed
a) Specimen 8A-1, b) Specimen 8A-2,
c) Specimen 8A-3, and d) Specimen 8A-4

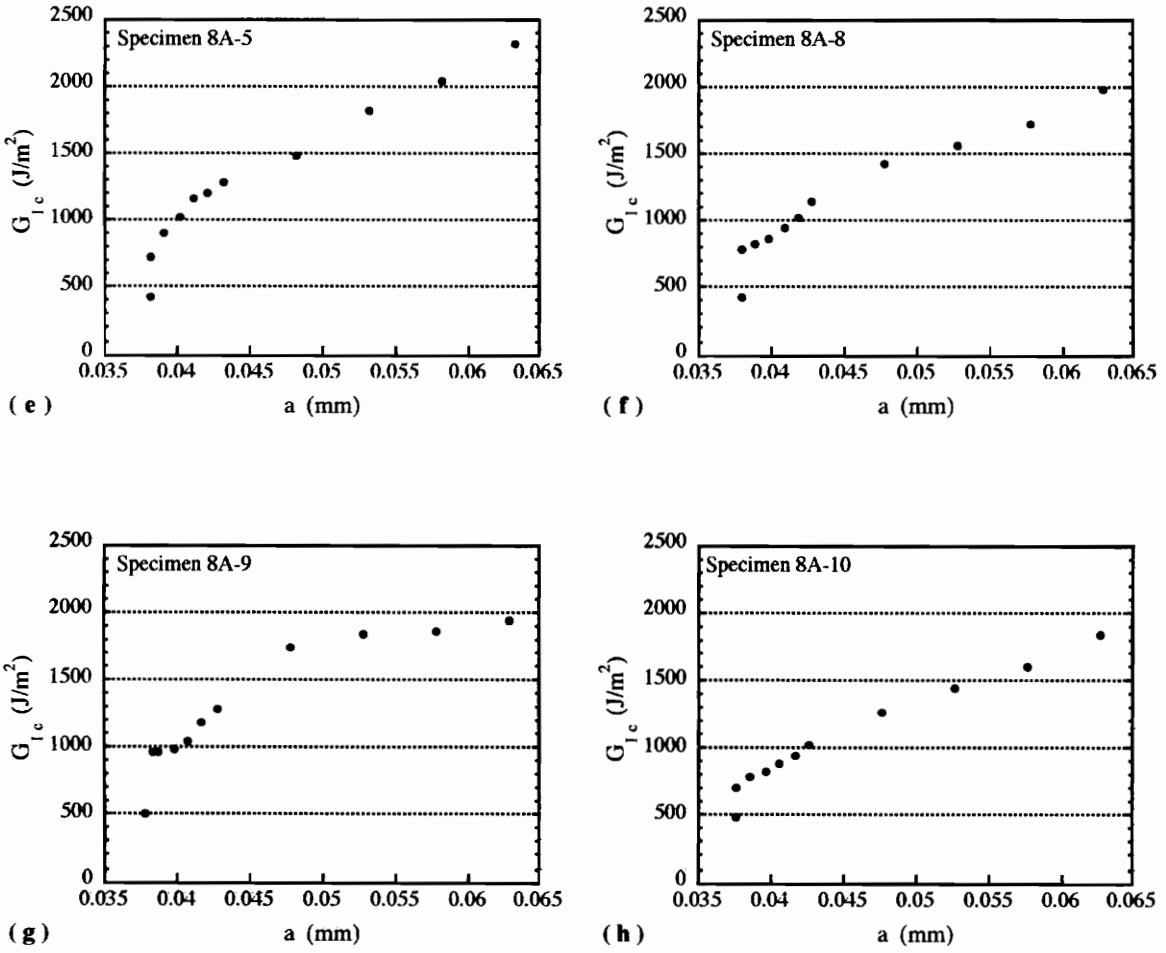

Figures A2.5 (continued): Delamination Resistance Curves for Specimens from the Panel Cooled at 8°C/min and then Annealed
e) Specimen 8A-5, f) Specimen 8A-8,
g) Specimen 8A-9, and h) Specimen 8A-10

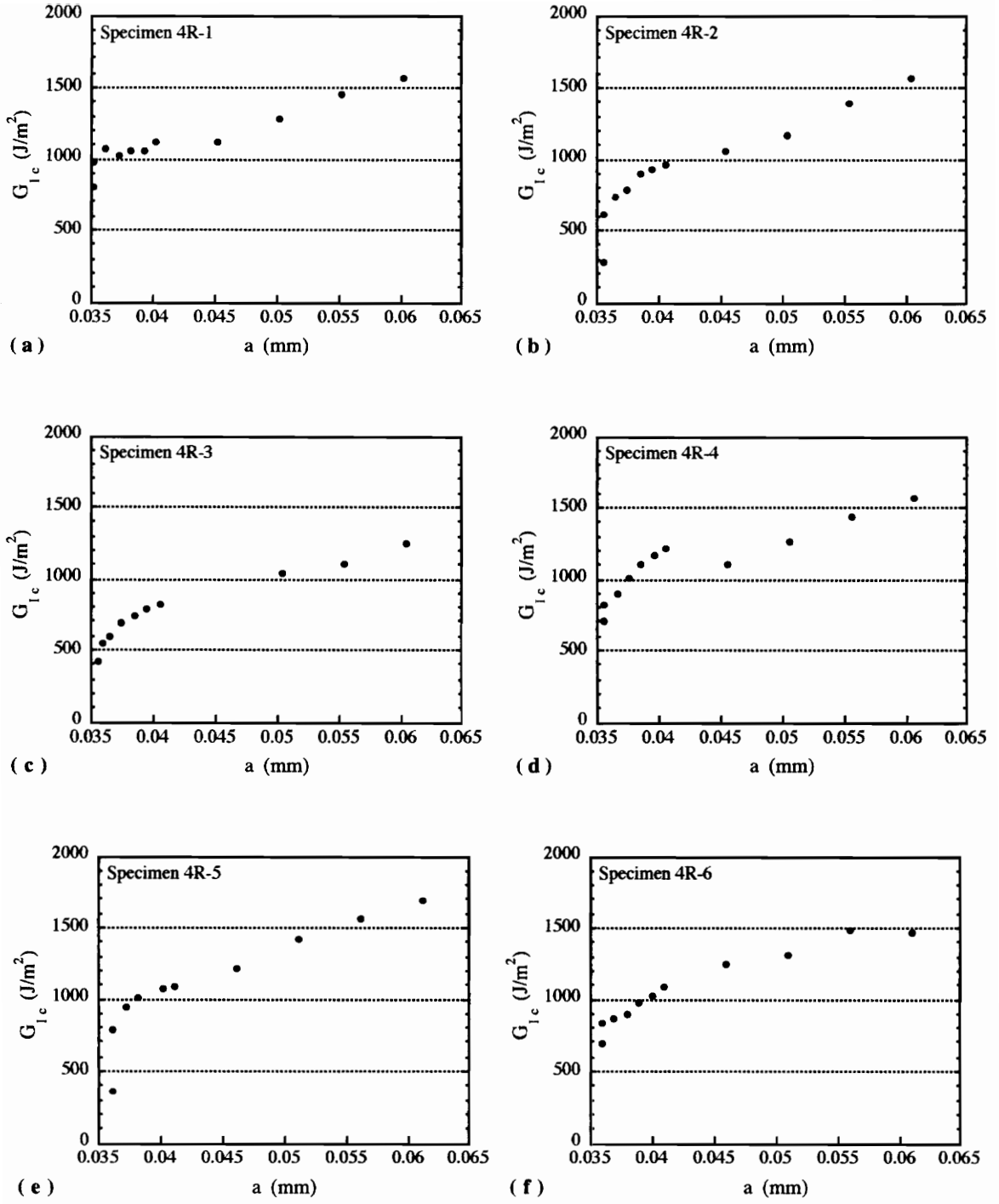

Figures A2.6: Delamination Resistance Curves for Specimens from the Panel Made with Recovered Polymer Cooled at 4°C/min a) Specimen 4R-1, b) Specimen 4R-2, c) Specimen 4R-3, d) Specimen 4R-4, e) Specimen 4R-5, and f) Specimen 4R-6

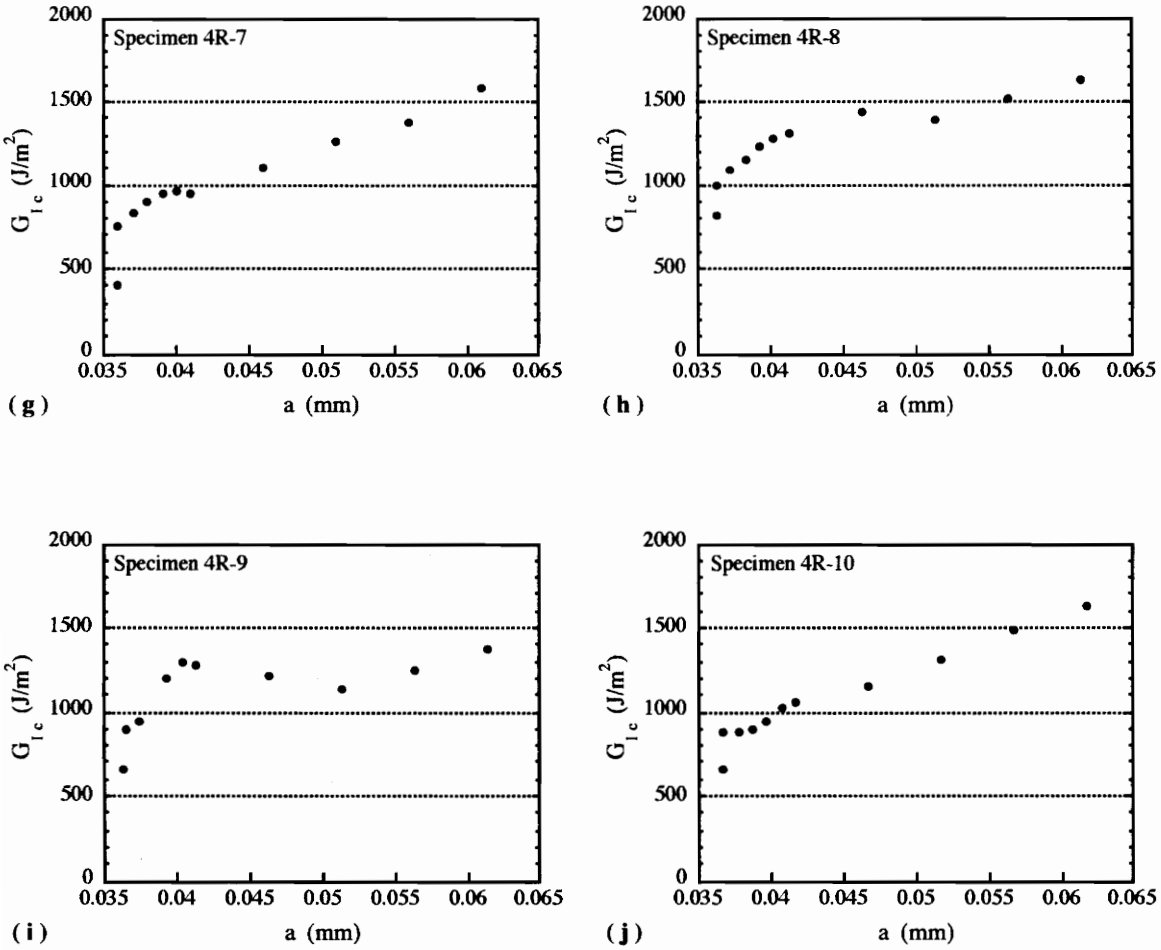

Figures A2.6 (continued) : Delamination Resistance Curves for Specimens from the Panel Made with Recovered Polymer Cooled at 4°C/min
g) Specimen 4R-7, h) Specimen 4R-8
i) Specimen 4R-9, and j) Specimen 4R-10

Appendix B - End Notch Flexure Data

ENF Load Displacement Curves

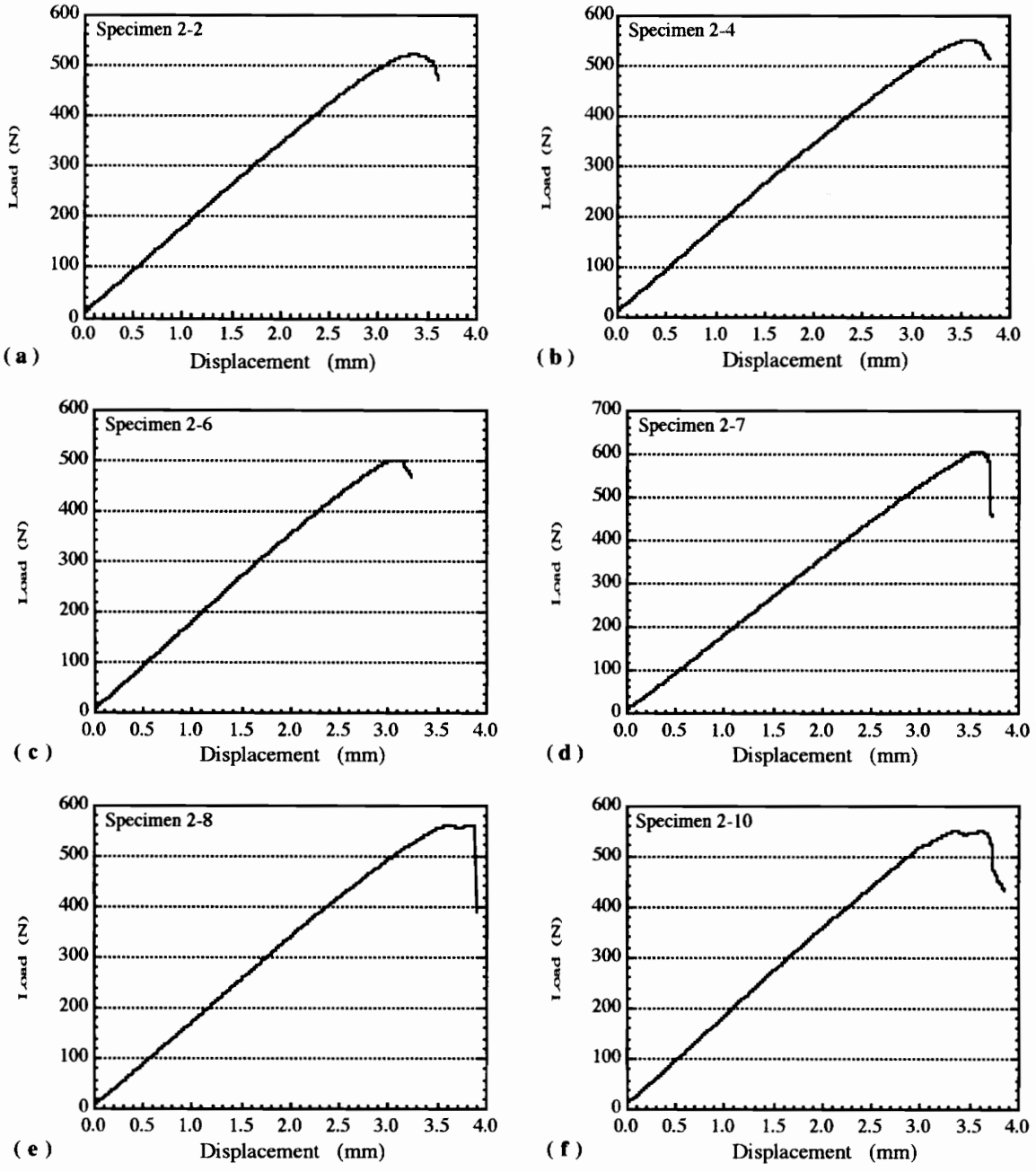

Figures B1.1: Load-Displacement Curves for Specimens from the Principal Panel Cooled at 2°C/min
a) Specimen 2-2, b) Specimen 2-4, c) Specimen 2-6,
d) Specimen 2-7, e) Specimen 2-8, and f) Specimen 2-10

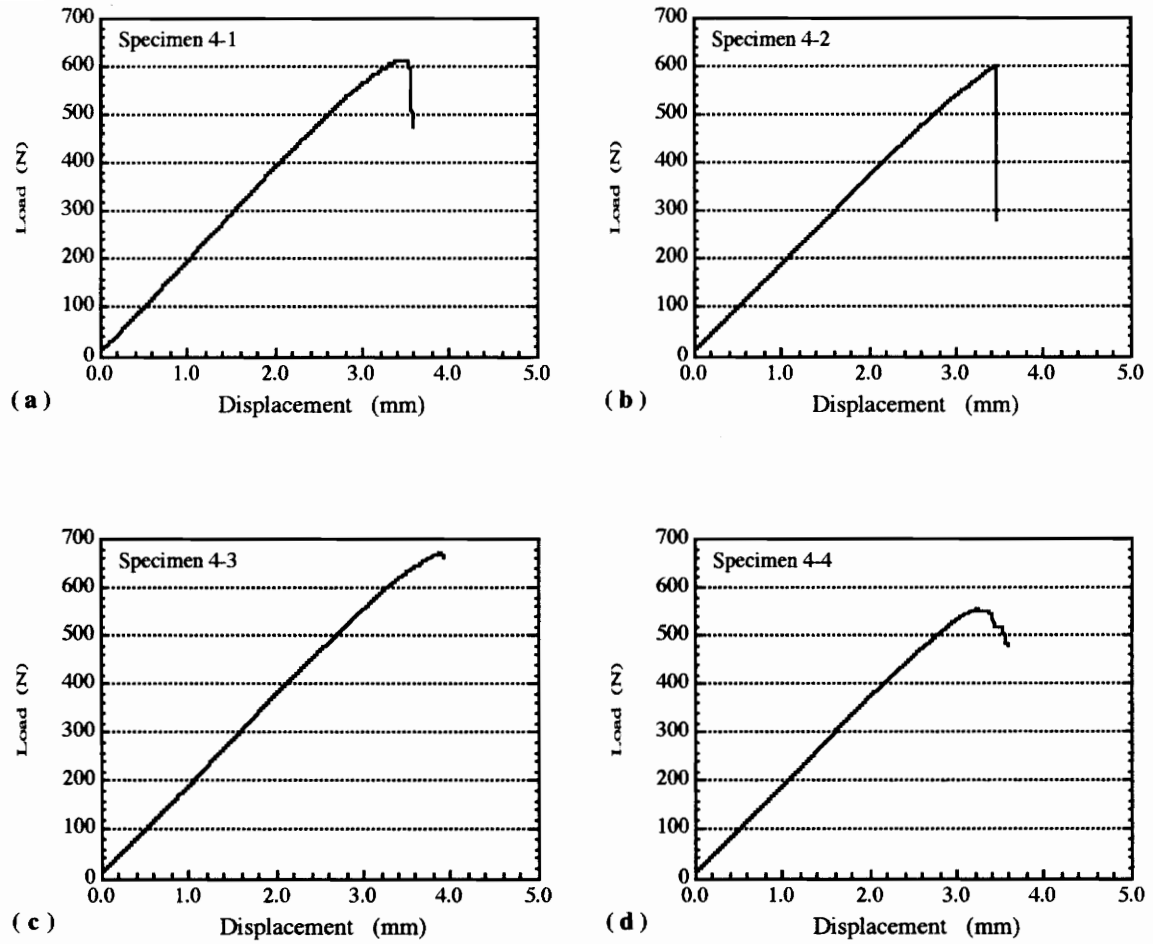

Figures B1.2: Load-Displacement Curves for Specimens from the Principal Panel Cooled at 4°C/min
a) Specimen 4-1, b) Specimen 4-2,
c) Specimen 4-3, and d) Specimen 4-4

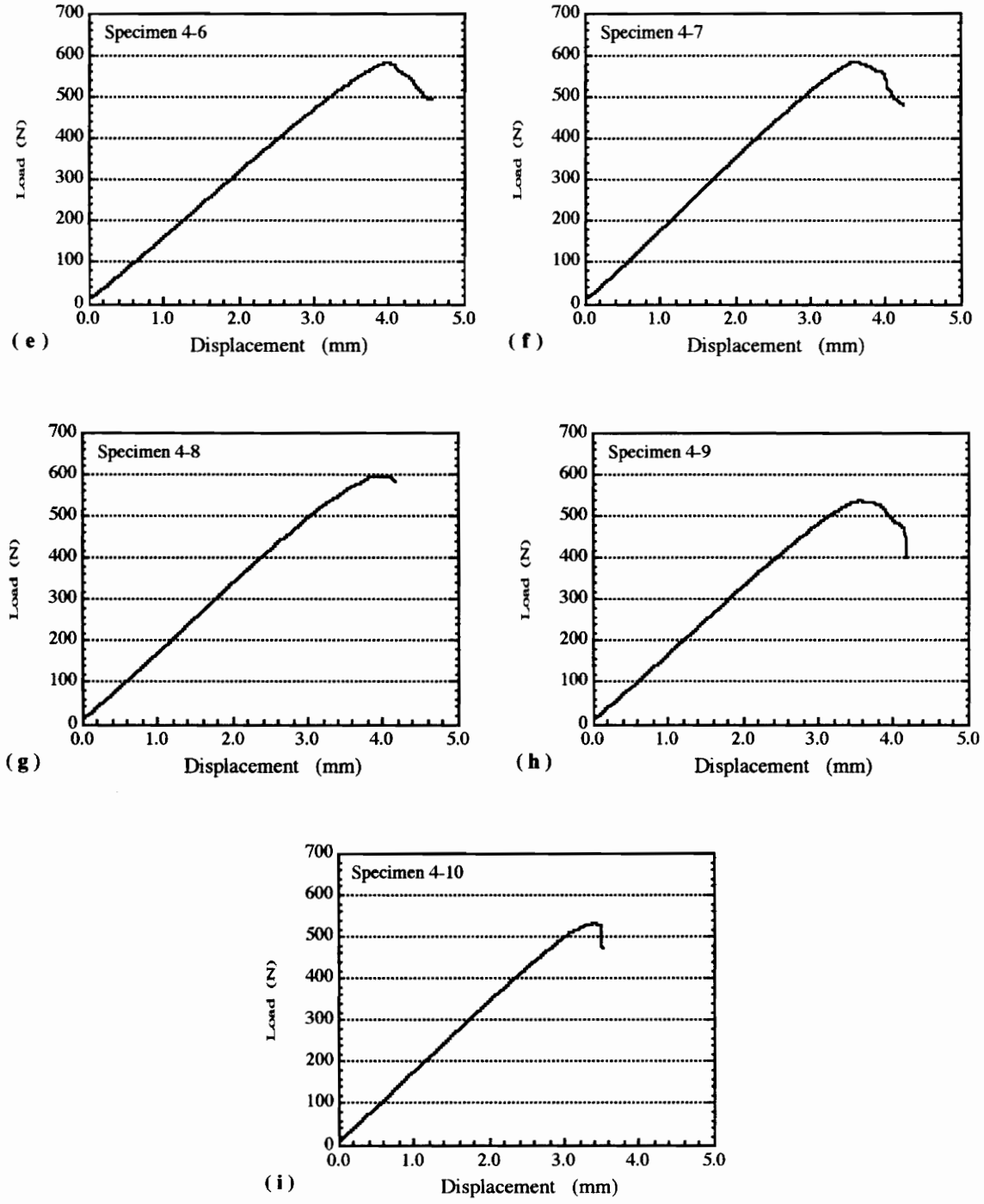

Figures B1.2 (continued): Load-Displacement Curves for Specimens from the Principal Panel Cooled at 4°C/min
e) Specimen 4-6, f) Specimen 4-7, g) Specimen 4-8,
h) Specimen 4-9, and i) Specimen 4-10

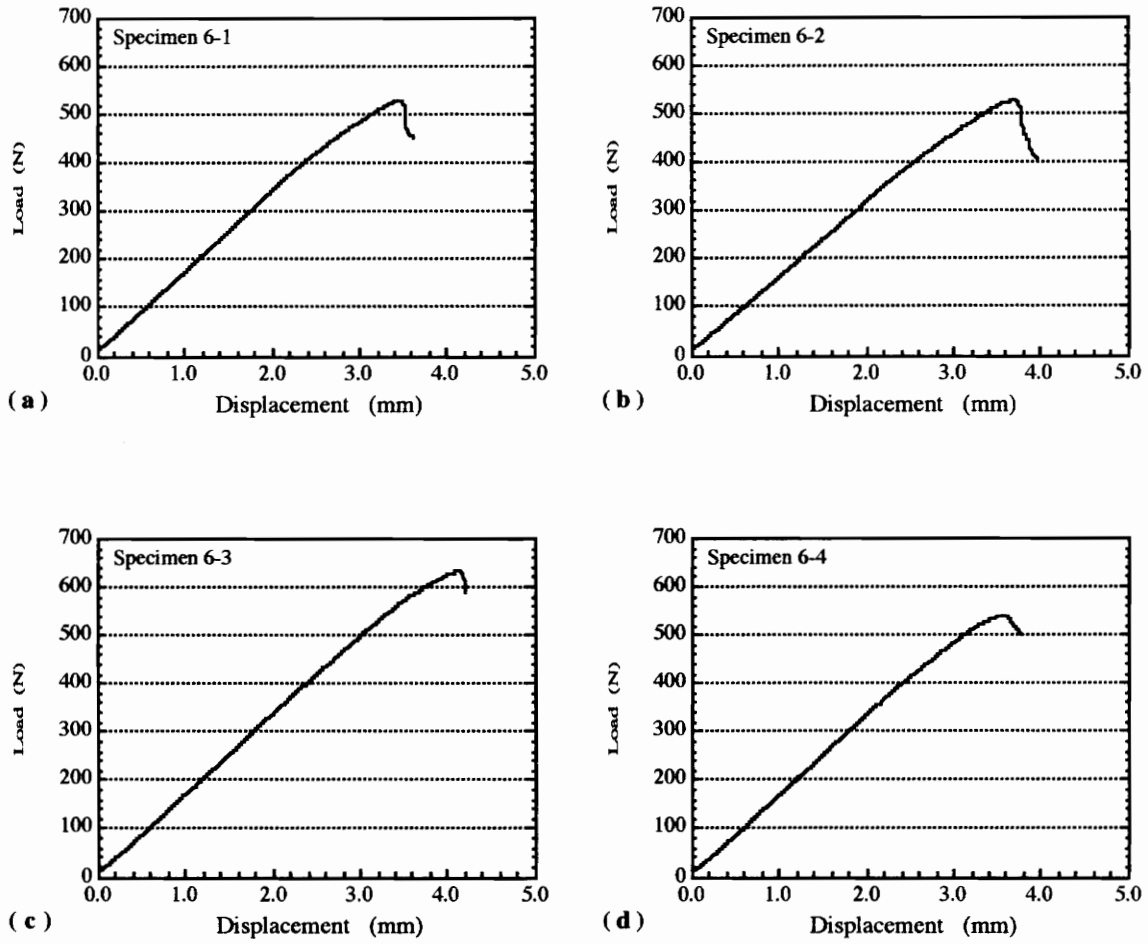

Figures B1.3: Load-Displacement Curves for Specimens from the Principal Panel Cooled at 6°C/min
a) Specimen 6-1, b) Specimen 6-2,
c) Specimen 6-3, and d) Specimen 6-4

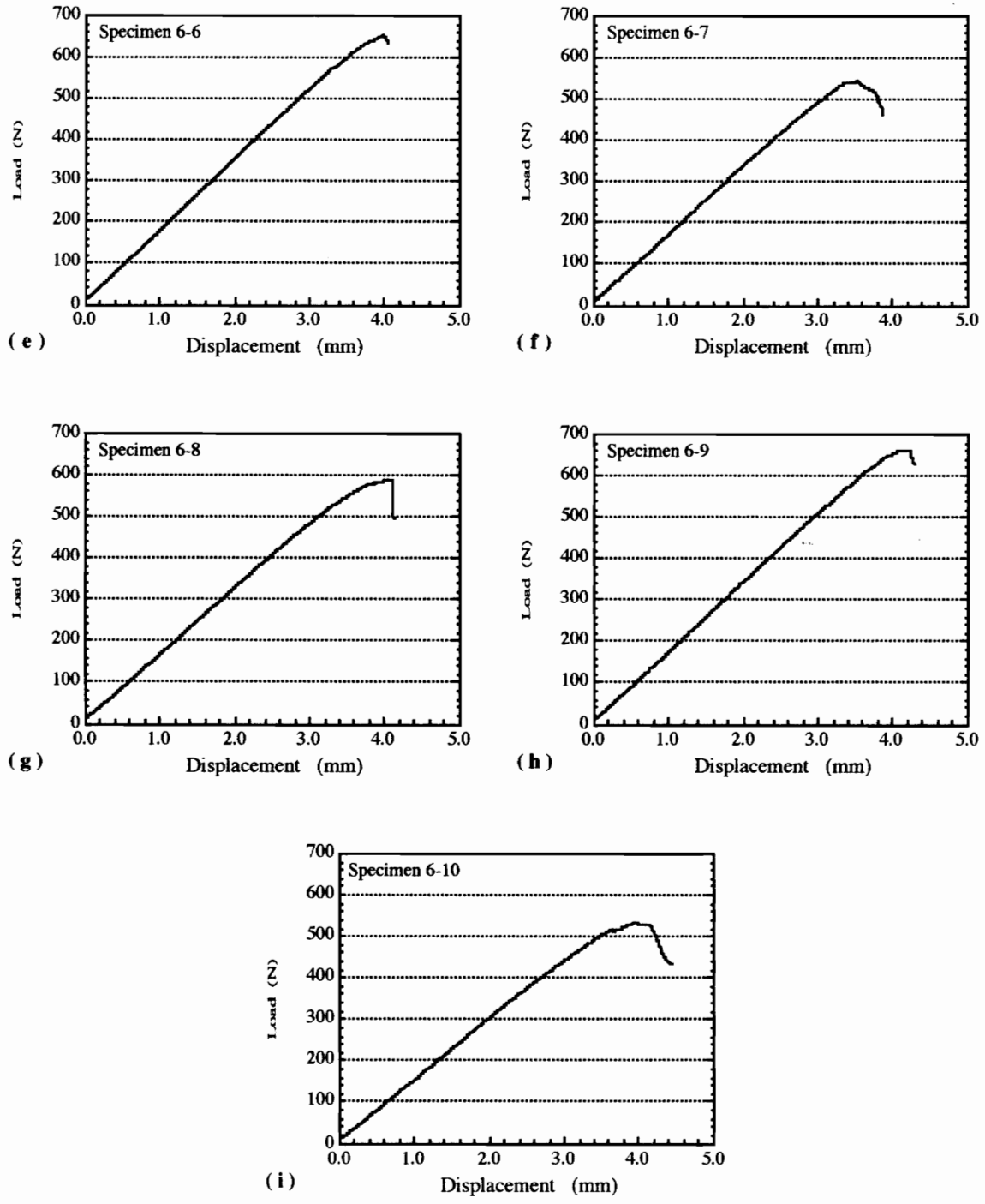

Figures B1.3 (continued): Load-Displacement Curves for Specimens from the Principal Panel Cooled at 6°C/min
e) Specimen 6-6, f) Specimen 6-7, g) Specimen 6-8
h) Specimen 6-9, and i) Specimen 6-10

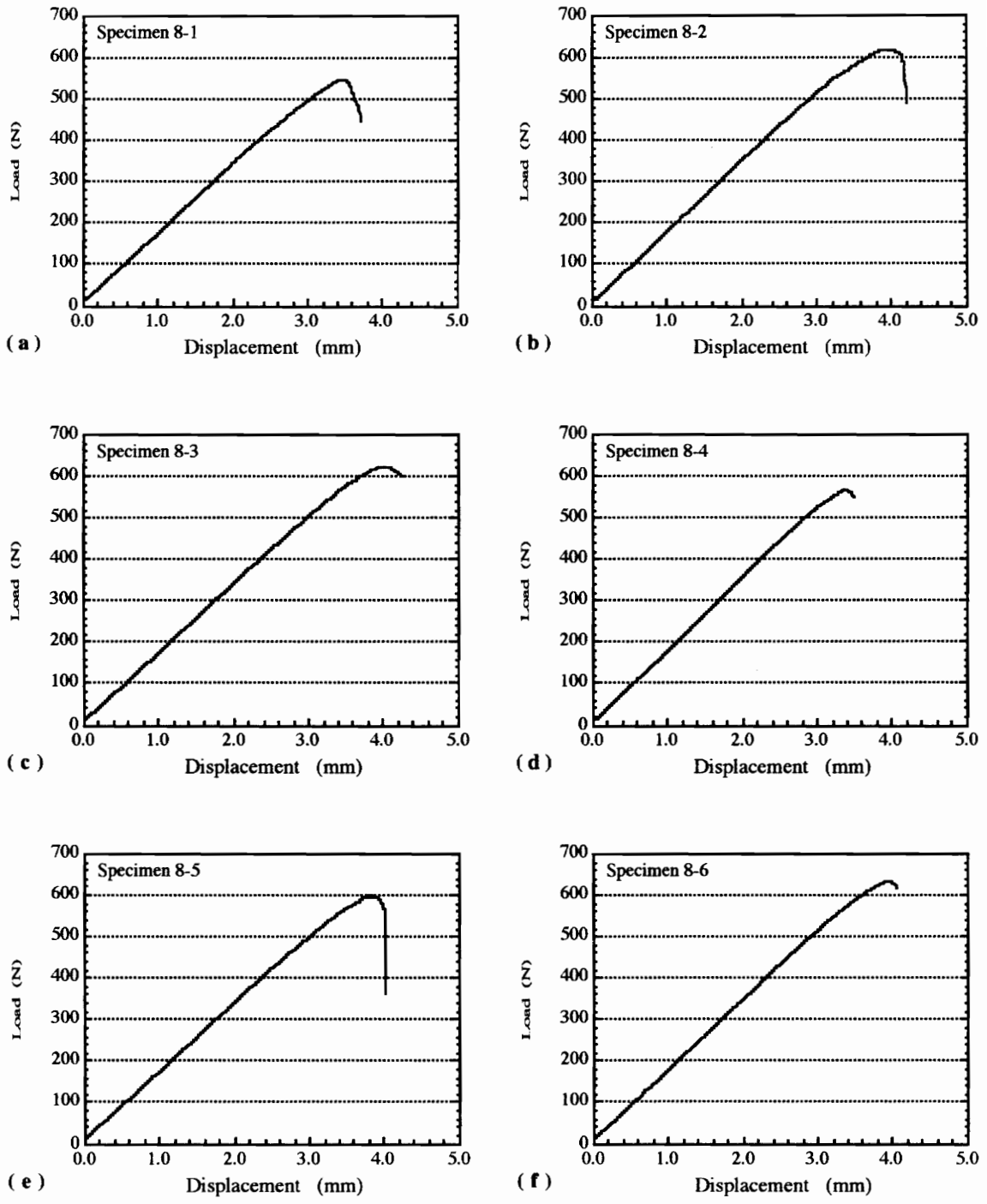

Figures B1.4: Load-Displacement Curves for Specimens from the Principal Panel Cooled at 8°C/min
a) Specimen 8-1, b) Specimen 8-2, c) Specimen 8-3
d) Specimen 8-4, e) Specimen 8-5, and f) Specimen 8-6

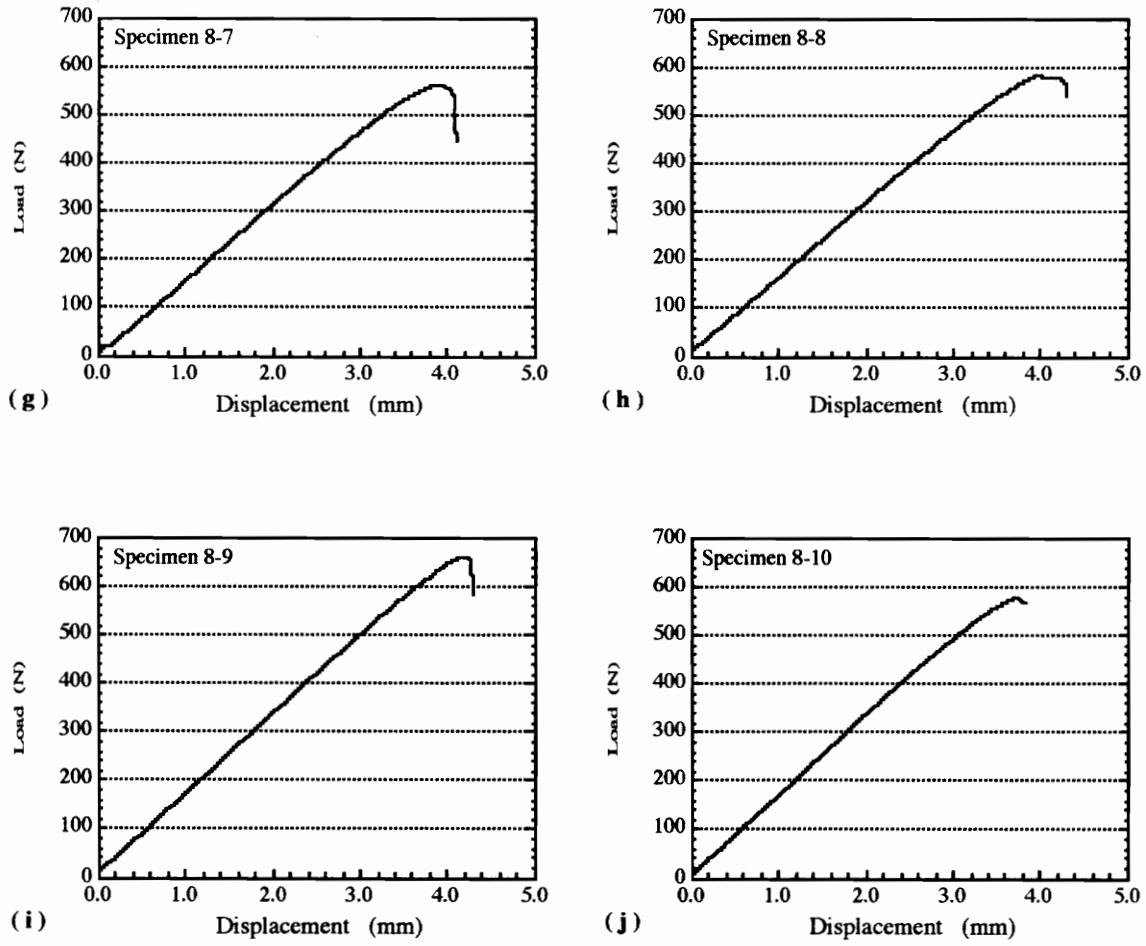

Figures B1.4 (continued): Load-Displacement Curves for Specimens from the Principal Panel Cooled at 8°C/min
g) Specimen 8-7, h) Specimen 8-8,
i) Specimen 8-9, and j) Specimen 8-10

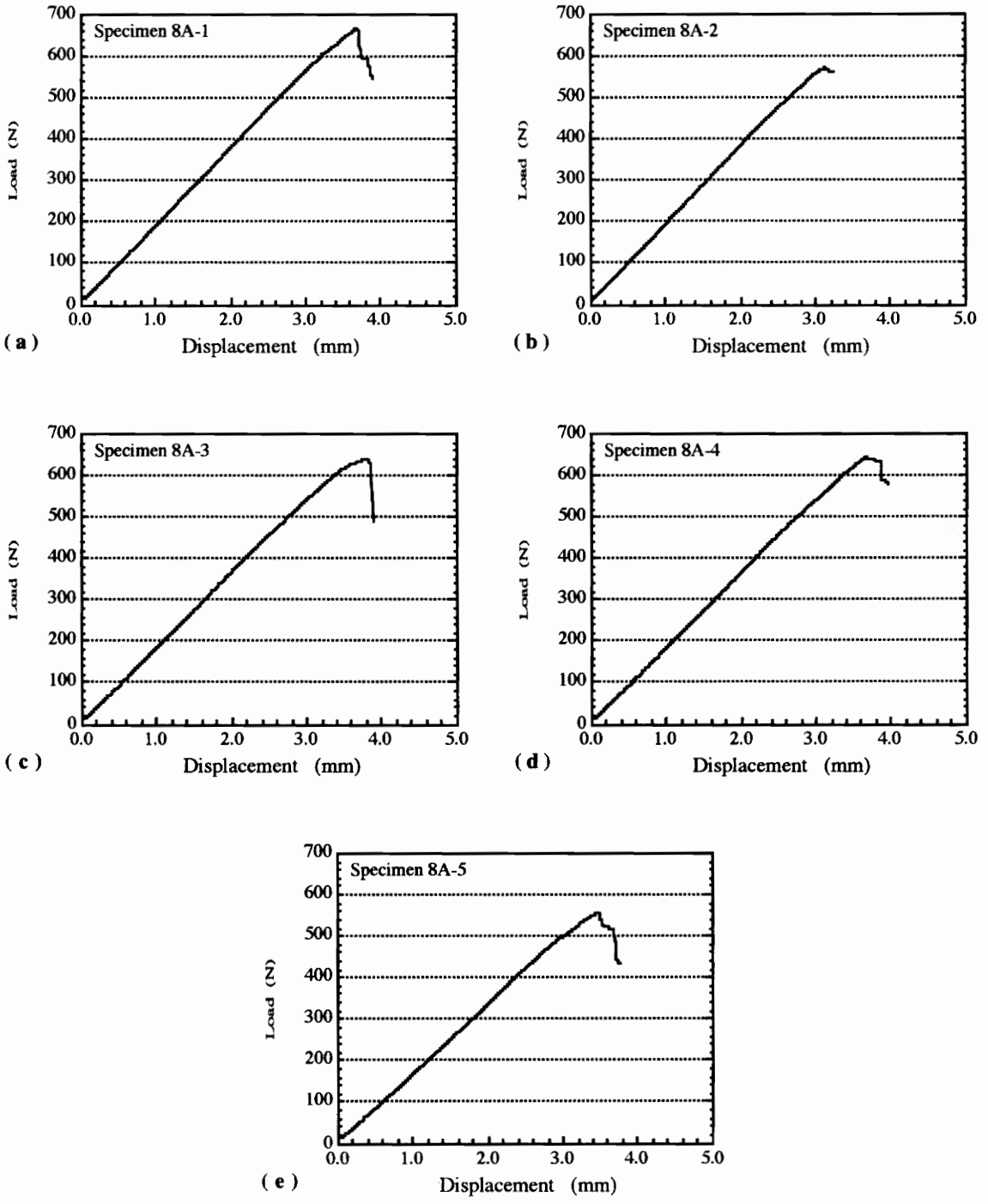

Figures B1.5: Load-Displacement Curves for Specimens from the Panel Cooled at 8°C/min and then Annealed
a) Specimen 8A-1, b) Specimen 8A-2, c) Specimen 8A-3
d) Specimen 8A-4, and e) Specimen 8A-5

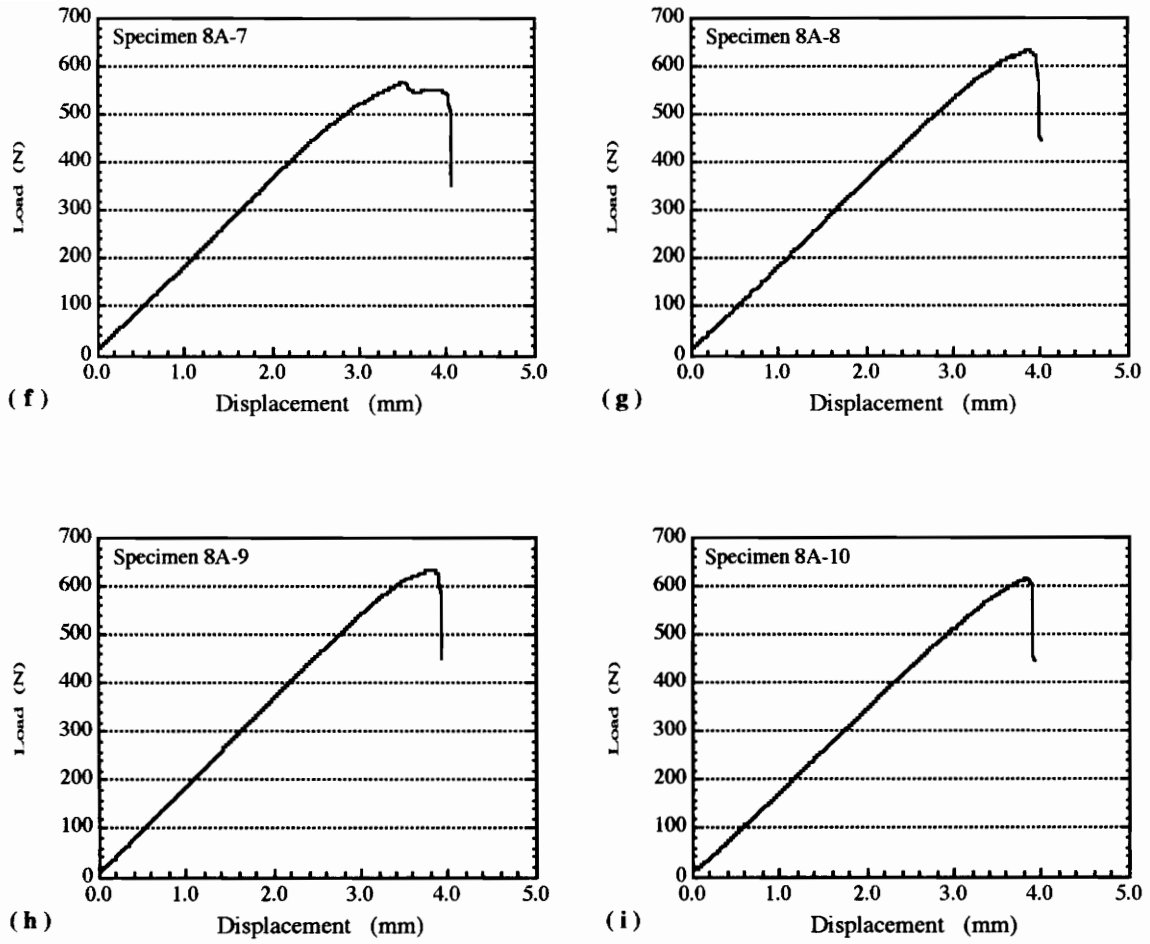

Figures B1.5 (continued): Load-Displacement Curves for Specimens from the Panel Cooled at 8°C/min and then Annealed
f) Specimen 8A-7, g) Specimen 8A-8,
h) Specimen 8A-9, and i) Specimen 8A-10

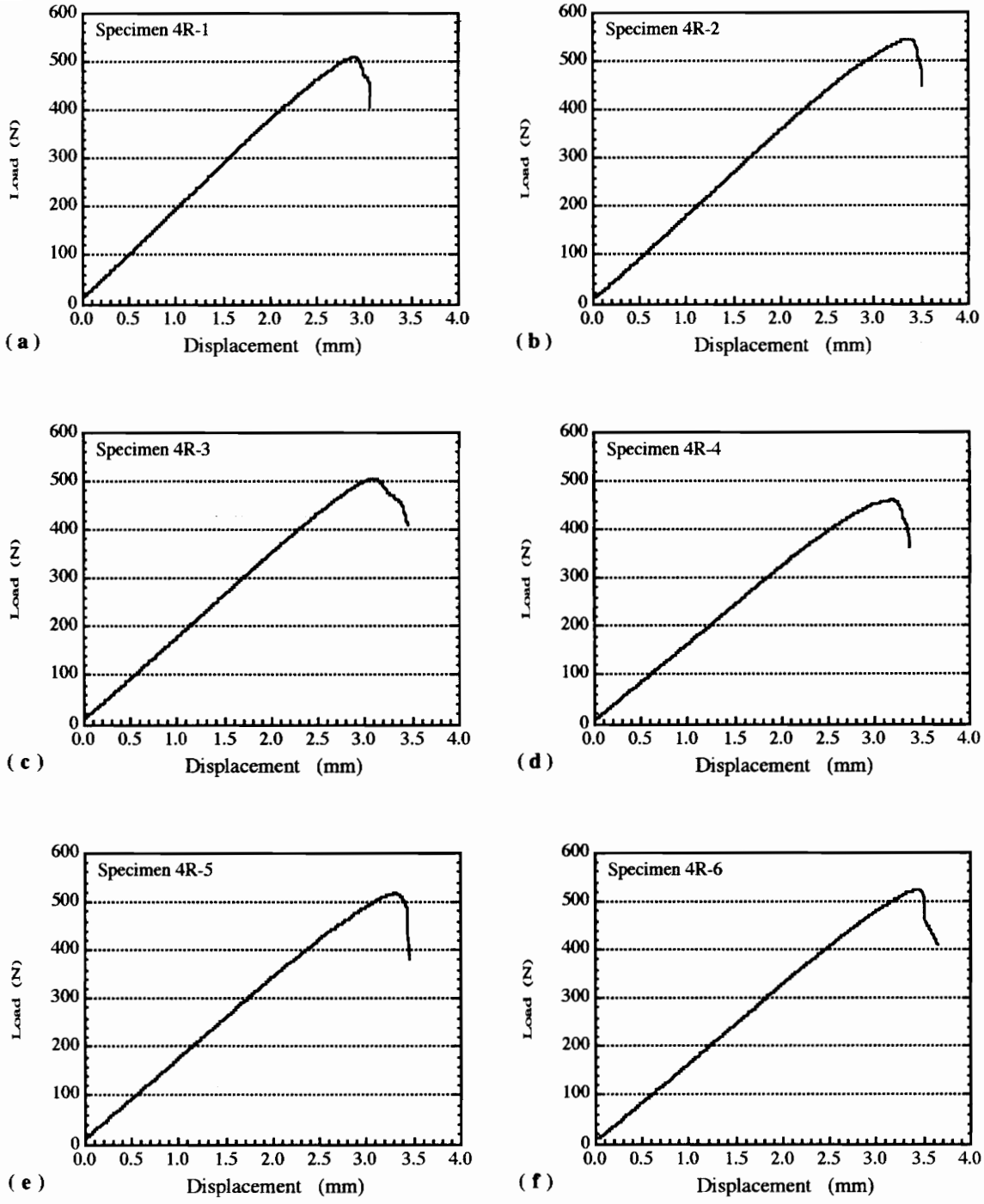

Figures B1.6: Load-Displacement Curves for Specimens from the Panel Made with Recovered Polymer and Cooled at 4°C/min a) Specimen 4R-1, b) Specimen 4R-2, c) Specimen 4R-3 d) Specimen 4R-4, e) Specimen 4R-5, and f) Specimen 4R-6

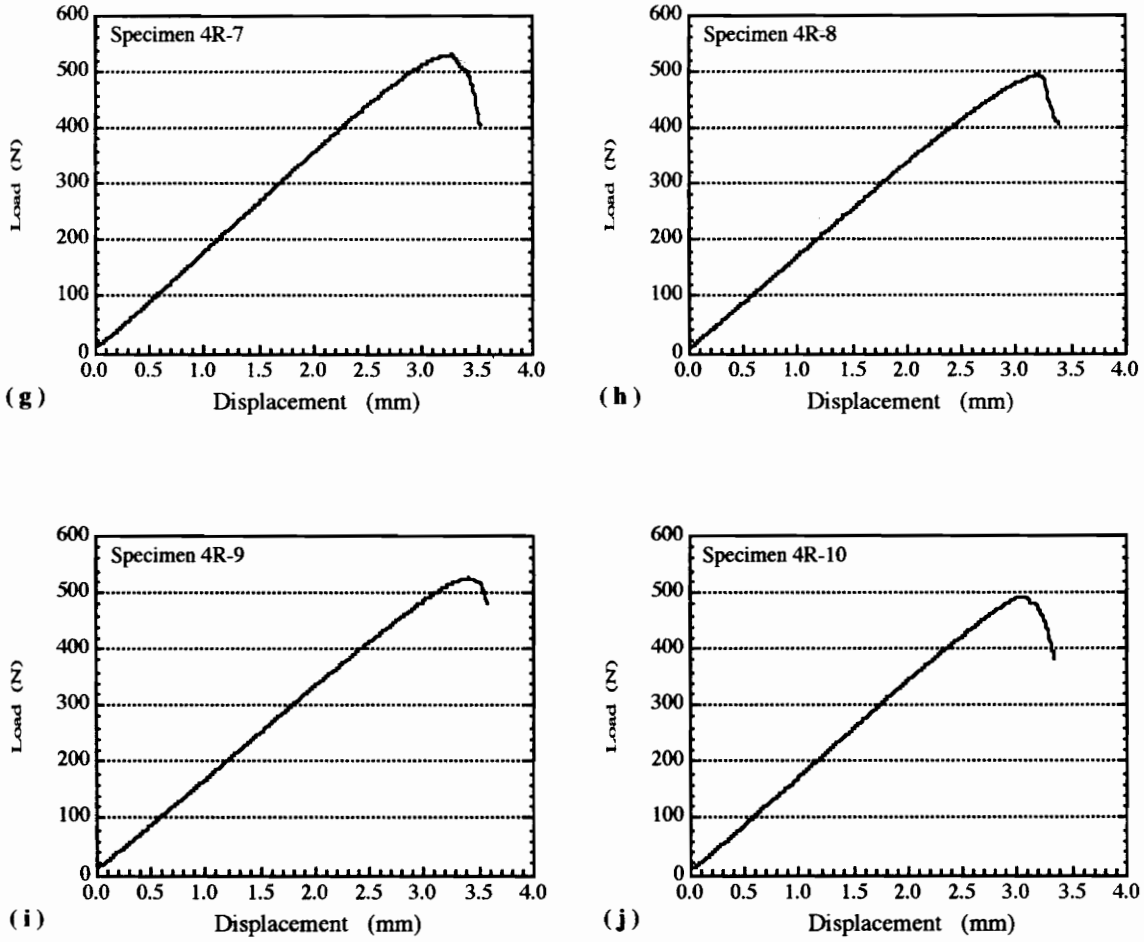

Figures B1.6 (continued): Load-Displacement Curves for Specimens from the Panel Made with Recovered Polymer and Cooled at 4°C/min
g) Specimen 4R-7, h) Specimen 4R-8,
i) Specimen 4R-9, and j) Specimen 4R-10

ENF Compliance Calibration Plots

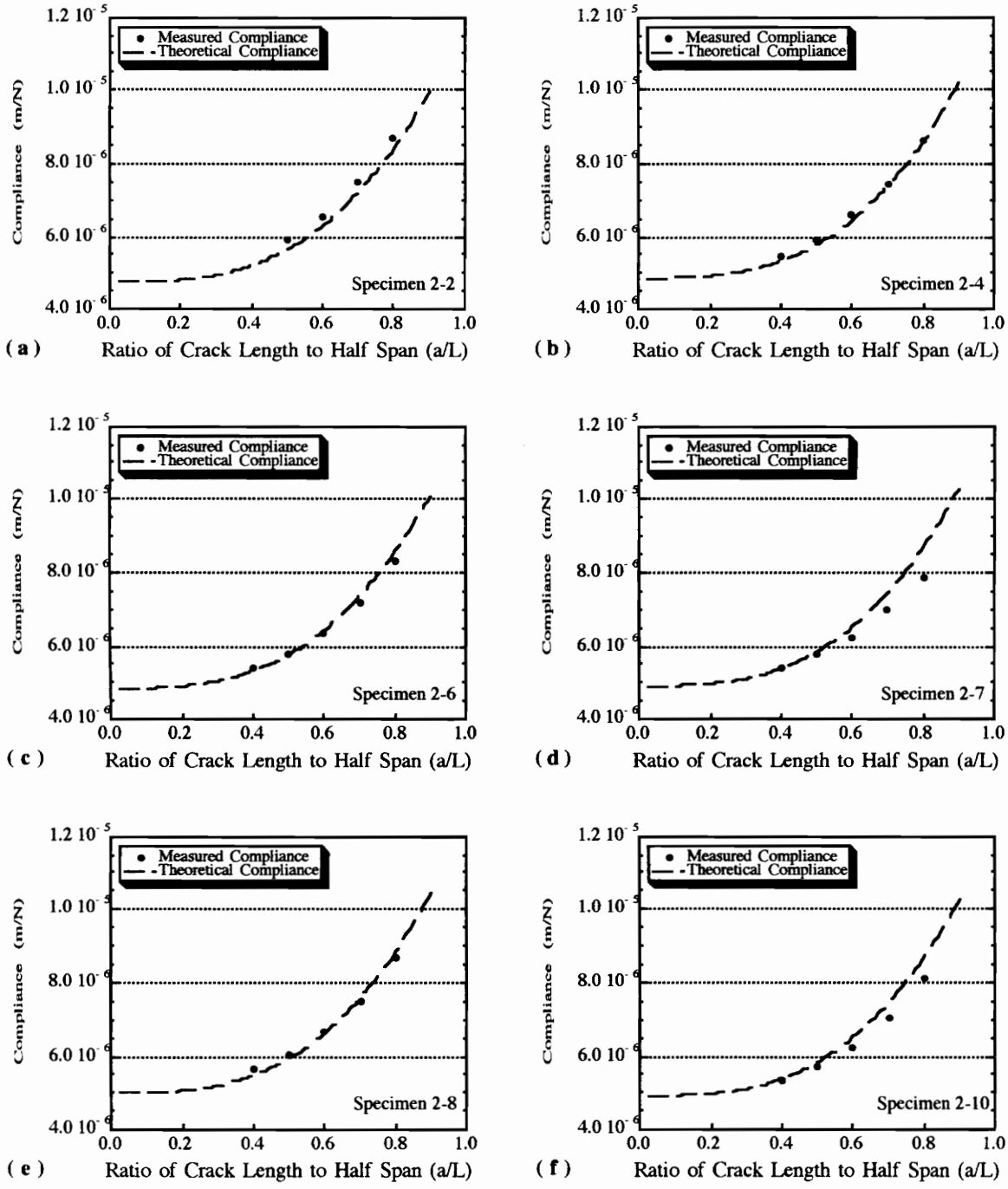

Figures B2.1: Compliance Calibration Curves for Specimens from the Principal Panel Cooled at 2°C/min
a) Specimen 2-2, b) Specimen 2-4, c) Specimen 2-6,
d) Specimen 2-7, e) Specimen 2-8, and f) Specimen 2-10

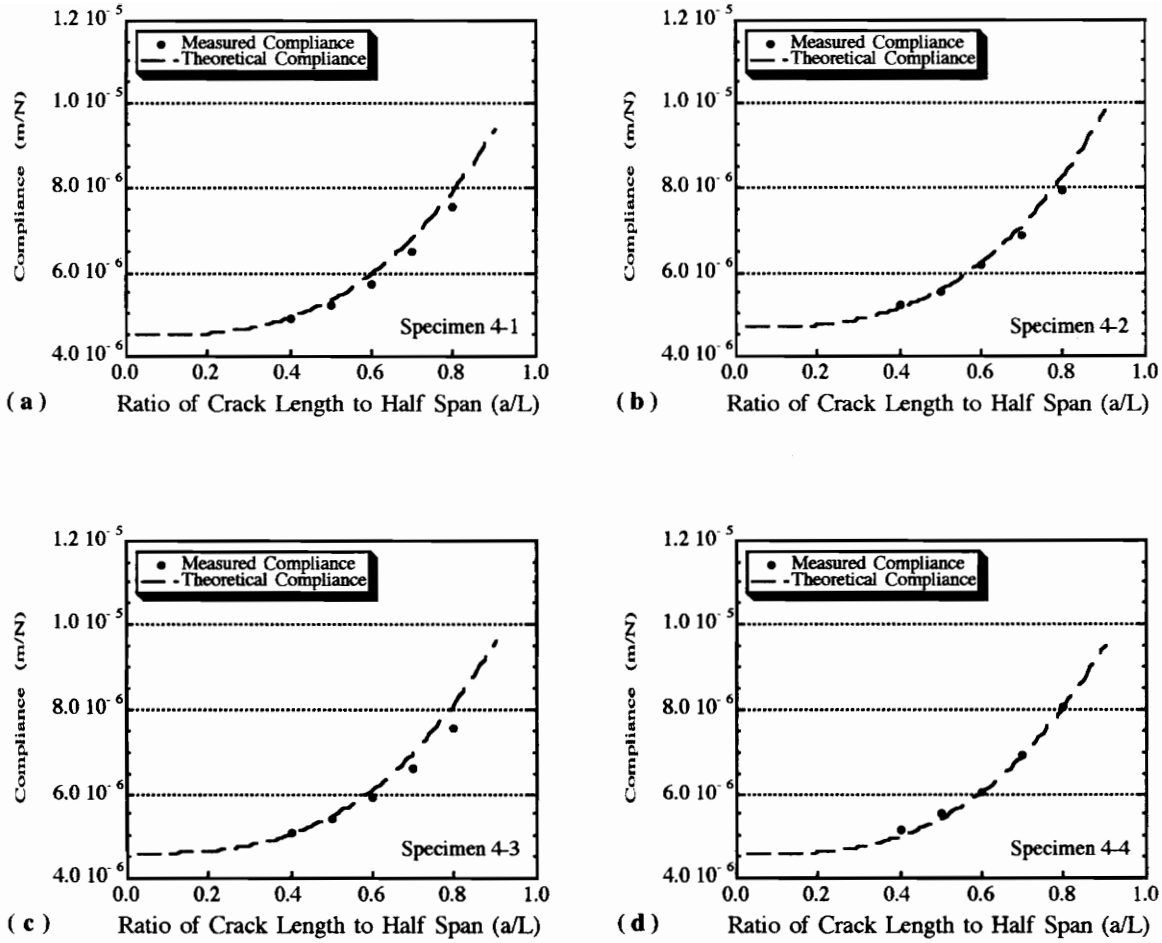

Figures B2.2: Compliance Calibration Curves for Specimens from the Principal Panel Cooled at 4°C/min
a) Specimen 4-1, b) Specimen 4-2,
c) Specimen 4-3, and d) Specimen 4-4

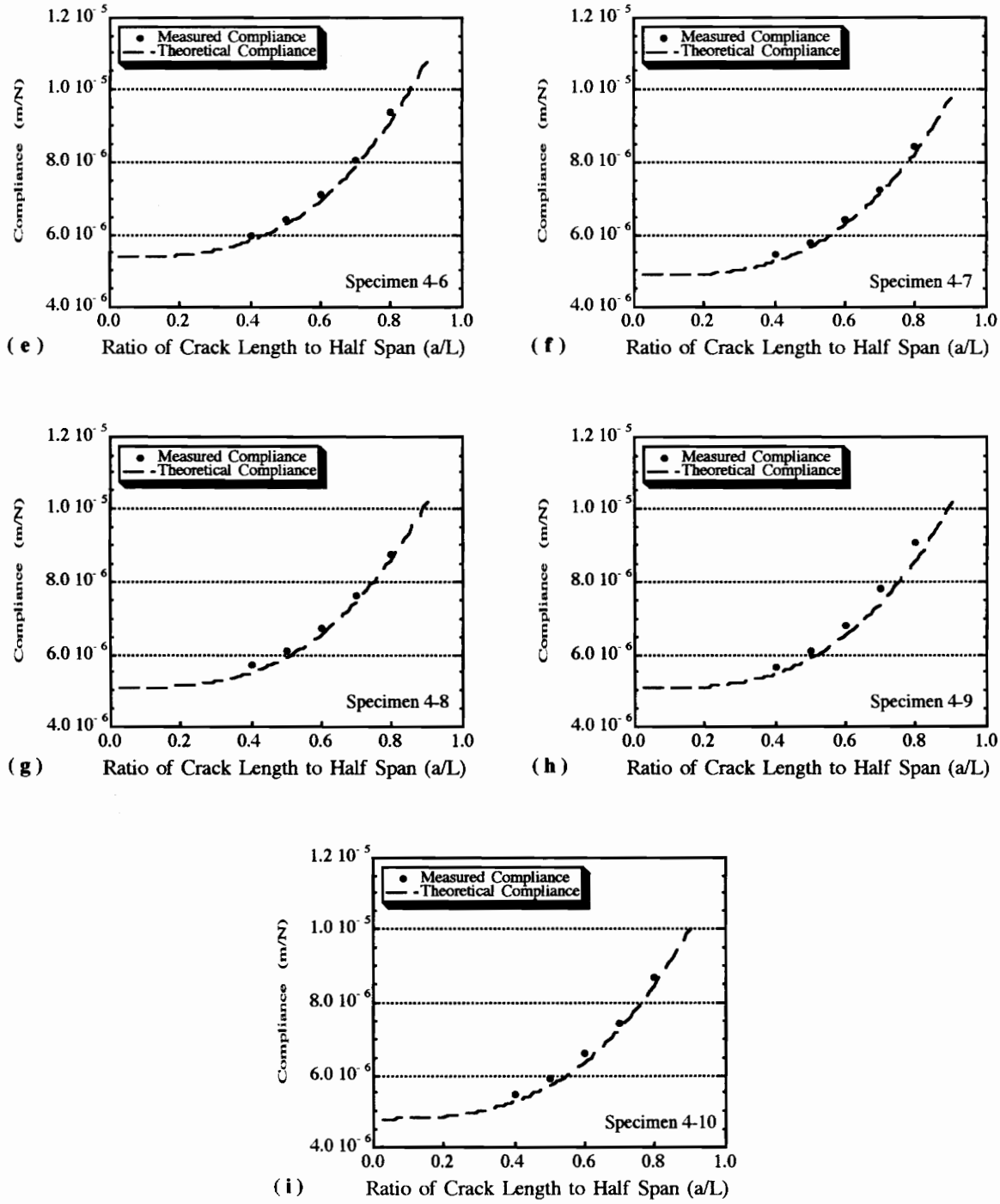

Figures B2.2 (continued): Compliance Calibration Curves for Specimens from the Principal Panel Cooled at 4°C/min
e) Specimen 4-6, f) Specimen 4-7, g) Specimen 4-8
h) Specimen 4-9, and i) Specimen 4-10

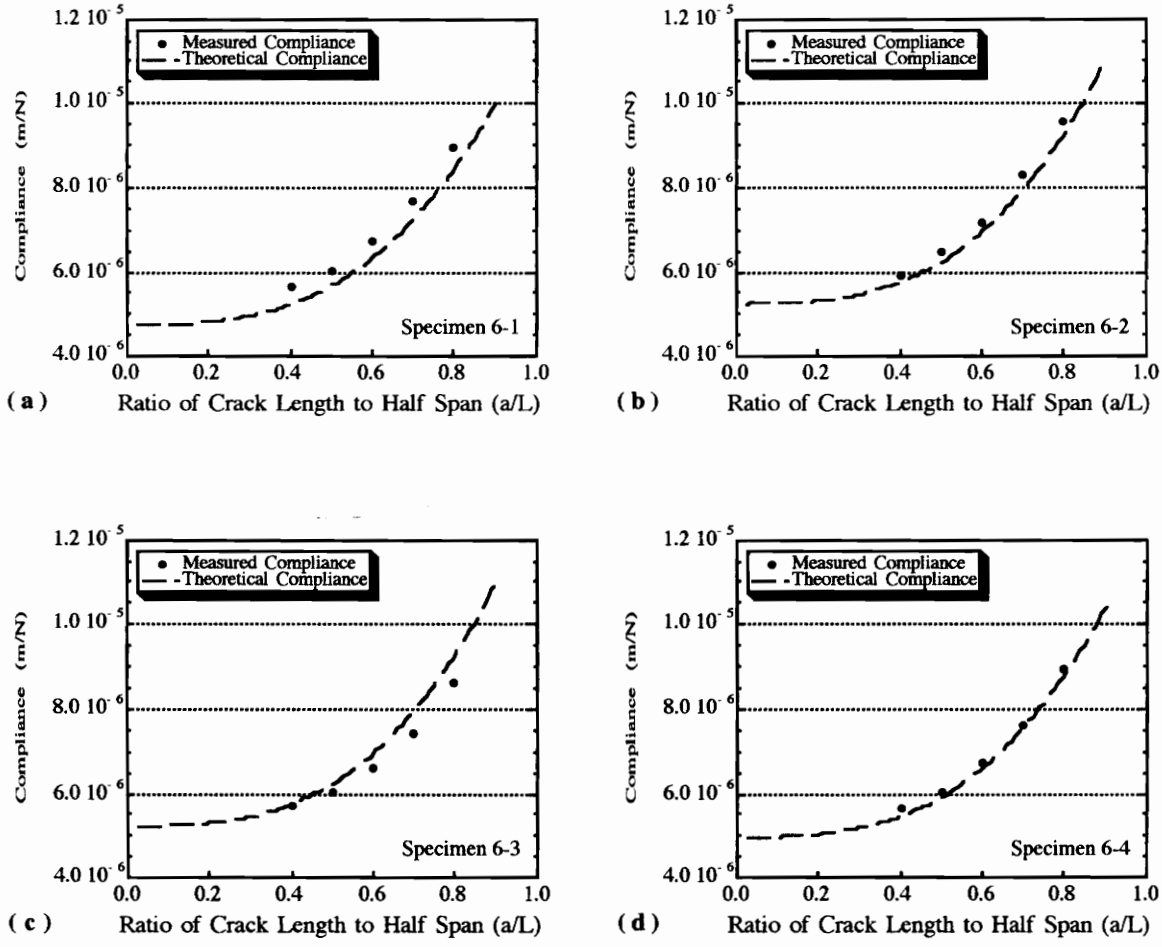

Figures B2.3: Compliance Calibration Curves for Specimens from the Principal Panel Cooled at 6°C/min
a) Specimen 6-1, b) Specimen 6-2,
c) Specimen 6-3, and d) Specimen 6-4

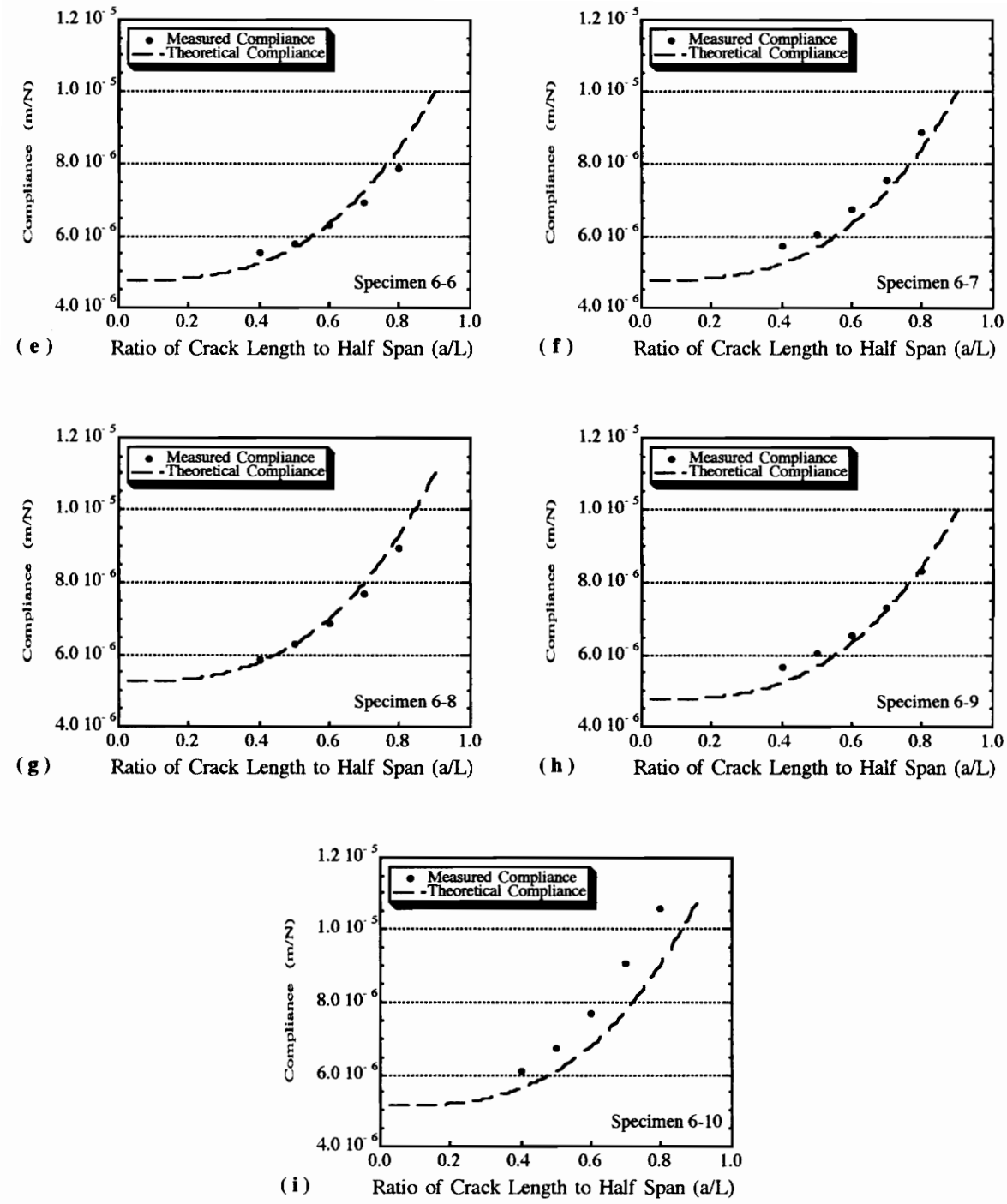

Figures B2.3 (continued): Compliance Calibration Curves for Specimens from the Principal Panel Cooled at 6°C/min
e) Specimen 6-6, f) Specimen 6-7, g) Specimen 6-8
h) Specimen 6-9, and i) Specimen 6-10

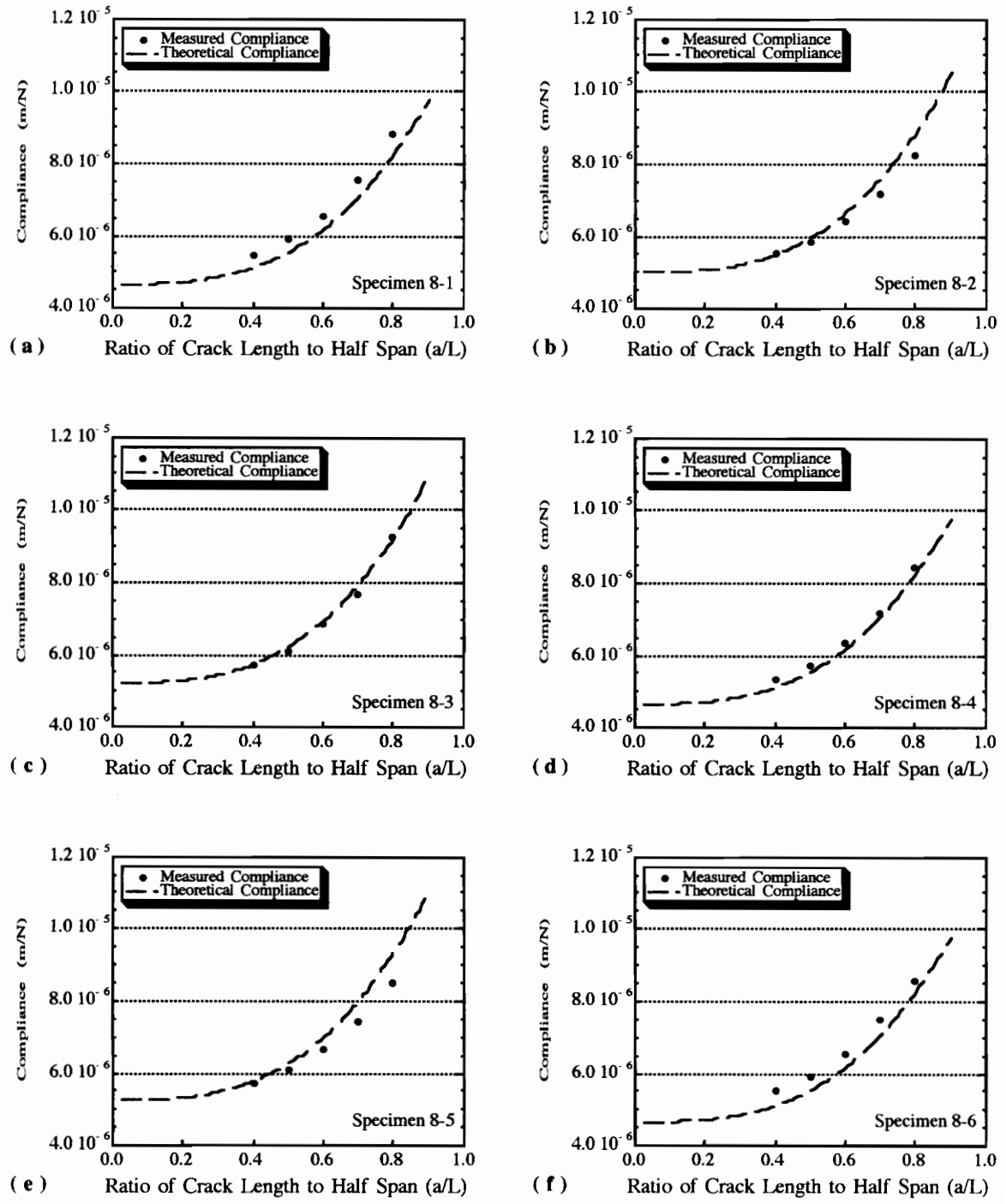

Figures B2.4: Compliance Calibration Curves for Specimens from the Principal Panel Cooled at 8°C/min
a) Specimen 8-1, b) Specimen 8-2, c) Specimen 8-3
d) Specimen 8-4, e) Specimen 8-5, and f) Specimen 8-6

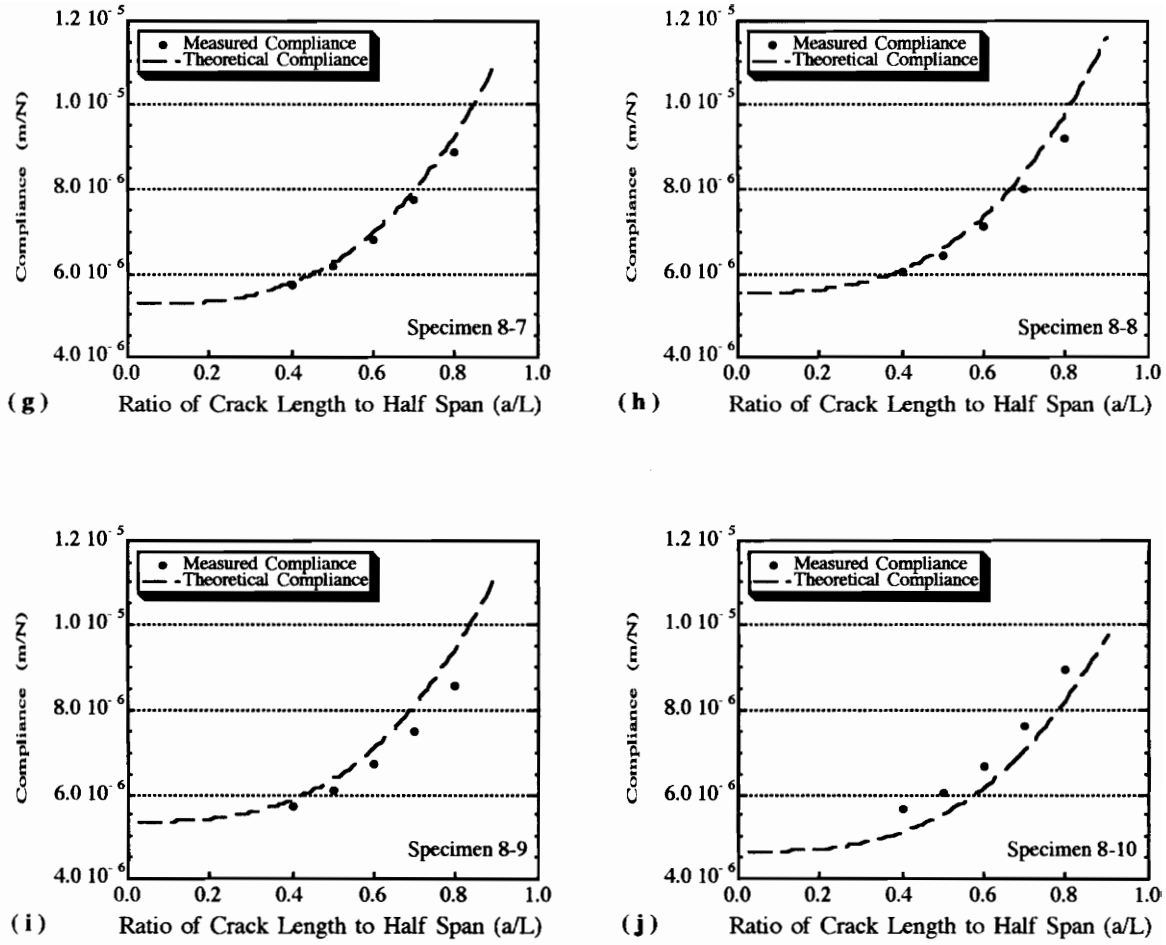

Figures B2.4 (continued): Compliance Calibration Curves for Specimens from the Principal Panel Cooled at 8°C/min
g) Specimen 8-7, h) Specimen 8-8,
i) Specimen 8-9, and j) Specimen 8-10

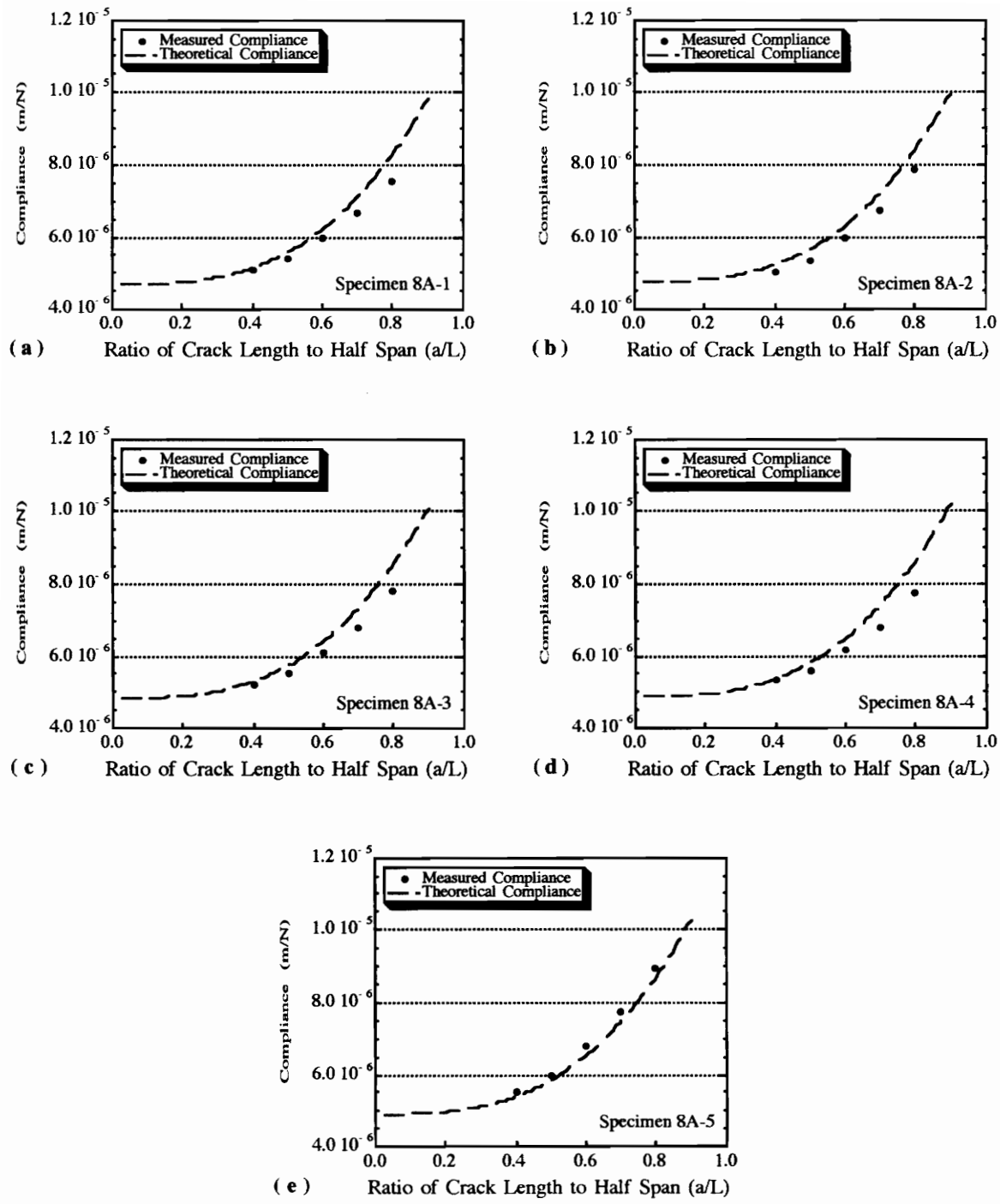

Figures B2.5: Compliance Calibration Curves for Specimens from the Panel Cooled at 8°C/min and then Annealed
a) Specimen 8A-1, b) Specimen 8A-2, c) Specimen 8A-3
d) Specimen 8A-4, and e) Specimen 8A-5

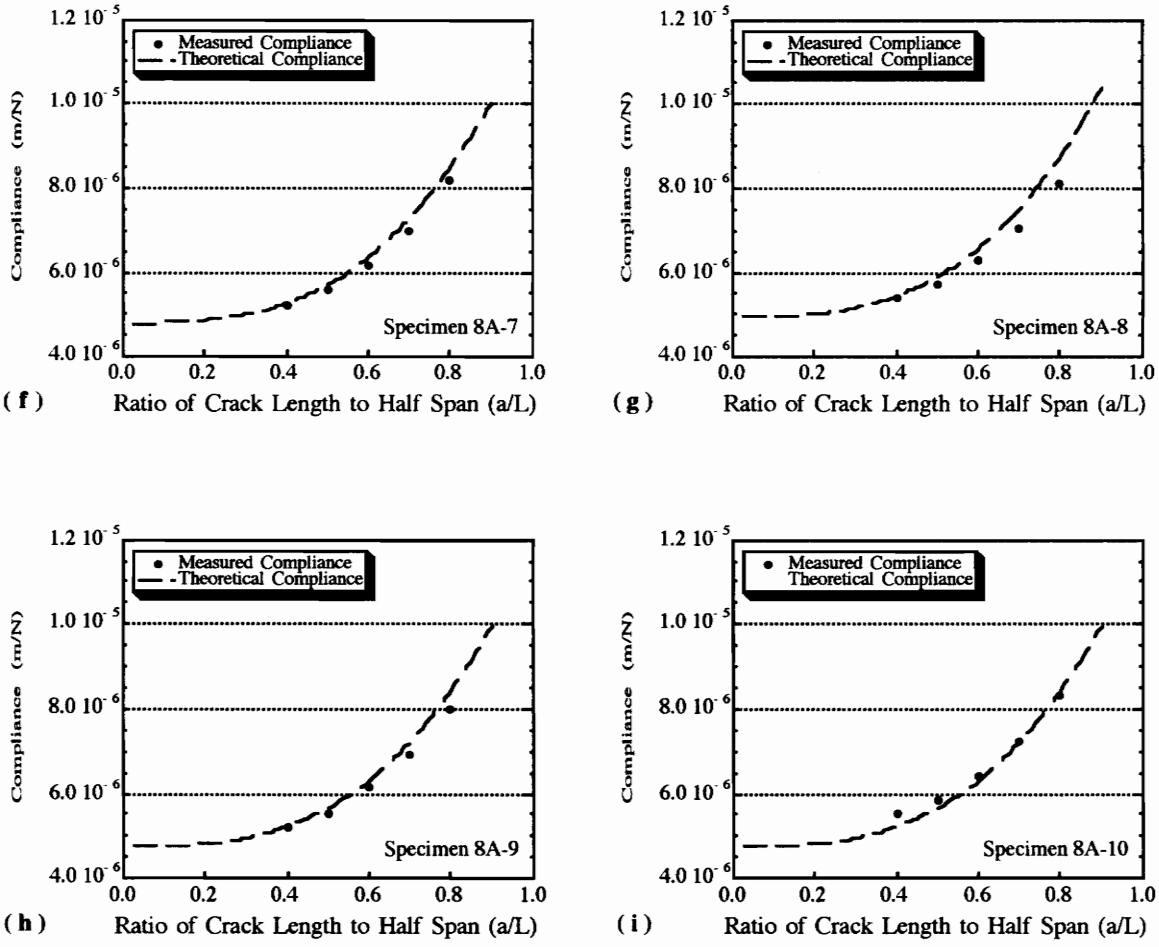

Figures B2.5 (continued): Compliance Calibration Curves for Specimens from the Panel Cooled at 8°C/min and then Annealed
f) Specimen 8A-7, g) Specimen 8A-8
h) Specimen 8A-9, and i) Specimen 8A-10

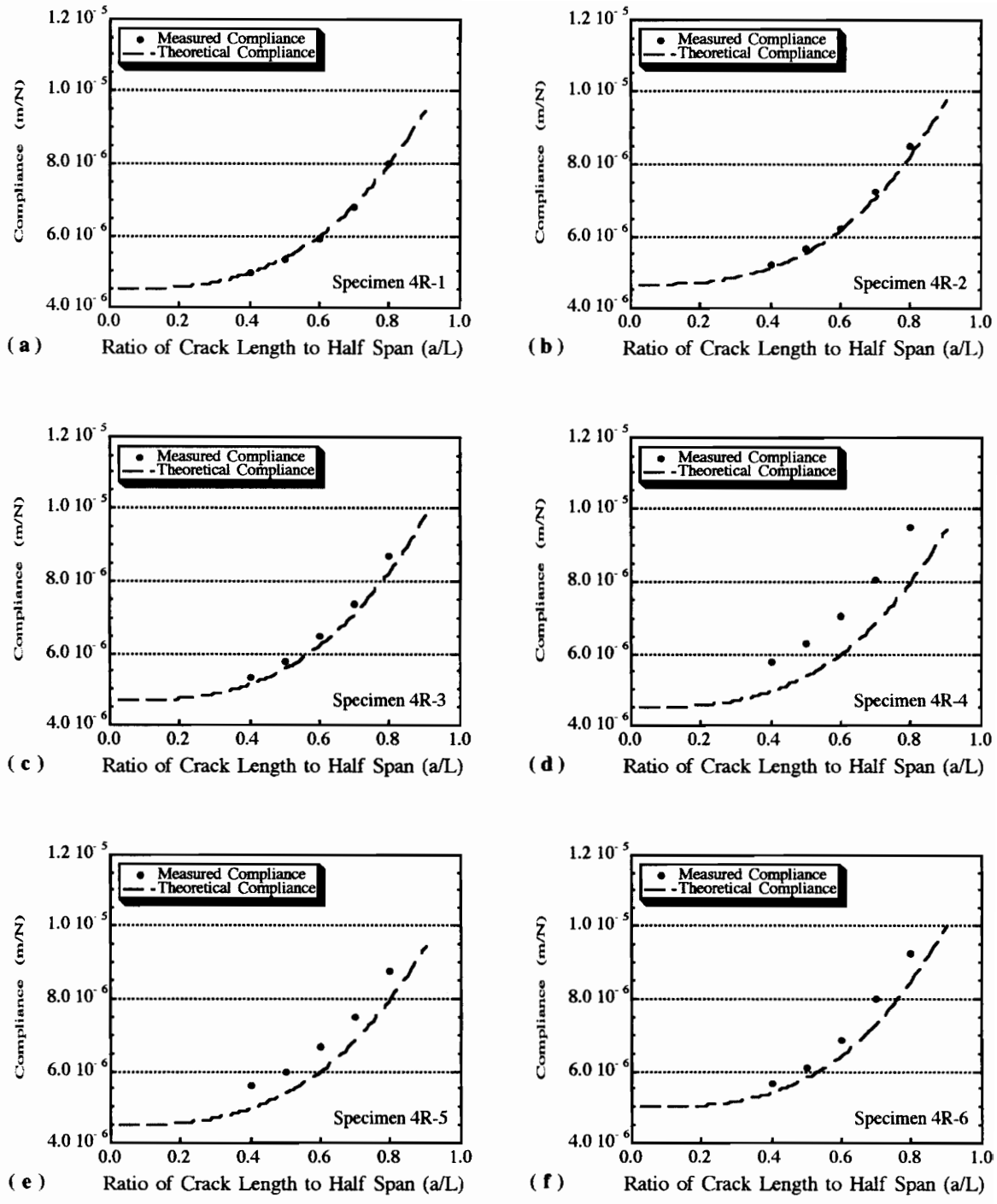

Figures B2.6: Compliance Calibration Curves for Specimens from the Panel Made with Recovered Polymer and Cooled at 4°C/min a) Specimen 4R-1, b) Specimen 4R-2, c) Specimen 4R-3 d) Specimen 4R-4, e) Specimen 4R-5, and f) Specimen 4R-6

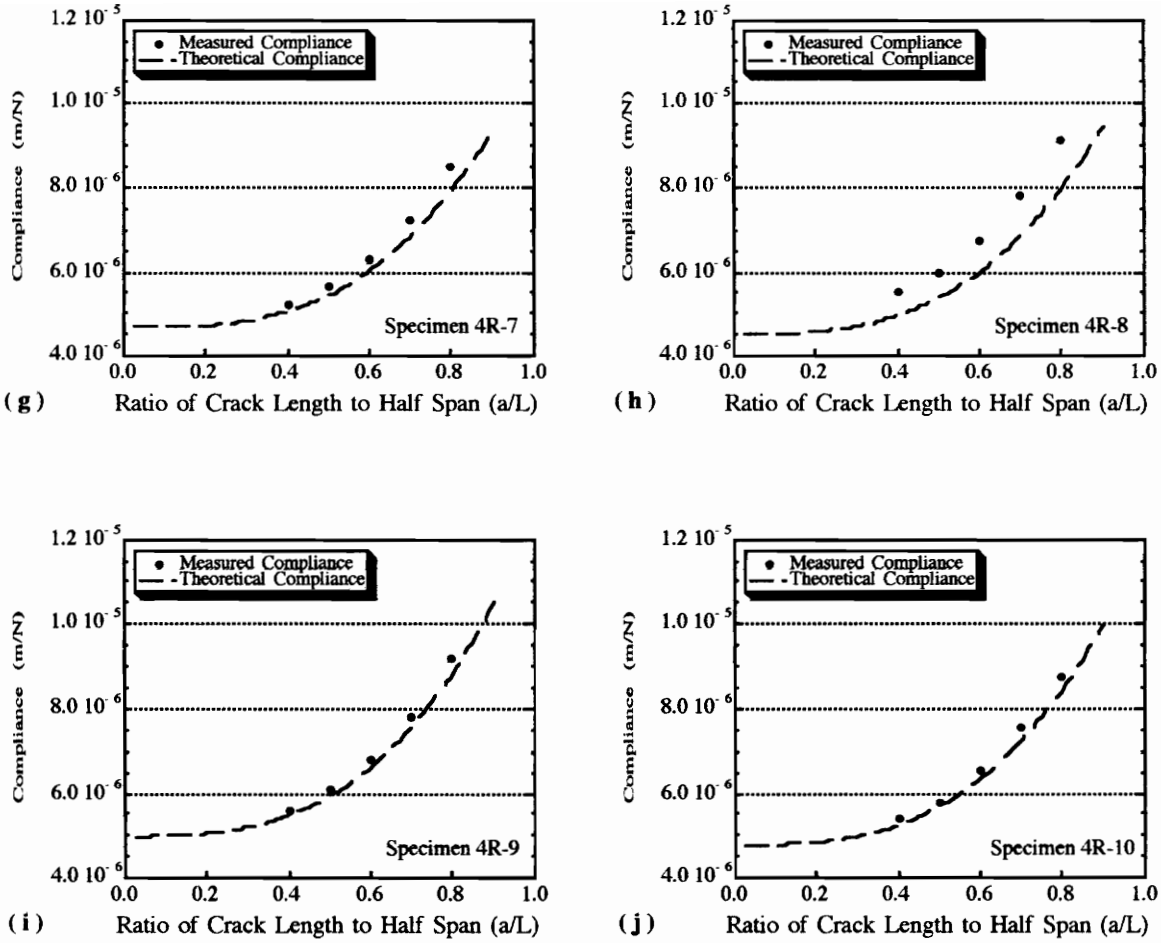

Figures B2.6: Compliance Calibration Curves for Specimens from the Panel Made with Recovered Polymer and Cooled at 4°C/min g) Specimen 4R-7, h) Specimen 4R-8, i) Specimen 4R-9, and j) Specimen 4R-10

Appendix C - Statistical Concepts[1]

In experimental work, there is always a distribution to the possible values of a property. This distribution of an experimental value is called the population. The true population for a particular property is rarely known; therefore, experiments are conducted to obtain samples from the population.

Experimental values, although they come from the population, will not be exactly equal to the population mean. Consequently, an experimentally measured value will be different for different samples. This makes it very unlikely that the experimental mean will be equal to the true population mean, unless the sample size is very large. As a result, to determine whether two population means are equal when given two sets of experimental data, the variance in the data must be considered as well as the mean values. Statistical tests are used to combine the knowledge from the means and the variances of two or more data sets to determine whether experimental values have come from populations with equal means.

Comparing Two Independent Samples

To compare two independent random samples for which the population variance is unknown, a "t-test" is used. The t-test assumes that the population from which the sample is drawn is a normal distribution. There are two types of t-tests, a pooled-variance t-test and separate variance t-test. A pooled-variance t-test can be used when either the sample sizes are equal or when the variance of the two samples varies by less than a factor of two. A separate-variance t-test must be used in all other cases.

In either variation of the t-test, the difference between the two sample means are normalized. This normalized value, called the test statistic, is used to determine whether the difference between the two experimental values is large enough to verify that the two population values are unequal. The value to which the normalized value is compared is called the cut-off. The cut-off is determined from the rejection region.

---

[1] This appendix is designed to only give an overview of the statistical tests used in this work. A more detailed discussion and explanation of these tests is available in Reference 44.

A rejection region is used to specify the probability of experimentally measured values from multiple groups of specimens coming from populations with equal means. Both populations are assumed to be normal distributions. The question is how much the two populations overlap. When a test statistic falls within a rejection region this indicates that the two populations have a small overlap and therefore and unequal. A result is classified as "significant" when two values are shown to be unequal. A 5% rejection region indicates that for the two means to be declared unequal, one experimental mean must lie within a given 5% area of the normal curve that is described by the other group's mean and variance. A one-tailed test indicates that the 5% of the curve is contained within one tail of the distribution, Figure C.1. A two-tailed test refers to splitting the 5% area between the tails, Figure C.2.

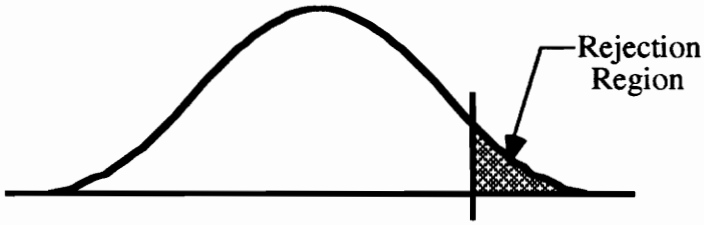

Figure C.1: A One-Tailed Rejection Region

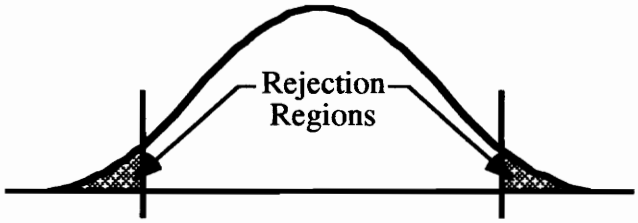

Figure C.2: A Two-Tailed Rejection Region

Comparing a Group of Samples

When several groups are to be compared, they could be compared using a series of t-tests. Each t-test, however, has a 5% chance that it will indicate that a difference exists when that is not true. Consequently, the more comparisons that are made, the better the probability that a comparison will result in a false answer. If a group of related data is being compared, the chance of finding a difference that does not really exist can be reduced through the use of a multiple range test.

The Duncan Multiple Range test provides a 5% chance of finding a difference that does not exist within each "step" of comparisons. If there are n group means, then there are n-1 steps to compare. The mean values are ordered in increasing value from the smallest mean to the largest mean. The first step will compare the largest mean to the smallest mean. The second step will compare the second largest mean to the smallest mean and compare the largest mean to the second smallest mean. The steps continue to decrease in size and increase in number of comparisons per step until all data is included in a "nonsignificant" group or all means have been compared to each other. These tests do identify "non-significant" results, i.e. these tests search for values which are equal. Note that the "significant" results of this test still refer to means which are unequal.

References

[1] Moore, D.R.; Seferis, J.C.; "Toughness Characterization of Carbon Fiber/Poly Ether Ether Ketone (CF/PEEK) Laminates", *Pure and Applied Chemistry*, v63, n11 (1991) pg. 1609-1625.

[2] Seferis, J.C.; "Polyetheretherketone (PEEK): Processing-Structure and Properties For a Matrix in High Performance Composites", *Polymer Composites*, v6, n3 (1986) pg. 158-169.

[3] Nguyen, H.X.; Ishida, H.; "Poly(Aryl-Ether-Ether-Ketone) and Its Advanced Composites: A Review", Polymer Composites, v8, n2 (1987) pg. 57-73.

[4] Chen, E.J.H.; Hsiao, B.S.; "The Effects of Transcrystalline Interphase in Advanced Polymer Composites", *Polymer Engineering and Science*, v32, n4 (1992) pg. 280-286.

[5] Hsiao, B.S.; Chang, I.Y.; Sauer, B.B.; "Novel Crystallization Kinetics Modeling of Advanced Polymer Composites", Conference Proceedings: In Search of Excellence -- ANTEC '91, 49th Annual Technical Conference, pg. 2084-2087.

[6] Song, J.W.; "Thermoplastic Composites for Ballistic Applications", 26th International SAMPE Technical Conference, Oct 17-20 (1994) pg. 627-641.

[7] Cebe, P.; "Non-Isothermal Crystallization of Poly(Etheretherketone) Aromatic Polymer Composite", *Polymer Composites*, v9, n4 (1988) pg. 271- 279.

[8] Schultz, J.M.; "Microstructural Aspects of Failure in Semicrystalline Polymers", *Polymer Engineering Science*, v24 n10 (1984) pg. 770-785.

[9] Cebe, P.; "Crystallization and Annealing of High Performance Semicrystalline Polymers: PEEK and PPS", ANTEC '89, pg. 1413-1415.

[10] Cebe, P.; Chung, S.Y.; Hong, S.-D.; "Effect of Thermal History on Mechanical Properties of Polyetheretherketone Below the Glass Transition Temperature", *Journal of Applied Polymer Science*, v33 (1987) pg. 487-503.

[11] Chu, J.-N.; Schultz, J.M.; "The Influence of Microstructure on the Failure Behavior of PEEK", *Journal of Materials Science*, v25 (1990) pg. 3746-3752.

[12] Ho, R-M.; et al; "Crystal Morphology and Phase Identifications in Poly(Aryl Ether Ketone)s and Their Copolymers. 2. Poly(oxy-1,4-Phenylene-carbonyl-1,3-phenylenecarbonyl-1,4-phenylene)", Macromolecules, v27 (1994) pg. 5787-5793.

[13] Lee, Y.; Porter, R.S.; "Crystallization of Poly(etheretherketone) (PEEK) in Carbon Fiber Composites", Polymer Engineering and Science, v26, n9 (1986) pg. 633-639.

[14] Gardner, K.H.; Hsiao, B.S.; Faron, K.L.; "Polymorphism in Poly(Aryl Ether Ketone)s", Polymer, v35, n11 (1994) pg. 2290-2295.

[15] Hsiao, B.S.; Gardner, K.H.; Cheng, S.Z.D.; "Crystallization of Poly(Aryl Ether Ketone Ketone) Copolymers Containing Terephthalate/Isophthalate Moieties", Journal of Polymer Science: Part B: Polymer Physics, v22 (1994) 2585-2594.

[16] Hsiao, B.S.; Chen, E.J.H.; "Study of Transcrystallization in Polymer Composites", Materials Research Society Symposium Proceedings - Interfaces in Composites, v170 (1990), ed. C.G. Pantano, E.J.H. Chen.

[17] Bessell, T.; Shortall, J.B.; "The Crystallization and Interfacial Bond Strength of Nylon 6 at Carbon and Glass Fiber Surfaces", *Journal of Materials Science*, v10 (1975) pg. 2035-2043.

[18] Incardona, S.D.; DiMaggio, R.; Fambri, L.; Migliaresi, C.; Marom, G.; "Crystallization in J-1 Polymer/Carbon-Fiber Composites: Bulk and Interface Processes", Journal of Materials Science, v28 (1993) pg. 4983-4987.

[19] Folkes, M.J.; Hardwick, S.T.; "The Mechanical Properties of Glass/Polypropylene Multilayer Laminates", *Journal of Materials Science*, v25 (1990) pg. 2598-2606.

[20] Huson, M.G.; McGill, W.J.; "Transcrystallinity in Polypropylene", *Journal of Polymer Science: Polymer Chemistry Edition*, v22 (1984) pg. 3571-3580.

[21] Teishev, A.; Marom, G.; "The Effect of Transcrystallinity on the Transverse Mechanical Properties of Single-Polymer Polyethylene Composites", *Journal of Applied Polymer Science*, v56 (1995) pg. 959-966.

[22] Campbell, D.; Qayyum, M.M.; "Melt Crystallization of Polypropylene: Effect of Contact with Fiber Substrates", *Journal of Polymer Science: Polymer Physics Edition*, v18 (1980) pg. 83-93.

[23] He, T.; Porter, R.S.; "Melt Transcrystallinity of Polyethylene on High Modulus Polyethylene Fibers", *Journal of Applied Polymer Science*, v35 (1988) pg. 1945-1953.

[24] Moon, C-K.; "The Effect of Interfacial Microstructure on the Interfacial Strength of Glass Fiber/Polypropylene Resin Composites", *Journal of Applied Polymer Science*, v54 (1994) pg. 73-82.

[25] Hodge, I.; "Physical Aging in Polymer Glasses", *Science*, v267 (1995) pg. 1945-1947.

[26] Ogale, A.A.; McCullough, R.L.; "Physical Aging Characteristics of Poly Ether Ether Ketone", *Composites Science and Technology*, v30 (1987) pg. 137-148.

[27] Mijovic, J.; "Interplat of Physical and Chemical Aging in Graphite/Epoxy Composites", *Journal of Composite Materials*, v19 (1985) pg. 178-191.

[28] Lee, A.; McKenna, G.B.; "Physical Aging of Polymer Composite Matrices", *Polymer*, v31 (1990) pg. 423-430.

[29] Kemmish, D.J.; Hay, J.N.; "The Effect of Physical Aging on the Properties of Amorphous PEEK", *Polymer*, v26 (1985) pg. 905-912.

[30] Struik, L.C.E.; Physical Aging in Amorphous Polymers and Other Materials, Elsevier, New York (1971).

[31] Tant, M.R.; Wilkes, G.L.; "An Overview of the Nonequilibrium Behavior of Polymer Glasses", *Polymer Science and Engineering*, v21 (1981) pg. 875-895.

[32] Goodwin, A. A.; Hay, J.N.; "Temperature Range of Physical Aging", *Polymer Communications*, v31 (1990) pg. 338-340.

[33] Carfagna, C.; Amendola, E.; D'Amore, A.; Nicolais, L.; "Physical Aging of Amorphous Poly(Etheretherketone) (PEEK)", *Polymer Engineering and Science*, v28 n18 (1988) pg. 1203-1206.

[34] Lustiger, A.; "Considerations in the Utilization of Semicrystalline Thermoplastic Advanced Composites", *SAMPE Journal*, v20, n5 (1984) pg. 13-16.

[35] Carvalho, W.S.; Bretas, R.E.S.; "Thermoplastic/Carbon Fibre Composites: Correlation Between Interphase Morphology and Dynamic Mechanical Properties", *European Polymer Journal*, v26, n7 (1990) pg. 817-821.

[36] Chu, J.-N.; Schultz, J.M.; "The Influence of Microstructure on the Failure Behavior of PEEK", *Journal of Materials Science*, v25 (1990) pg. 3746-3752.

[37] Talbott, M.F.; Springer, G.S.; Berglund, L.A.; "The Effects of Crystallinity on the Mechanical Properties of PEEK Polymer and Graphite Fiber Reinforced PEEK", *Journal of Composite Materials*, v21 (1987) pg. 1056-1080.

[38] Tregub, A.; Harel, H.; Marom, G.; "Thermal Treatment Effects on the Crystallinity and the Mechanical Behavior of Carbon Fiber-Poly(Ether Ether Ketone) Composites", *Journal of Materials Science Letters*, v13, n5 (1994) pg. 329-331.

[39] Chow, T.S.; "Stress-Strain Behaviour of Physically Aging Polymers", *Polymer*, v34 (1993) pg. 541-546.

[40] Chang, I.Y.; "Carbon Fiber Reinforced Thermoplastic Composites with Poly(Ether Ketone Ketone) Matrix", Proceedings of the ACS Division of Polymeric Materials: Science and Engineering, (1988) pg. 1094-1100.

[41] Bucher, R.A.; Loos, A.C.; "High Performance Thermoplastic Matrix Composite Processing: Dry Powder Prepregging, Plasma Treatment, Consolidation/ Crystallization Analysis", Viriginia Tech Center for Composite Materials and Structures Report 95-02, December 1994.

[42] O'Brien, T.K.; Martin, R.H.; "Results of ASTM Round Robin Testing for Mode I Interlaminar Fracture Toughness of Composite Materials," *ASTM Journal of Composites Technology and Research*, v15, n4 (1993) pg. 269-281.

[43] Rau, A.; "Processing of Toughened Cyanate Ester Maxtrix Composites", Ph.D. Dissertation, Virginia Polytechnic Institute and State University, 1996.

[44] Ott, R.L.; An Introduction to Statistical Methods and Data Analysis, Duxbury Press, Belmont, CA, 1993.

[45] Russell, A.J.; Street, K.N.; "Moisture and Temperature Effects on the Mixed-Mode Delamination Fracture of Unidirectional Graphite/Epoxy", Delamination and Debonding of Materials, ASTM STP 876, W.S. Johnson, Ed. (1985) pg. 349-370.

[46] Whitney, J.M. "Experimental Characterization of Delamination and Fracture", Chapter 4 of Interlaminar Response of Composite Materials, N.J. Pagano, Ed. (1989), pg. 161-247.

Vita

Kedzie Davis completed a Bachelor of Science degree in Aeronautical and Astronautical Engineering at the University of Illinois at Urbana-Champaign in May 1994. Her engineering experience includes three terms as a co-op with the McDonnell Douglas Corporation, seven semesters as an Undergraduate Research Assistant in the Department of Aeronautical and Astronautical Engineering at the University of Illinois at Urbana-Champaign, two summers as an intern in the Langley Aerospace Research Summer Scholars Program at NASA-Langley Research Center, and one summer as an intern in the Carderock Division of the Naval Surface Warfare Center. She currently holds an Office of Naval Research Graduate Fellowship. Upon completion of her Master's program, Kedzie plans to pursue a Doctoral degree at Virginia Polytechnic Institute and State University.

Kedzie Davis